Approximate account of connected quadruply excited clusters in single-reference coupled-cluster theory via cluster analysis of the projected unrestricted Hartree-Fock wave function

Piotr Piecuch,[1,*] Robert Toboła,[2] and Josef Paldus[1,3]
[1]*Department of Applied Mathematics, University of Waterloo, Waterloo, Ontario, Canada N2L 3G1*
[2]*Technical University of Wrocław, Institute of Physical and Theoretical Chemistry, Wybrzeże Wyspiańskiego 27, 50-370 Wrocław, Poland*
[3]*Department of Chemistry and Guelph-Waterloo Center for Graduate Work in Chemistry, Waterloo Campus, University of Waterloo, Waterloo, Ontario, Canada N2L 3G1*
(Received 26 February 1996)

Extension of the applicability of the closed-shell coupled-cluster (CC) theory with doubly (CCD) or singly and doubly (CCSD) excited clusters to quasidegenerate situations requires the inclusion of the connected triply and quadruply excited cluster components T_3 and T_4. Since an explicit consideration of these clusters for larger systems is computationally very demanding, we explore the possibility of estimating the T_4 contribution using the projected unrestricted Hartree-Fock (PUHF) wave function. The resulting CCDQ′ and CCSDQ′ approaches are shown to correctly approximate the effect of the quadruply (Q') excited T_4 clusters, even when the PUHF wave function itself cannot serve as a good source of the lower-order pair-cluster components. It is important that the results of the cluster analysis of the PUHF solution are used directly and no further approximations are made. Only when both pair-cluster and T_4 cluster components are reasonably well approximated by the PUHF wave function, the T_4 cluster contributions cancel out certain CCSD diagrams, and good CC results can be obtained with the approximate coupled-pair approaches. It is also demonstrated that it may be more difficult to balance T_3 and T_4 clusters relying on simple perturbative approaches, such as CCSDQ′+T(CCSDQ′). The results of formal considerations, including a thorough investigation of the cluster structure of the PUHF wave function, are illustrated on several examples. These include a few model systems composed of four and eight hydrogen atoms in various geometrical arrangements, as described using minimum and double zeta plus polarization basis sets, for which the exact full configuration interaction data are available. The orthogonally spin-adapted formulation of CC theory is used throughout. [S1050-2947(96)07407-0]

PACS number(s): 31.10.+z, 31.15.Dv, 31.15.Ar, 31.25.−v

I. INTRODUCTION

The single-reference (SR) coupled-cluster (CC) theory [1] is currently widely exploited for an *ab initio* description of the electronic structure of atomic and molecular systems [3–9]. Its success in describing nondegenerate ground states has stimulated considerable activity aiming to extend its applicability to quasidegenerate and excited electronic states. Particularly significant are several formulations and implementations of multireference (MR) CC formalisms of both genuine (Fock or Hilbert space) and state-selective (SS) types (cf., e.g., Refs. [7–14], and references therein). These advances have been paralleled by the development and coding of various SRCC methods that account for connected triexcited and tetraexcited cluster components [15–25,27–31].

Although the genuine MRCC theories may represent an expedient solution in general open-shell situations, their application to real systems is far from being routine and remains rather limited. Proper choice of the reference space, which depends on the fragmentation pathway considered, and of truncation schemes required for realistic calculations, is rather delicate, so that one often experiences intruder state [32] or convergence problems [33,34]. On the other hand, the inclusion of higher than pair clusters in the standard SRCC formalism can often successfully describe the complicated cluster structure of quasidegenerate wave functions (cf., e.g., the so-called SSCC approach [14], including selected types of triexcited and tetraexcited clusters [31,35–37]). Thus, in spite of all the recent progress in the area of MRCC theory, it is still worthwhile to seek efficient SRCC approaches that are capable of accounting for connected triexcited and tetraexcited clusters. Likewise, many excited and ionized states of both closed- and open-shell systems can be successfully described using a single, yet effectively multiconfigurational, spin-free reference of the unitary group approach (UGA) in the so-called UGA coupled cluster singles and doubles (CCSD) method [38,39].

A full, explicit account of higher than pair clusters in the SRCC theory leads to methods that are computationally very demanding [e.g., for the CCSDT [20,21] and CCSDTQ [27–29] methods, considering triples (T) and quadruples (Q) in addition to singles (S) and doubles (D), the number of floating point operations scale as n^8 and n^{10}, respectively, where n is the dimension of the one-electron space involved; cf., e.g., Refs. [27,28], and [40]]. In addition, special provisions must be made to avoid convergence problems when solving the resulting nonlinear CC equations (cf., e.g., Refs. [28] and [30]). While the performance of CCSDT and CCSDTQ codes can be substantially improved by using recur-

* Present address: Department of Chemistry, University of Toronto, Toronto, Ontario, Canada M5S 3H6.

sively generated intermediates, leading to a fully vectorizable computer algorithm [27,28], much less can be done to reduce large storage requirements for triexcited and tetraexcited cluster amplitudes. Orthogonal spin adaptation [22,41–44] and adaptation to spatial symmetry (or other available symmetries) certainly help here (cf., e.g., Refs. [23, 43, 45], and [46]), but the primary problem of large memory requirements can hardly be eliminated.

For these reasons one often employs various approximate approaches, such as, for example, noniterative perturbative estimates of singly (T_1), triply (T_3), and quadruply (T_4) excited clusters, referred to as the CCD+ST(CCD) or CCD[ST] [18,22,24], CCSD+T(CCSD) or CCSD[T] [17,22,24], CCSD(T) [19], CCSDT+Q(CCSDT) or CCSDT[Q] [25], and CCSD+TQ*(CCSD) or CCSD[TQ]* [26] schemes, or their iterative CCSDT-*n* [15,16,20,22] and CCSDTQ-*n* [25] counterparts (cf., also, Refs. [4,6,27,28], and [40]). In these approaches, the quadruply and/or triply excited cluster amplitudes are approximated via many-body perturbation theory (MBPT) in terms of lower-order T_1 and T_2 clusters and thus need not be stored. This leads to substantial savings in computational costs (cf. Ref. [40], and references therein), even though these may still be excessive when larger systems are considered. Moreover, even when computationally feasible, the perturbative CC approaches are often limited to near equilibrium geometries. For example, when computing potential energy surfaces (PES) of simple diatomics, such as HF or N_2, the perturbative CC methods yield incorrect shapes of PES at large internuclear distances (cf., e.g., Refs. [37], [47], and [48]).

Replacing the restricted Hartree-Fock (RHF) reference by its unrestricted (UHF) analog may improve the results, but the corresponding wave functions are spin contaminated and the computational costs of such CC-UHF calculations substantially increase due to the fact that we must use twice as many molecular (spin) orbitals than in CC-RHF calculations (cf., e.g., Ref. [47]). In general, when the configurational quasidegeneracy [49] (or nondynamical correlation) sets in, the connected quadruply excited clusters are no longer negligible relative to their disconnected $\frac{1}{2}(T_2)^2$ counterparts, and it becomes difficult to balance the effect of large T_3 and T_4 contributions (cf., e.g., Refs. [23,24,31,40], and [50]). In severe cases of quasidegeneracy, such as those found in cyclic polyenes in the strongly correlated limit, where orbital and configurational degeneracies are heavily mixed [49], and where T_4 components are large [51], the conventional CCSD, or even CCSDT approaches, completely break down (in fact become singular) [23,52].

An alternative category of SRCC approaches, which exploits easily available wave functions of non-CC origin to estimate the contribution from T_4 (and, if possible, T_3) clusters, was initiated by Paldus, Čížek, and Takahashi in Ref. [53]. In this particular case, the projected UHF (PUHF) wave function, which has a relatively simple yet sufficiently rich structure, was used to provide information about the T_4 cluster components. The motivation for this choice was the fact that for the Pariser-Parr-Pople (PPP) model Hamiltonians the (P)UHF method often yields the exact energy in the fully correlated limit (i.e., when the resonance integral $\beta \rightarrow 0$). Specifically, for cyclic polyenes $C_N H_N$ with a nondegenerate ground state, $N = 4\nu + 2$, $\nu = 1,2,\ldots$, the CCD (CC with doubles) method corrected by T_4 contributions extracted from the PUHF wave function yields the exact energy in this limit, in spite of the fact that the standard uncorrected CCD approach becomes singular in the strongly correlated region [23,52], and in spite of the fact that the T_3 cluster components generally do not vanish. In fact, the cyclic polyene ground state becomes highly degenerate in the fully correlated limit (fivefold degenerate for benzene, $N=6$, 42-fold degenerate for $N=10$ cycle, etc.) and the analytic continuation from $\beta<0$ region of the true ${}^1A_{1g}^-$ ground-state wave function of the benzene model to $\beta=0$ limit does contain T_3 clusters [54]. However, one can show that there exists a linear combination of two ${}^1A_{1g}^-$ states, which at $\beta=0$ does not contain T_3 clusters [55].

Using additional simplifications in the form of the PUHF wave function (relevant to the PPP Hamiltonians; cf. Sec. III), a SRCC method accounting for the effect of quadruple excitations, termed CCDQ′, has been suggested, and the explicit CCDQ′ equations derived [53]. Further theoretical analysis of CCDQ′ equations has shown that whenever PUHF provides exact T_2 components (as it does, for example, in the fully correlated limit of cyclic polyenes [56]), the corrections due to the T_4 clusters cancel certain nonlinear diagrams of CCD theory, so that CCDQ′ method reduces in this case to one of the approximate coupled-pair (ACP) or approximate CCD (ACCD) approaches [57–60], in which only those $\frac{1}{2}(T_2)^2$ diagrams that can be factorized over one or more hole lines [diagrams 4 and 5 in Fig. 1 of Ref. [57] or (d) and (e) in Fig. 4 of Ref. [22]] are retained [53]. This led to the formulation of a slightly modified approach, termed ACPQ (approximate coupled-pair theory with quadruples), which is identical to ACP-45 method of Refs. [57] and [58] or ACCD method of Ref. [60] up to a numerical factor of 9 in the nonlinear diagram 5 (Fig. 1 of Ref. [57]) when projected onto the so-called triplet-coupled biexcited states (see Sec. II). This simple formulation of the ACPQ approach (hereafter referred to as the ACCD′ method) was possible thanks to the orthogonally spin-adapted (OSA) formulation of the SRCC theory [22,41–44]. Other possible cancellations of nonlinear diagrams in the fully correlated limit of cyclic polyene model were analyzed in Ref. [56].

The original CCDQ′ method [53] itself has never been implemented and tested. However, the ACCD′ method and its ACCSD′ counterpart have been implemented and proved highly successful in a number of model [23,24,52,59] as well as actual [24,48] applications, eliminating the singular behavior of CCSD theory in the strongly correlated regime of cyclic polyene model and improving in most cases the CC(S)D results. The ACCD′ and ACCSD′ approaches, when applied in conjunction with perturbative estimates of triply and/or singly excited clusters {ACCD′+ST(ACCD′) ≡ ACPQ+ST(ACPQ) or ACCD′[ST], ACCSD′+T(ACCSD′) or ACCSD′[T], and ACCSDT′ ≡ ACPTQ methods [23]}, proved successful as well, providing a reasonable estimate of the effect of T_3 clusters in nondegenerate and quasidegenerate cases [23,24]. The ACCD′[ST] or ACCSD′[T] approaches were particularly useful in cases where the conventional CCD and CCSD methods fail due to the neglect of T_4 clusters [23]. In these difficult cases, the ACCD′ or ACCSD′ methods were the only CC procedures that enabled us to calculate pair-cluster

components that were in turn used to estimate the T_3 cluster contributions using the MBPT-like expressions [23].

In a recent study, Kucharski, Balková, and Bartlett [40] questioned the ability of ACCD′ or ACCSD′ approaches to estimate the effect of T_4 cluster contributions. They showed [40] that in some quasidegenerate systems the inclusion of T_4 clusters in the CCSD formalism changes the CCSD energy in the opposite direction than suggested by ACCD′ or ACCSD′ calculations [i.e., contrary to ACC(S)D′ results, the ''true'' T_4 contributions worsen the CCSD results, and one needs T_3 terms, which are absent in ACC(S)D′ theories, to compensate the energy changes due to T_4]. A similar situation was found in the corresponding semiempirical four-electron models by Planelles, Paldus, and Li [54,61] who used the valence bond (VB) corrected CC theory [62], in which the T_3 and T_4 clusters are extracted from simple VB wave functions and subsequently used to correct the standard CCSD method. However, this study also clearly showed that the T_3 and T_4 contributions to the energy may be highly nonadditive, particularly in quasidegenerate situations where the relative importance of these clusters is high (cf., also, Refs. [23] and [31]). Furthermore, in spite of an excellent performance of ACCSD′-type methods in a number of instances [23,24,48,52,56–60] and of a convincing analysis in the cyclic polyene case [53] which indicates the ability of these approaches to account for the T_4 clusters, we must keep in mind that the basic assumptions for their validity may not always hold. We cannot expect, for example, that simple PUHF wave function will always be a good source of T_4 clusters or that the PUHF wave function will always give good estimates of both T_2 and T_4 components, as assumed in the derivation of ACCD′ formalism [53]. While the first problem can be resolved by examining other sources of T_3 and T_4 contributions (cf. the VB corrected CC results mentioned above [54,61,62]), the latter problem requires an exploration of the original CCDQ′ approach [53], or its more accurate CCSDQ′ analog (see Sec. IV), in order to find out to what extent the assumptions of ACC(S)D′ approximations are satisfied in realistic calculations. This should enable us to better understand the behavior of ACC(S)D′-type approaches and the reasons why in some cases the ACC(S)D′ theory gives the results that seem to contradict the results of more accurate CC calculations with explicit inclusion of quadruply excited clusters [40].

We thus decided to examine the cluster structure of PUHF solutions and to implement and test CC(S)DQ′ methods at the *ab initio* level, using the same type of exponential expansions for UHF and PUHF wave functions (cf. Thouless′ theorem for single-determinantal wave functions [63,64]) as utilized in the original study [53]. In general, we have to consider all possible contributions appearing in these expansions, including those that vanish in cyclic polyenic case. In particular, we explore the role of monoexcited clusters defining these exponential expansions in relationship with the problem of triplet instability of HF solutions (cf., e.g., Ref. [64]), using the symbolic manipulation language MAPLE [65] and double zeta (DZ) molecular hydrogen model. After deriving the pertinent equations, we describe our general-purpose FORTRAN program performing the cluster analysis of PUHF wave functions and correcting the CCSD equations for T_4 cluster contributions obtained by such an analysis.

The resulting *ab initio* method, designated as CCSDQ′, and its perturbative version corrected for triexcited clusters, referred to as CCSDQ′+T(CCSDQ′) or CCSDQ′[T], are applied to model systems in which the amount of configurational degeneracy can be continuously varied by changing a single parameter describing their geometries. These include H_4 systems with two different geometries (the so-called H4 and P4 models of Jankowski and Paldus [57]), using both minimum basis set (MBS) [57] and double zeta plus polarization basis set (DZP) [59], as well as the MBS H8 model of Jankowski, Meissner, and Wasilewski [66], composed of eight hydrogen atoms. The latter model involves a larger number of electrons, has a sizable quadruply excited manifold and up to eightfold excitations in the full configuration interaction (FCI) expansion. We investigate the DZP H4 model, since the same model was used by Kucharski, Balková, and Bartlett in their critical study [40]. To assess the quality of T_4 clusters resulting from CCSDQ′ and ACCSD′ calculations, we compare the CCSDQ′ and CCSDQ′[T] results with ACCSD′ and ACCSD′[T] ones, as well as with limited CI and CC methods involving quadruple excitations. The quality of CCSDQ′ and CCSDQ′[T] results is also assessed by comparing them with the exact FCI data.

Throughout the present paper we use the OSA formulation of SRCC method [22,41–44], both in theoretical developments and programming, which enables substantial computational memory and time savings [67] (cf., also, Ref. [68]). This formulation has the advantage of using the minimum number of cluster amplitudes, in addition to an obvious appeal of exploiting the spin symmetry of the Hamiltonian and a direct connection with the corresponding spin-adapted CI approaches. We use the OSA version of CC theory in diagrammatic form based on graphical methods of spin algebras [69].

We organize the paper as follows. Section II contains a brief outline of the SRCC approach, with emphasis on the CCSDTQ method and its various approximate versions of both standard and nonstandard types (cf., e.g., Ref. [40]). The structure of UHF and PUHF wave functions in relationship to Thouless′ theorem, stability of HF solutions, and the role of various cluster components is analyzed in Sec. III. In Sec. IV we present basic equations of the OSA CCSDQ′ approach and discuss their connection with the ACCSD′ method. Section V then describes the details of computer implementation of CCSDQ′ and CCSDQ′[T] methods, and Sec. VI presents the results of our study of P4, H4, and H8 systems. Section VII summarizes the results, while the diagrammatic derivation of CCSDQ′ equations is given in the Appendix.

II. SINGLE-REFERENCE COUPLED-CLUSTER THEORY

To introduce CCSDQ′ and CCSDQ′[T] approaches and derive the required equations, we briefly review the basic SRCC formalism. We divide the existing CC approaches into standard and nonstandard ones.

A. Standard approaches

The SRCC theory generates the exact eigenfunction $|\Psi_0\rangle$ of the many-electron Hamiltonian H through action of

an exponential operator e^T on a suitable independent particle model reference configuration $|\Phi_0\rangle$,

$$|\Psi_0\rangle = e^T|\Phi_0\rangle, \quad \langle\Phi_0|\Psi_0\rangle = \langle\Phi_0|\Phi_0\rangle = 1. \tag{1}$$

For an N-electron system, the cluster operator T is given by a sum

$$T = \sum_{j=1}^{N} T_j, \tag{2}$$

and the j-body cluster components T_j are expanded in terms of suitably chosen set of excitation operators $G_{I_j}^{(j)}$ generating the j-fold excited configurations $|\Phi_{I_j}^{(j)}\rangle = G_{I_j}^{(j)}|\Phi_0\rangle$,

$$T_j = \sum_{I_j} t_{I_j}^{(j)} G_{I_j}^{(j)}. \tag{3}$$

The coefficients $t_{I_j}^{(j)}$ are referred to as cluster amplitudes.

The cluster operator T generates all possible fully connected [5,7] components of $|\Psi_0\rangle$ when acting on $|\Phi_0\rangle$. There is a simple relationship between the excitation operators C_j defining CI expansion for the wave function $|\Psi_0\rangle$,

$$|\Psi_0\rangle = (1+C)|\Phi_0\rangle, \quad C = \sum_{j=1}^{N} C_j, \tag{4}$$

and the cluster components T_j (see, e.g., Refs. [4–7]),

$$C_1 = T_1, \tag{5}$$

$$C_2 = T_2 + \tfrac{1}{2}(T_1)^2, \tag{6}$$

$$C_3 = T_3 + T_1T_2 + \tfrac{1}{6}(T_1)^3, \tag{7}$$

$$C_4 = T_4 + \tfrac{1}{2}(T_2)^2 + T_1T_3 + \tfrac{1}{2}(T_1)^2T_2 + \tfrac{1}{24}(T_1)^4 \tag{8}$$

(for general relationship, cf., e.g., Refs. [7] and [8]).

The general SRCC equations for the wave function $|\Psi_0\rangle$ (as represented by the cluster operator T) and for the corresponding energy E then take the following form [5,7]:

$$\langle\Phi_0|(G_{I_j}^{(j)})^\dagger(H_Ne^T)_C|\Phi_0\rangle = 0 \quad (j=1,2,\ldots,N), \tag{9}$$

$$\langle\Phi_0|(H_Ne^T)_C|\Phi_0\rangle = \Delta E \equiv E - \langle\Phi_0|H|\Phi_0\rangle, \tag{10}$$

where the subscript C designates the connected part of a given expression and

$$H_N \equiv H - \langle\Phi_0|H|\Phi_0\rangle = F_N + V_N \tag{11}$$

designates the normal-product form of the Hamiltonian [5,7,70]. In the closed-shell case considered here ($N=2n$), the reference $|\Phi_0\rangle$ involves only doubly occupied orbitals, and the one- and two-body components of the spin-independent Hamiltonian H_N, designated as F_N and V_N, respectively, are defined in terms of one- and two-electron integrals $\langle k|z|k'\rangle$ and $\langle kl|v|k'l'\rangle$ as follows:

$$F_N = \sum_{k,k'} \langle k|f|k'\rangle N[E_{kk'}], \tag{12}$$

$$V_N = \tfrac{1}{2} \sum_{k,l,k',l'} \langle kl||k'l'\rangle N[E_{kk'}E_{ll'}], \tag{13}$$

where, for simplicity, we dropped the interaction operator v from $\langle kl|v|k'l'\rangle$ and

$$\langle k|f|k'\rangle = \langle k|z|k'\rangle + \sum_{a=1}^{n} (2\langle ka||k'a\rangle - \langle ka||ak'\rangle). \tag{14}$$

Here, $N[\ ]$ denotes the normal product relative to the Fermi vacuum $|\Phi_0\rangle$ and $E_{kk'}$ are the orbital unitary group generators [71],

$$E_{kk'} = \sum_{\sigma=-1/2}^{1/2} X_{k\sigma}^\dagger X_{k'\sigma}, \tag{15}$$

with $X_{k\sigma}^\dagger$ ($X_{k\sigma}$) designating the usual Fermion creation (annihilation) operators associated with a given orthonormal spin-orbital basis $|k\sigma\rangle \equiv |k\rangle \otimes |\tfrac{1}{2},\sigma\rangle$, $\sigma = \pm\tfrac{1}{2}$. The orbitals occupied in $|\Phi_0\rangle$ (holes) are labeled by a, b, a', b', etc., and the unoccupied ones (particles) by r, s, r', s', etc. The indices k,l,k',l' run over all (occupied and unoccupied) orbitals. Choosing the RHF solution for $|\Phi_0\rangle$ makes the operator f diagonal,

$$\langle k|f|k'\rangle = \delta_{kk'}\varepsilon^k, \tag{16}$$

with ε^k representing the RHF orbital energies. Note that the energy ΔE (correlation energy when $|\Phi_0\rangle$ is the RHF reference) involves at most pair clusters T_2,

$$\Delta E = \langle\Phi_0|[H_N(T_1 + T_2 + \tfrac{1}{2}T_1^2)]_C|\Phi_0\rangle. \tag{17}$$

In *standard* SRCC approaches, expansion (2) is truncated at a suitable (preferably low) excitation level, $j = j_{\max}$, and equations projected on higher than $j_{\max}$-fold excited configurations are eliminated from system (9). For example, equations of the standard CCSDTQ approach (cf. Refs. [27–31]), where

$$T \cong T^{\mathrm{CCSDTQ}} = T_1 + T_2 + T_3 + T_4, \tag{18}$$

take the form

$$\langle\Phi_0|(G_{I_1}^{(1)})^\dagger[H_N(1 + T_1 + T_2 + \tfrac{1}{2}T_1^2 + T_3 + T_1T_2 + \tfrac{1}{6}T_1^3)]_C|\Phi_0\rangle = 0, \tag{19}$$

$$\langle\Phi_0|(G_{I_2}^{(2)})^\dagger[H_N(1 + T_1 + T_2 + \tfrac{1}{2}T_1^2 + T_3 + T_1T_2 + \tfrac{1}{6}T_1^3 + T_4 + T_1T_3 + \tfrac{1}{2}T_2^2 + \tfrac{1}{2}T_1^2T_2 + \tfrac{1}{24}T_1^4)]_C|\Phi_0\rangle = 0, \tag{20}$$

$$\langle\Phi_0|(G_{I_3}^{(3)})^\dagger[H_N(T_2 + T_3 + T_1T_2 + T_4 + T_1T_3 + \tfrac{1}{2}T_2^2 + \tfrac{1}{2}T_1^2T_2 + T_1T_4 + T_2T_3 + \tfrac{1}{2}T_1^2T_3 + \tfrac{1}{2}T_1T_2^2 + \tfrac{1}{6}T_1^3T_2)]_C|\Phi_0\rangle = 0, \tag{21}$$

$$\langle\Phi_0|(G_{I_4}^{(4)})^\dagger[H_N(T_3+T_4+T_1T_3+\tfrac{1}{2}T_2^2+T_1T_4+T_2T_3+\tfrac{1}{2}T_1^2T_3+\tfrac{1}{2}T_1T_2^2+T_2T_4+\tfrac{1}{2}(T_3)^2$$
$$+\tfrac{1}{2}T_1^2T_4+T_1T_2T_3+\tfrac{1}{6}T_2^3+\tfrac{1}{6}T_1^3T_3+\tfrac{1}{4}T_1^2T_2^2]\}_C|\Phi_0\rangle=0. \tag{22}$$

In nondegenerate situations, it is sufficient to truncate T at the doubly excited level

$$T\cong T^{\mathrm{CCSD}}=T_1+T_2. \tag{23}$$

However, when quasidegeneracy becomes appreciable (as it does, for example, in metalliclike or extended systems [23,49,51,52] or in highly distorted systems [25,26,28,31,40,47,48,50,57,59,66]), the basic assumption of CCD and CCSD approaches, which we symbolically express as

$$T_4\ll\tfrac{1}{2}(T_2)^2, \tag{24}$$

no longer applies and T_4 clusters must be accounted for. Otherwise the CCSD or CCSDT approaches may suffer a singular behavior [23,53].

The standard CCSD equations [Eqs. (19) and (20) with $T_3=T_4=0$] assume a particularly transparent form when we use the OSA formalism of Refs. [22] and [41–44]. In this case T_1 and T_2 take the form [22,24,42–44,67]

$$T_1=\sum_{a,r}\langle r|t_1|a\rangle G_a^r=\sum_{a,r}\langle r|\tau_1|a\rangle\Gamma_a^r, \tag{25}$$

$$T_2=\sum_{\substack{a\leqslant b\\ r\leqslant s}}\sum_{i=0}^{1}\langle rs|t_2|ab\rangle_i G_{ab}^{rs}(i)$$
$$=\tfrac{1}{4}\sum_{a,b,r,s}\sum_{i=0}^{1}\langle rs|\tau_2|ab\rangle_i\Gamma_{ab}^{rs}(i), \tag{26}$$

where G_a^r (Γ_a^r) and $G_{ab}^{rs}(i)$ [$\Gamma_{ab}^{rs}(i)$], $i=0,1$, designate the OSA monoexcited and biexcited operators, which generate normalized (unnormalized) monoexcited and particle-particle–hole-hole coupled biexcited singlet configurations with respect to $|\Phi_0\rangle$ (see, e.g., Refs. [22], [44], and [67]), and $\langle r|t_1|a\rangle$ ($\langle r|\tau_1|a\rangle$) and $\langle rs|t_2|ab\rangle_i$ ($\langle rs|\tau_2|ab\rangle_i$) are the corresponding normalized (unnormalized) cluster amplitudes. These operators represent special cases of general excitation operators $G_a^r(S,M_S)$ [$\Gamma_a^r(S,M_S)$] and $G_{ab}^{rs}(S_{ab},S^{rs};S,M_S)$ [$\Gamma_{ab}^{rs}(S_{ab},S^{rs};S,M_S)$], which generate OSA singlet ($S=0$) or triplet ($S=1$) monoexcited configurations and singlet ($S=0$), triplet ($S=1$) or quintet ($S=2$) doubly excited configurations, when acting on $|\Phi_0\rangle$, namely,

$$G_a^r=\Gamma_a^r\equiv G_a^r(0,0), \tag{27}$$

$$G_{ab}^{rs}(i)=N_{ab}^{rs}\Gamma_{ab}^{rs}(i)\equiv G_{ab}^{rs}(i,i;0,0),$$
$$N_{ab}^{rs}=[(1+\delta_{ab})(1+\delta^{rs})]^{-1/2}. \tag{28}$$

Here, N_{ab}^{rs} is the normalization factor that also relates $\langle rs|t_2|ab\rangle_i$ and $\langle rs|\tau_2|ab\rangle_i$ cluster amplitudes,

$$\langle rs|t_2|ab\rangle_i=N_{ab}^{rs}\langle rs|\tau_2|ab\rangle_i. \tag{29}$$

The general multiplet operators G_a^r [Γ_a^r] and G_{ab}^{rs} [Γ_{ab}^{rs}] are defined as follows [41]:

$$G_a^r(S,M_S)=\Gamma_a^r(S,M_S)=([S]/2)^{1/2}\sum_{\sigma_a,\sigma^r}\langle SM_S,\tfrac{1}{2}\sigma_a|\tfrac{1}{2}\sigma^r\rangle X_{r\sigma^r}^\dagger X_{a\sigma_a}, \tag{30}$$

$$G_{ab}^{rs}(S_{ab},S^{rs};S,M_S)\equiv N_{ab}^{rs}\Gamma_{ab}^{rs}(S_{ab},S^{rs};S,M_S)=N_{ab}^{rs}([S]/[S^{rs}])^{1/2}\sum_{\sigma_a,\sigma_b,\sigma^r,\sigma^s}\sum_{\sigma_{ab},\sigma^{rs}}\langle\tfrac{1}{2}\sigma_a,\tfrac{1}{2}\sigma_b|S_{ab}\sigma_{ab}\rangle\langle\tfrac{1}{2}\sigma^r,\tfrac{1}{2}\sigma^s|S^{rs}\sigma^{rs}\rangle$$
$$\times\langle SM_S,S_{ab}\sigma_{ab}|S^{rs}\sigma^{rs}\rangle X_{r\sigma^r}^\dagger X_{a\sigma_a}X_{s\sigma^s}^\dagger X_{b\sigma_b}, \tag{31}$$

where $\langle j_1m_1,j_2m_2|jm\rangle$ designates the standard SU(2) Clebsch-Gordan coefficient and $[X]\equiv 2X+1$ for any spin quantum number X. Notice that in Eq. (31) we reversed the order of coupling for holes in comparison to Ref. [41], so that the biexcited configurations

$$\left|\begin{matrix}r & s\\ a & b\end{matrix};SM_S\right\rangle_{S_{ab}}^{S^{rs}}=G_{ab}^{rs}(S_{ab},S^{rs};S,M_S)|\Phi_0\rangle \tag{32}$$

differ from those of Ref. [41] by the phase factor $(-1)^{S_{ab}+1}$.

With the above definitions, the OSA CCSD equations can be written in the following symbolic form [44]:

$$\sum_{n=0}^{3}\Lambda_n(G_r^a)=0, \tag{33}$$

$$\sum_{n=0}^{4} \Lambda_n[G_{rs}^{ab}(i)]=0 \quad (i=0,1), \tag{34}$$

where $G_r^a \equiv (G_a^r)^\dagger$ and $G_{rs}^{ab}(i) \equiv [G_{ab}^{rs}(i)]^\dagger$. The individual contributions

$$\Lambda_n(G_I^\dagger)=\langle \Phi_0|G_I^\dagger (H_N C_n')_C|\Phi_0\rangle \quad [G_I=G_a^r, G_{ab}^{rs}(i)], \tag{35}$$

are defined in terms of CI-like excitation operators C_n', $n=0-4$, where [cf. Eqs. (5)–(8)]

$$C_0'=1, \tag{36}$$

$$C_j'=C_j \quad (j=1,2), \tag{37}$$

$$C_3'=T_1T_2+\tfrac{1}{6}(T_1)^3, \tag{38}$$

$$C_4'=\tfrac{1}{2}(T_2)^2+\tfrac{1}{2}(T_1)^2T_2+\tfrac{1}{24}(T_1)^4. \tag{39}$$

Explicit expressions for $\Lambda_n(G_r^a)$, $n=0-3$, and $\Lambda_n[G_{rs}^{ab}(i)]$, $i=0,1$, $n=0-4$, in terms of cluster amplitudes $\langle r|\tau_1|a\rangle$ and $\langle rs|\tau_2|ab\rangle_i$ and one- and two-electron molecular integrals $\langle k|f|k'\rangle$ and $\langle kl||k'l'\rangle$ were given in Ref. [44]. Every term $\Lambda_n(G_r^a)$ and $\Lambda_n[G_{rs}^{ab}(i)]$ reduces to a sum of several diagrammatic contributions, which are evaluated using the diagrammatic approach based on the graphical methods of spin algebras [22,41–44]. For example, the $\frac{1}{2}(T_2)^2$ term of the OSA CCD theory, $\Lambda_4^{\mathrm{CCD}}[G_{rs}^{ab}(i)]$, splits into five contributions corresponding to five distinct Goldstone-Hugenholtz diagrams (see Fig. 1 of Ref. [57] or Fig. 4 of Ref. [22]),

$$\Lambda_4^{\mathrm{CCD}}[G_{rs}^{ab}(i)] \equiv \tfrac{1}{2}\langle \Phi_0|(H_N T_2^2)_C|\Phi_0\rangle = \sum_{k=1}^{5} \Lambda_4^{(k)}[G_{rs}^{ab}(i)], \tag{40}$$

where $\Lambda_4^{(k)}[G_{rs}^{ab}(i)]$ designates the contribution from the kth diagram. In the following, we label these diagrams in the same way as in Ref. [22] or [57].

As already mentioned, in degenerate cases we must go beyond the CCSD approximation and account for the T_3 and T_4 clusters. Unfortunately, CCSDT and CCSDTQ involve a large number of triply and quadruply excited cluster amplitudes and are computationally very demanding [cf. Eqs. (19)–(22)]. A spin-free formulation helps to reduce computational costs [20,21,27,28], but special precautions must be taken to eliminate linear dependencies among spin-free triexcited and tetraexcited cluster amplitudes [2], since otherwise CCSDT and CCSDTQ equations may become ill-conditioned and the iterative procedures used to solve them may diverge [28]. The above difficulty can be avoided by switching to the OSA formulation that employs the minimum number of amplitudes, but its implementation for the full CCSDT or CCSDTQ method is rather complex (cf. Ref. [43]). In any case, the standard CCSDT and CCSDTQ methods are computationally too demanding to be used for larger systems and, at least for the time being, they will remain most useful in benchmark calculations, particularly in cases where the exact FCI calculations are difficult to perform. This leaves room for approximate CC approaches of *nonstandard* type, which do not store or iterate T_3 and T_4 clusters. Another useful alternative is to employ the concept of multi-dimensional reference space and reduce the number of triples and quadruples rather than to approximate them as in nonstandard SRCC methods. Such procedures (the so-called SSCC formalism of Refs. [14], [31], and [35–37]) will not be discussed in this paper as they no longer represent pure SRCC approach.

B. Nonstandard approaches. Decoupling the CCSDTQ equations

We define the *nonstandard* CC methods as those SRCC approaches in which clusters higher than pair clusters, in particular T_3 and T_4, are no longer treated as independent variables whose values are determined simultaneously with T_1 and T_2 by solving CC equations. Instead, we estimate their values from some independent source or using MBPT arguments, and accordingly correct the standard CCSD equations (CCSDT equations if only T_4 is being approximated). In the following we concentrate on the corrections to the OSA CCSD equations of Ref. [44] [cf. Eqs. (33) and (34)].

Rewriting the first two equations of the complete CCSDTQ system, Eqs. (19) and (20), in the OSA form [when $G_{I_1}^{(1)}=G_a^r$ and $G_{I_2}^{(2)}=G_{ab}^{rs}(i)$], we obtain [cf. Eqs. (33) and (34)]

$$\sum_{n=0}^{3} \Lambda_n(G_r^a)+\Theta_3(G_r^a)=0, \tag{41}$$

$$\sum_{n=0}^{4} \Lambda_n[G_{rs}^{ab}(i)]+\Theta_3[G_{rs}^{ab}(i)]+\Theta_4[G_{rs}^{ab}(i)]+\Theta_{1,3}[G_{rs}^{ab}(i)] = 0 \quad (i=0,1), \tag{42}$$

where

$$\Theta_3(G_I^\dagger)=\langle \Phi_0|G_I^\dagger (H_N T_3)_C|\Phi_0\rangle \quad [G_I=G_a^r, G_{ab}^{rs}(i)], \tag{43}$$

$$\Theta_4[G_{rs}^{ab}(i)]=\langle \Phi_0|G_{rs}^{ab}(i)(H_N T_4)_C|\Phi_0\rangle, \tag{44}$$

$$\Theta_{1,3}[G_{rs}^{ab}(i)]=\langle \Phi_0|G_{rs}^{ab}(i)(H_N T_1 T_3)_C|\Phi_0\rangle \tag{45}$$

are the corrections to CCSD equations involving T_3 and T_4. Once T_3 and T_4 are available, we can calculate corrections Θ, Eqs. (43)–(45), and solve the resulting CCSD-like system, Eqs. (41) and (42), for T_1 and T_2 (cf. Ref. [62]). In particular, using the exact T_3 and T_4 amplitudes when calculating these corrections, the exact T_1 and T_2 clusters result, and thus the exact energy [cf. Eq. (17)]. Clearly, the exact T_3 and T_4 components are only available if we know the FCI wave function, so that in practical exploitations of this idea we must rely on approximations of T_3 and T_4 in order to decouple the CCSD-like system, Eqs. (41) and (42), from the rest of the CCSDTQ chain.

Basically, there are two options available to us. We can either use the MBPT analysis of CC equations to relate T_3 and T_4 clusters with their lower-order T_1 and T_2 counterparts, or utilize some readily available wave function of non-CC type to estimate T_3 and T_4 contributions. The former

approach is widely exploited and was briefly reviewed in the Introduction. For example, in the iterative CCSDT-1 or CCSDT-1a approaches of Ref. [15], the corrections to CCSD equations due to T_3 clusters, $\Theta_3(G_I^\dagger)$, Eq. (43), modify the linear T_2 terms by expressions involving $R_0^{(3)}V_N$, where $R_0^{(p)}$ designates the p-body part of the reduced resolvent,

$$R_0^{(p)}=\frac{Q^{(p)}}{-F_N}\equiv\frac{\Sigma_{I_p}|\Phi_{I_p}^{(p)}\rangle\langle\Phi_{I_p}^{(p)}|}{-F_N}. \tag{46}$$

This gives [22]

$$\Theta_3^{\text{CCSDT-1}}(G_I^\dagger)=\langle\Phi_0|G_I^\dagger V_N R_0^{(3)}V_N T_2|\Phi_0\rangle \quad [G_I=G_a^r,G_{ab}^{rs}(i)], \tag{47}$$

so that the linear term

$$\Lambda_{2,3}(G_I^\dagger)\equiv\langle\Phi_0|G_I^\dagger[V_N(T_2+T_3)]_C|\Phi_0\rangle =\langle\Phi_0|G_I^\dagger W_N T_2|\Phi_0\rangle \quad [G_I=G_a^r,G_{ab}^{rs}(i)], \tag{48}$$

where

$$W_N=V_N+V_N R_0^{(3)}V_N \tag{49}$$

represents an ''effective interaction'' operator, which accounts for T_3 components. In the noniterative CCSD[T] method we evaluate the triple-excitation contribution according to the formula that is reminiscent of the well-known MBPT(4) energy expression, namely,

$$\Delta E^{\text{T(CCSD)}}=\langle\Phi_0|(T_2^{\text{CCSD}})^\dagger V_N R_0^{(3)}V_N T_2^{\text{CCSD}}|\Phi_0\rangle, \tag{50}$$

where T_2^{CCSD} is the CCSD T_2 cluster component. The total CCSD[T] energy is defined as a sum

$$E^{\text{CCSD[T]}}=E^{\text{CCSD}}+\Delta E^{\text{T(CCSD)}}. \tag{51}$$

All such perturbative approaches provide useful information about T_3 and T_4 clusters at a relatively small cost when compared to CCSDT or CCSDTQ methods. However, these approaches are likely to fail in quasidegenerate situations for a number of reasons. When configurational quasidegeneracy becomes appreciable, both T_3 and T_4 contributions may be large and the assumption of their additivity as well as the MBPT arguments may no longer hold (cf. Refs. [23,24,31,40,50]). In severe cases of quasidegeneracy, such as those found in cyclic polyene PPP model, both the standard CCSD method and the iterative CCSDT-1 approach completely break down and become singular [23]. Thus, the CC(S)D amplitudes are no longer available to calculate energy corrections, Eq. (50), and another method of accounting for T_3 and T_4 clusters must be found.

An alternative to the MBPT arguments, which often no longer apply in quasidegenerate situations, is to exploit a suitable non-CC wave function as a source of information about the T_3 and T_4 clusters. By performing cluster analysis of such a wave function we are able, at least in principle, to evaluate approximate values of triples and quadruples and use them to calculate the required corrections Θ, Eqs. (43)–(45), in order to decouple Eqs. (41) and (42) from the rest of the CC chain.

Approaches of this kind constitute the second category of nonstandard methods, since they do not result from general CC theory by conventional truncation at a given excitation level. The main characteristic of these approaches, considered by Paldus, Čížek, and Takahashi [53], is the fact that the three- and four-body cluster components are determined *before* initiating the CC iterative procedure. Recall that in the above-mentioned perturbative CC approaches, the corrections due to T_3 and T_4 are calculated *during* or *after* the CC iterative procedure.

As may be expected, the effectiveness of nonstandard methods will strongly depend on the initial choice of the wave function used to evaluate T_3 and T_4 components. A compromise must be found between the accuracy and the cost of the calculated T_3 and/or T_4 amplitudes, since otherwise we could end up with an impractical method, which is inapplicable to larger systems.

It was suggested by Planelles and co-workers [54,61,62] that very good results may be obtained by extracting the T_3 and T_4 components from a VB wave function involving a small number of covalent (and, if necessary, ionic) structures that are chosen to reasonably describe a given quasidegenerate situation, for example, a given bond breaking or bond formation process. Another suggestion was made by Stolarczyk [72], who proposed to use the complete active space self-consistent field (CASSCF) wave function. This may have a number of advantages, since the CASSCF method with a proper choice of the active space correctly describes all quasidegenerate situations involving the dissociation of the system into open-shell fragments. Simultaneously, the CASSCF method uses orthogonal orbitals, which are much easier to handle than nonorthogonal orbitals of VB approaches. Finally, CASSCF wave functions are currently easily available thanks to a number of standard electronic structure packages, such as GAMESS [73], HONDO [74], GAUSSIAN 92 [75], or MOLCAS [76]. The only open problem with Stolarczyk's suggestion is the proposed computational strategy (even though no actual implementation nor explicit formalism was presented in Ref. [72]). He suggests using one of the CASSCF configurations (presumably, the dominant one) as a reference. In such a case, his formalism will represent an approximation to the SSCC theory developed earlier by Piecuch, Oliphant, and Adamowicz [14], in which a few internal (all-active) triexcited and tetraexcited cluster amplitudes are fixed to their CASSCF values instead of being iterated as suggested in Ref. [14] (in fact, SSCC calculations using CASSCF reference were performed in Ref. [36]). It might be worthwhile to contemplate another computational strategy, in which a transformation of the CASSCF wave function to the RHF molecular orbital (MO) basis is carried out prior to its cluster analysis. Clearly, this will lead to quite rich triexcitation and tetraexcitation manifolds even when small active space is used in CASSCF calculations. Both strategies are now investigated by us and the results will be presented elsewhere [77].

In fact, the aforementioned distinction between the CASSCF corrected SRCCSD theory using the RHF refer-

ence and its variant using the dominant CASSCF configuration as a reference is reminiscent, to some degree, of the distinction between the CCSD approach employing RHF orbitals, which we subsequently correct for T_4 components by analyzing the cluster structure of the PUHF wave function, and the standard spin-orbital CCSD approach using the UHF reference. No explicit T_4 contributions (relative to the UHF vacuum) are present in the latter case, whereas quite a rich T_4 manifold (relative to the RHF reference) is generated in the former case. The T_4-corrected SRCCSD theory, in which T_4 clusters are extracted from the PUHF wave function, is discussed next.

III. CLUSTER STRUCTURE OF THE PUHF WAVE FUNCTION

The UHF wave functions of the DODS (different orbitals for different spins) type are currently available even for large molecular systems, and it is well known that the UHF approach or its projected PUHF version correctly describe the dissociation of many molecular systems into the open-shell fragments. In the strongly correlated regime of the PPP cyclic polyene model, where the standard CCSD theory using the RHF reference breaks down [23,52], the PUHF method provides exact pair clusters, and thus the exact energy [56,78]. This indicates that the PUHF wave function may serve as a reliable source of information about the T_4 clusters.

Of course, instead of extracting T_4 cluster components from the PUHF wave function (CCSDQ′ approach), we can simply use the UHF solution as a reference in the spin-orbital CCSD theory (CCSD-UHF method). Although the usefulness of the latter approach lies primarily in its simplicity and generality, we find the CCSDQ′ procedure worth exploring for the following reasons. First of all, in the triplet unstable region of RHF [64,79,80], the UHF wave function is spin contaminated and the level of spin contamination may remain relatively high at the correlated CCSD-UHF level, particularly for systems involving multiple bond breaking, such as N_2 [47,81]. As a result, the transition between the triplet stable and triplet unstable regions may manifest itself by a nonanalytic behavior of CC and MBPT PES′s, in spite of relatively good CCSD-UHF results in the bond-breaking region [47,81]. With T_4 cluster components extracted from the PUHF wave function, we should be able to describe bond-breaking phenomena without introducing the spin contamination of the CCSD-UHF approach. Second, CCSD-UHF uses twice as many (spin) orbitals as CCSD-RHF or CCSDQ′, and does not allow for a number of simplifications in the CC formalism that are normally possible due to the presence of spin and spatial symmetries of the system (UHF wave functions have not only broken spin symmetry, but often break the spatial symmetry of the Hamiltonian as well). Consequently, the CCSD-UHF method is computationally more demanding than OSA CCSD-RHF, or the T_4-corrected CCSDQ′ method.

In fact, projection of the closed-shell ground-state UHF wave function onto the singlet subspace automatically projects out components that are not totally symmetric with respect to the spatial symmetry group of the Hamiltonian. Thus, if we use the lowest symmetry-adapted RHF solution as a CC reference (even though there may exist broken-symmmetry RHF solutions with lower energy in a singlet unstable region [64,79], we are not going to use them as $|\Phi_0\rangle$; cf., e.g., Ref. [82]), the T_4 components resulting from the cluster analysis of the PUHF wave function as well as the corresponding corrections $\Theta_4[G^{ab}_{rs}(i)]$, Eq. (44), will be automatically symmetry adapted. We will thus be able to fully exploit both spin and point-group symmetries in T_4-corrected CCSDQ′ calculations (cf. Sec. V), making the CCSDQ′ method no more expensive than the standard OSA CCSD approach.

Although we employ PUHF wave functions throughout this paper, we wish to emphasize that the same procedure would apply to the projected Hartree-Fock (PHF) methods [83], such as the alternant molecular orbital (AMO) approach [84]. In both cases, the broken-symmetry single-determinantal wave function of the DODS type and variational principle are employed. However, in the PHF approaches, the single-determinantal wave function is first projected onto the appropriate subspace of the spin space (singlet for the ground-state closed-shell problem) before the actual orbital optimization is carried out. The PUHF wave function exploited in this paper is obtained by first performing the orbital optimization using the DODS wave function (UHF approach) followed by the projection of the resulting UHF solution onto the appropriate spin subspace. This distinction is immaterial for the cluster analysis performed below, and the formal results presented in this paper would be the same for any broken-symmetry solution of DODS or even RHF type (including UHF, PHF, and AMO wave functions or closed-shell solutions found for singlet unstable [64,79] RHF cases; for a general classification of various types of UHF solutions, see Refs. [82] and [85]). However, in actual implementation of the CCSDQ′ method, we use the ground-state UHF or PUHF wave function as a source of T_4 cluster components (cf. Sec. V).

To analyze the cluster structure of a single-determinantal DODS (UHF, PHF, AMO) or broken space symmetry RHF wave functions, it is useful to recall Thouless′ theorem [63,64], which states that any single-determinantal wave function $|\Phi^X_0\rangle$, having a nonzero overlap with the reference configuration $|\Phi_0\rangle$, can be written in the form

$$|\Phi^X_0\rangle = e^{U^X_1}|\Phi_0\rangle, \tag{52}$$

where U^X_1 is a monoexcitation operator. In our case, $|\Phi^X_0\rangle$ represents the ground-state UHF, PHF, or AMO wave function ($X=$ UHF, PHF, or AMO), or broken-symmetry RHF solution, which we will use as a source of T_4 components, and $|\Phi_0\rangle$ is the standard closed-shell, symmetry-adapted reference configuration (usually, the ground-state RHF solution, the same one as used later in CC calculations). Since we assume $|\Phi^X_0\rangle$ and $|\Phi_0\rangle$ to be eigenfunctions of S_z with $M_S=0$, the operator U^X_1 takes the form

$$U^X_1 = \sum_{a,r}\sum_{\sigma} \langle r\sigma|u^{(\sigma)}_1|a\sigma\rangle X^\dagger_{r\sigma}X_{a\sigma} = \langle r\alpha|u^{(\alpha)}_1|a\alpha\rangle X^\dagger_{r\alpha}X_{a\alpha} + \langle r\beta|u^{(\beta)}_1|a\beta\rangle X^\dagger_{r\beta}X_{a\beta}, \tag{53}$$

where $\alpha=|\frac{1}{2},\frac{1}{2}\rangle$ ($\beta=|\frac{1}{2},-\frac{1}{2}\rangle$) designates the usual spin-up (spin-down) spin function. We can thus express U_1^X in terms of the OSA singlet ($S=0$) and triplet ($S=1$) monoexcitation operators $G_a^r(S,0)$, Eq. (30), obtaining

$$U_1^X = U_1^X(0,0) + U_1^X(1,0), \tag{54}$$

where

$$U_1^X(S,0) = \sum_{a,r} \langle r|u_1|a\rangle_S \; G_a^r(S,0) \quad (S=0,1) \tag{55}$$

designate the singlet ($S=0$) and triplet ($S=1$) components of U_1^X and $\langle r|u_1|a\rangle_S$ the corresponding amplitudes. Since the operators $U_1^X(0,0)$ and $U_1^X(1,0)$ mutually commute, we can write

$$|\Phi_0^X\rangle = e^{U_1^X(0,0)} e^{U_1^X(1,0)} |\Phi_0\rangle. \tag{56}$$

We can also write

$$U_1^X(S,0) = \sum_{a,r} \langle r||a\rangle_S \, [X_{r\beta}^\dagger X_{a\beta} + (-1)^S X_{r\alpha}^\dagger X_{a\alpha}], \tag{57}$$

where

$$\langle r||a\rangle_S = 2^{-1/2}\langle r|u_1|a\rangle_S = \tfrac{1}{2}[\langle r\beta|u_1^{(\beta)}|a\beta\rangle + (-1)^S\langle r\alpha|u_1^{(\alpha)}|a\alpha\rangle]. \tag{58}$$

Clearly, the numerical values of the OSA amplitudes $\langle r||a\rangle_S$ or $\langle r|u_1|a\rangle_S$ depend on the specific form of $|\Phi_0^X\rangle$ employed.

Prior to cluster analyzing $|\Phi_0^X\rangle$, we project out higher spin multiplets (triplets, quintets, etc.) that are irrelevant for the ground-state singlet problem. This must be done with care, since some terms contain both the singlet and triplet components of U_1^X. The role of these components is discussed next.

The initial formulation of CCDQ′ and ACCD′ methods [53] neglected the singlet component $U_1^X(0,0)$, which is absent in the UHF solution for PPP cyclic polyene models that were examined in our earlier study of ACCD′ theory [52]. As will be seen below, it is the triplet component $U_1^X(1,0)$ that is responsible for the energy lowering whenever the RHF solution is triplet unstable, so it was reasonable to assume that $U_1^X(0,0)=0$. Even in other minimum basis set models, or models having a sufficiently high symmetry, the assumption $U_1^X(0,0)=0$ is justified (cf. Sec. VI). In general, however, the $U_1^X(0,0)$ component does not vanish and must be considered together with its triplet counterpart. This is the case in most *ab initio* applications. We thus consider both components $U_1^X(S,0)$ ($S=0,1$) in the cluster analysis of $|\Phi_0^X\rangle$.

A. A simple example

We illustrate the role of both $U_1^X(0,0)$ and $U_1^X(1,0)$ components for a DZ model of the hydrogen molecule (eliminating the $2p$ polarization function from the DZP basis set of Ref. [59]). The resulting two-electron–four-orbital model is rich enough to provide information about the relative importance of $U_1^X(S,0)$ components, yet simple enough to enable a graphical visualization of various components of the UHF wave function. In the simpler MBS H_2 model, the singlet component $U_1^X(0,0)$ vanishes.

Let us designate the four RHF molecular orbitals (MO's) of our DZ H_2 model by ϕ_i ($\phi_1=1\sigma_g, \phi_2=1\sigma_u, \phi_3=2\sigma_g, \phi_4=2\sigma_u$), and their UHF counterparts corresponding to spin-up and spin-down spin functions by $\phi_{i,\alpha}^{\rm UHF}$ and $\phi_{i,\beta}^{\rm UHF}$, respectively ($i=1-4$). The coefficients $c_i^{(\sigma)}$ relating the occupied UHF MO's $\phi_{1,\sigma}^{\rm UHF}$ ($\sigma=\alpha,\beta$) with RHF MO's ϕ_i,

$$\phi_{1,\sigma}^{\rm UHF} = \sum_{i=1}^{4} c_i^{(\sigma)} \phi_i, \tag{59}$$

then satisfy the relations

$$c_i^{(\alpha)} = c_i^{(\beta)} \equiv c_i \quad (i=1,3), \tag{60}$$

$$c_j^{(\alpha)} = -c_j^{(\beta)} \equiv c_j \quad (j=2,4), \tag{61}$$

or, equivalently,

$$\phi_{1,\alpha}^{\rm UHF} = c_1\phi_1 + c_2\phi_2 + c_3\phi_3 + c_4\phi_4, \tag{62}$$

$$\phi_{1,\beta}^{\rm UHF} = c_1\phi_1 - c_2\phi_2 + c_3\phi_3 - c_4\phi_4. \tag{63}$$

As a consequence, the singlet and triplet components of the monoexcitation operator $U_1^{\rm UHF}$, relating the renormalized ground-state UHF solution $|\Phi_0^{\rm UHF}\rangle = c_1^{-2}|\phi_{1,\alpha}^{\rm UHF}\alpha\phi_{1,\beta}^{\rm UHF}\beta|$ with the RHF configuration $|\Phi_0\rangle = |\phi_1\alpha\phi_1\beta|$ via Eq. (56), assume a particularly simple form, namely,

$$U_1^{\rm UHF}(0,0) = \langle 3|u_1|1\rangle_0 \; G_1^3(0,0), \tag{64}$$

$$U_1^{\rm UHF}(1,0) = \langle 2|u_1|1\rangle_1 \; G_1^2(1,0) + \langle 4|u_1|1\rangle_1 \; G_1^4(1,0), \tag{65}$$

where

$$\langle 3|u_1|1\rangle_0 = \sqrt{2}c_3/c_1, \tag{66}$$

$$\langle 2|u_1|1\rangle_1 = -\sqrt{2}c_2/c_1, \tag{67}$$

$$\langle 4|u_1|1\rangle_1 = -\sqrt{2}c_4/c_1. \tag{68}$$

Notice that the operator $U_1^{\rm UHF}(0,0)$ is totally symmetric (Σ_g), while its triplet analog $U_1^{\rm UHF}(1,0)$ transforms according to the Σ_u representation of $D_{\infty h}$. This indicates that the decomposition of $U_1^{\rm UHF}$ into spin-adapted singlet and triplet components is equivalent to a splitting of the operator $U_1^{\rm UHF}$ into space-symmetry adapted and broken-symmetry components. As a result, the exponential operators of Eq. (56) that are associated with the individual cluster components $U_1^{\rm UHF}(0,0)$ and $U_1^{\rm UHF}(1,0)$ take the form

$$e^{U_1^{\rm UHF}(0,0)} = 1 + U_1^{\rm UHF}(0,0) + \tfrac{1}{2}[U_1^{\rm UHF}(0,0)]^2 = 1 + \langle 3|u_1|1\rangle_0 \; G_1^3 + \tfrac{1}{2}(\langle 3|u_1|1\rangle_0)^2 \; G_{11}^{33}(0), \tag{69}$$

and

$$e^{U_1^{\mathrm{UHF}}(1,0)} = 1 + U_1^{\mathrm{UHF}}(1,0) + \tfrac{1}{2}[U_1^{\mathrm{UHF}}(1,0)]^2$$
$$= 1 + \langle 2|u_1|1\rangle_1\, G_1^2(1,0) + \langle 4|u_1|1\rangle_1\, G_1^4(1,0) - \tfrac{1}{2}(\langle 2|u_1|1\rangle_1)^2\, G_{11}^{22}(0) - \tfrac{1}{2}(\langle 4|u_1|1\rangle_1)^2\, G_{11}^{44}(0)$$
$$- \frac{1}{\sqrt{2}}\langle 2|u_1|1\rangle_1\, \langle 4|u_1|1\rangle_1\, G_{11}^{24}(0). \tag{70}$$

Equations (69) and (70) enable us to analyze the cluster structure of the UHF solution $|\Phi_0^{\mathrm{UHF}}\rangle$, which now becomes

$$|\Phi_0^{\mathrm{UHF}}\rangle = e^{U_1^{\mathrm{UHF}}(0,0)} e^{U_1^{\mathrm{UHF}}(1,0)} |\Phi_0\rangle = [\Omega(^1\Sigma_g^+) + \Omega(^3\Sigma_u^+)]|\Phi_0\rangle, \tag{71}$$

where the operators $\Omega(^1\Sigma_g^+)$ and $\Omega(^3\Sigma_u^+)$ acting on $|\Phi_0\rangle$ generate, respectively, the singlet and triplet components of $|\Phi_0^{\mathrm{UHF}}\rangle$,

$$\Omega(^1\Sigma_g^+)|\Phi_0\rangle \equiv P_{S=0}|\Phi_0^{\mathrm{UHF}}\rangle \equiv |\Psi_0^{\mathrm{PUHF}}\rangle, \tag{72}$$

$$\Omega(^3\Sigma_u^+)|\Phi_0\rangle \equiv P_{S=1}|\Phi_0^{\mathrm{UHF}}\rangle, \tag{73}$$

with $P_{S=0,1}$ representing the corresponding projection operators. In particular, we find that

$$\Omega(^1\Sigma_g^+) = 1 + \langle 3|u_1|1\rangle_0\, G_1^3 + \tfrac{1}{2}(\langle 3|u_1|1\rangle_0)^2\, G_{11}^{33}(0) - \tfrac{1}{2}(\langle 2|u_1|1\rangle_1)^2\, G_{11}^{22}(0) - \tfrac{1}{2}(\langle 4|u_1|1\rangle_1)^2\, G_{11}^{44}(0)$$
$$- \frac{1}{\sqrt{2}}\langle 2|u_1|1\rangle_1\, \langle 4|u_1|1\rangle_1\, G_{11}^{24}(0), \tag{74}$$

$$\Omega(^3\Sigma_u^+) = \langle 2|u_1|1\rangle_1\, G_1^2(1,0) + \langle 4|u_1|1\rangle_1\, G_1^4(1,0) - \frac{1}{\sqrt{2}}\langle 2|u_1|1\rangle_1\, \langle 3|u_1|1\rangle_0\, G_{11}^{23}(0,1;1,0)$$
$$+ \frac{1}{\sqrt{2}}\langle 3|u_1|1\rangle_0\, \langle 4|u_1|1\rangle_1\, G_{11}^{34}(0,1;1,0). \tag{75}$$

To prove Eqs. (69)–(75), we used general relationships (cf. Refs. [41] and [53])

$$G_a^r(0,0)G_b^s(0,0) = \tfrac{1}{2}\Gamma_{ab}^{rs}(0,0;0,0) + (\sqrt{3}/2)\Gamma_{ab}^{rs}(1,1;0,0), \tag{76}$$

$$G_a^r(1,0)G_b^s(0,0) = (1/\sqrt{2})\Gamma_{ab}^{rs}(1,1;1,0) + \tfrac{1}{2}\Gamma_{ab}^{rs}(1,0;1,0) - \tfrac{1}{2}\Gamma_{ab}^{rs}(0,1;1,0), \tag{77}$$

$$G_a^r(1,0)G_b^s(1,0) = -\tfrac{1}{2}\Gamma_{ab}^{rs}(0,0;0,0) + [1/(2\sqrt{3})]\Gamma_{ab}^{rs}(1,1;0,0) + \sqrt{2/3}\Gamma_{ab}^{rs}(1,1;2,0), \tag{78}$$

which follow from definitions of the OSA excitation operators (30) and (31). Notice that the coefficients standing at various excitation operators in Eqs. (74) and (75), which in the exact (FCI) limit would be independent variables, are no longer independent and reflect the particular cluster structure of the UHF wave function, which in this case is fully described by only three independent coefficients $\langle 3|u_1|1\rangle_0$, $\langle 2|u_1|1\rangle_1$, and $\langle 4|u_1|1\rangle_1$ or [cf. Eqs. (66)–(68)] c_2, c_3, and c_4 (assuming the UHF orbitals to be normalized, i.e., $c_1 = \sqrt{1 - c_2^2 - c_3^2 - c_4^2}$). This simple three-parameter description enables us to analyze the relative importance of singlet and triplet components $U_1^{\mathrm{UHF}}(0,0)$ and $U_1^{\mathrm{UHF}}(1,0)$ in detail.

To carry out this analysis, we used the symbolic manipulation language MAPLE [65] in conjunction with a simple interface (written by ourselves in FORTRAN), which allowed us to access molecular integrals generated by GAMESS [73], so that they could be read, if necessary, into a MAPLE session. MAPLE formulas describing various energies, such as the UHF energy

$$E^{\mathrm{UHF}} = \langle \Phi_0^{\mathrm{UHF}}|H|\Phi_0^{\mathrm{UHF}}\rangle / \langle \Phi_0^{\mathrm{UHF}}|\Phi_0^{\mathrm{UHF}}\rangle, \tag{79}$$

its PUHF counterpart

$$E^{\mathrm{PUHF}} = \langle \Psi_0^{\mathrm{PUHF}}|H|\Psi_0^{\mathrm{PUHF}}\rangle / \langle \Psi_0^{\mathrm{PUHF}}|\Psi_0^{\mathrm{PUHF}}\rangle = \langle \Phi_0|[\Omega(^1\Sigma_g^+)]^\dagger H \Omega(^1\Sigma_g^+)|\Phi_0\rangle / \langle \Phi_0|[\Omega(^1\Sigma_g^+)]^\dagger \Omega(^1\Sigma_g^+)|\Phi_0\rangle, \tag{80}$$

or energies associated with individual cluster components $U_1^{\mathrm{UHF}}(S,0)$, e.g.,

$$E[U_1^{\mathrm{UHF}}(S,0)] = \langle \Phi_0|e^{[U_1^{\mathrm{UHF}}(S,0)]^\dagger} H e^{U_1^{\mathrm{UHF}}(S,0)}|\Phi_0\rangle / \langle \Phi_0|e^{[U_1^{\mathrm{UHF}}(S,0)]^\dagger} e^{U_1^{\mathrm{UHF}}(S,0)}|\Phi_0\rangle, \tag{81}$$

were calculated as CI expectation values $E=\Sigma_{I,J}C_I^* H_{IJ}C_J/\Sigma_I|C_I|^2$ ($H_{IJ}=\langle\Phi_I|H|\Phi_J\rangle$), with CI coefficients C_I expressed in terms of UHF MO coefficients c_2, c_3, and c_4 via Eqs. (64)–(75). This was possible thanks to the small dimension of the configuration spaces involved (6 for the singlet and 4 for the triplet). The matrix elements H_{IJ} between the OSA configurations were programmed using the formulas of Ref. [41]. The UHF energy formula was also programmed as a standard expression in terms of one-electron density matrices, with the UHF orbitals expressed as a linear combination of ground-state RHF MO's (first generated by GAMESS), Eqs. (62) and (63).

With the help of MAPLE we were able to explore the analytical properties of the UHF energy surface E^{UHF}, Eq. (79), regarded as a function of three variables $c_i\in(-1,1)$, $i=2,3,4$, in the region where the RHF solution is triplet unstable. For the DZ H_2 model with the internuclear separation $R=3.0$ a.u. (the RHF solution becomes triplet unstable for $R>2.25$ a.u.), we found that $E^{\mathrm{UHF}}(c_2,c_3,c_4)$ has a global minimum of -1.015761 hartree at two local minima $(c_2,c_3,c_4)=(0.467238,0.020604,-0.038059)$ and $(c_2,c_3,c_4)=(-0.467238,0.020604,0.038059)$ [assuming the phase convention in which c_1 is a positive square root of $(1-c_2^2-c_3^2-c_4^2)$], and a saddle point of $-0.983\,418$ hartree at $(c_2,c_3,c_4)=(0,0,0)$. Clearly, the global minimum of $E^{\mathrm{UHF}}(c_2,c_3,c_4)$ represents the ground-state UHF energy, whereas the saddle point $(c_2,c_3,c_4)=(0,0,0)$ corresponds to the ground-state RHF energy, which we independently confirmed by performing the UHF and RHF calculations using GAMESS. Notice that the UHF solution mixes the orbitals belonging to different irreducible representations of $D_{\infty h}$, so that the UHF wave function represents a broken-symmetry solution. If we restrict to symmetry-adapted solutions, i.e., if we vary only c_3 and set $c_2=c_4=0$, the RHF saddle point becomes a minimum. The minima on the $E^{\mathrm{UHF}}(c_2,c_3,c_4)$ surface are depicted in Figs. 1(a) and (b), for c_3 fixed to its optimum value of 0.020604. The presence of two minima reflects the invariance under a spin-flip operation, which in our parametrization implies that $c_{2(4)}\rightarrow -c_{2(4)}$ and $c_{1(3)}\rightarrow c_{1(3)}$, or $U_1^{\mathrm{UHF}}(S,0)\rightarrow(-1)^S U_1^{\mathrm{UHF}}(S,0)$ ($S=0,1$).

The important result is that at both E^{UHF} minima the coefficient c_3, defining the singlet component $U_1^{\mathrm{UHF}}(0,0)$, does not vanish. This is clearly illustrated by Fig. 1(c), where we plotted the UHF energy for the DZ H_2 model with $R=3.0$ a.u. as a function of c_3 for two different choices of the parameters c_2 and c_4. The first choice, namely, $(c_2,c_4)=(0.467238,-0.038059)$, corresponding to one of the minima on the E^{UHF} surface, clearly indicates that the ground-state UHF wave function is characterized by the nonzero value of c_3: The function $E^{\mathrm{UHF}}(0.467238,c_3,-0.038059)$ has a minimum at $c_3=0.020604$. The second choice, namely, $(c_2,c_4)=(0,0)$, shows that by eliminating the triplet component $U_1^{\mathrm{UHF}}(1,0)$, we only obtain a single minimum at $c_3=0$, which describes the symmetry-adapted RHF solution.

In order to see how the singlet and triplet components of U_1^{UHF} affect the UHF energy at various internuclear separations R, we plotted in Fig. 2 several potential energy curves

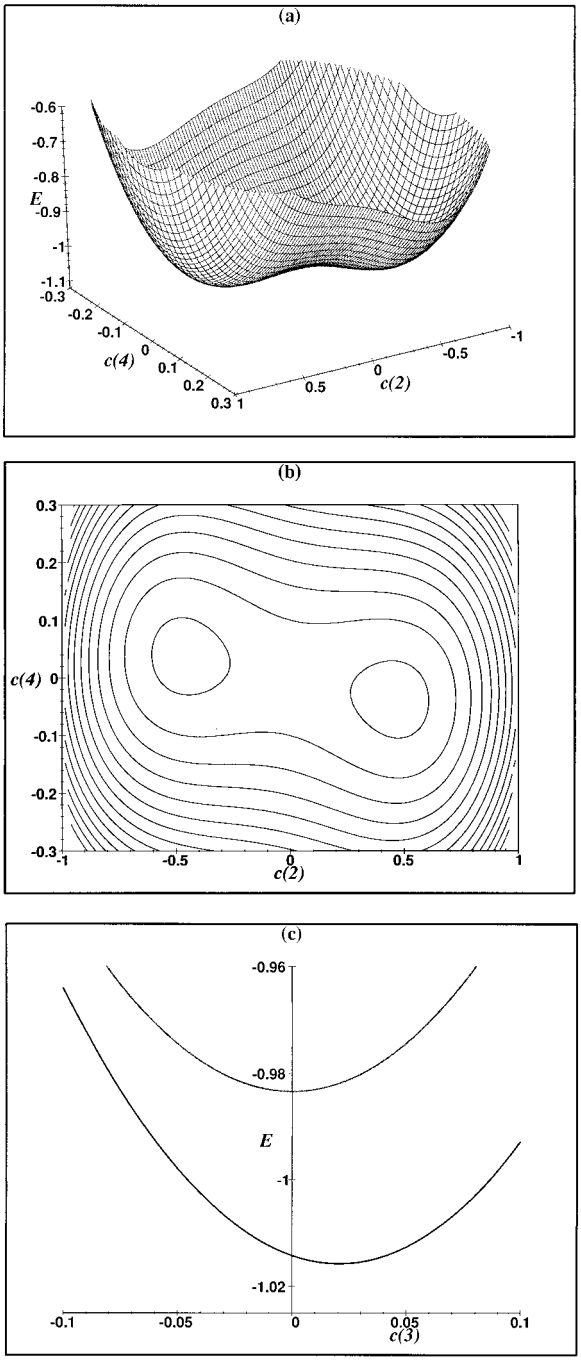

FIG. 1. Energy hypersurface $E^{\mathrm{UHF}}(c_2,c_3,c_4)$ (in hartree) for the DZ H_2 model with the internuclear separation $R=3.0$ a.u. (a) and (b) show the cross sections corresponding to the optimum value of c_3 for the UHF energy minimum, i.e., $E^{\mathrm{UHF}}(c_2,0.020604,c_4)$, while (c) shows the function $E^{\mathrm{UHF}}(0.467238,\ c_3,-0.038059)$ obtained from $E^{\mathrm{UHF}}(c_2,c_3,c_4)$ by fixing c_2 and c_4 to their optimum values at one of the two minima on the $E^{\mathrm{UHF}}(c_2,c_3,c_4)$ hypersurface that are apparent in cross sections (a) and (b) (see the text for details).

considering or ignoring the $U_1^{\mathrm{UHF}}(0,0)$ and $U_1^{\mathrm{UHF}}(1,0)$ contributions. In particular, we plotted the energies $E[U_1^{\mathrm{UHF}}(S,0)]$ ($S=0,1$), Eq. (81), which are associated with the wave functions $e^{U_1^{\mathrm{UHF}}(S,0)}|\Phi_0\rangle$, $S=0$ or 1, and their ap-

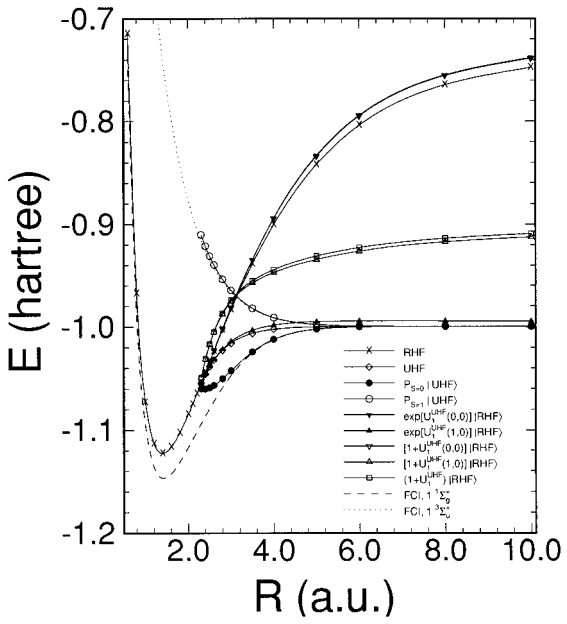

FIG. 2. Various potential energy curves for the DZ H_2 model obtained with RHF and various UHF wave functions involving or neglecting $U_1^{\mathrm{UHF}}(0,0)$ and $U_1^{\mathrm{UHF}}(1,0)$ contributions. FCI potential energy curves describing the lowest ${}^1\Sigma_g^+$ and ${}^3\Sigma_u^+$ states are shown for a comparison.

proximate versions obtained by retaining only the linear term in $U_1^{\mathrm{UHF}}(S,0)$. We find (see Fig. 2) that singlet and triplet components of U_1^{UHF} change the RHF energy in opposite directions. The singlet component $U_1^{\mathrm{UHF}}(0,0)$ raises the RHF energy, which is a consequence of the fact that the RHF solution is singlet stable, so that no further energy lowering can be achieved by the action of the totally symmetric singlet operator $e^{U_1^{\mathrm{UHF}}(0,0)}$. However, $U_1^{\mathrm{UHF}}(1,0)$ lowers the energy. In fact, we obtain quite a substantial energy lowering relative to the RHF energy when considering only linear terms in $U_1^{\mathrm{UHF}}(1,0)$ (i.e., using the wave function $[1+U_1^{\mathrm{UHF}}(1,0)]|\Phi_0\rangle$). Including the nonlinear terms as well, we obtain the energy curve $E[U_1^{\mathrm{UHF}}(1,0)]$, Eq. (81), which is very close to the UHF curve E^{UHF}. It is interesting to observe, however, that without the singlet component $U_1^{\mathrm{UHF}}(0,0)$, the energy curve $E[U_1^{\mathrm{UHF}}(1,0)]$ lies invariably above the UHF energy curve. Thus, the singlet and triplet components of U_1^{UHF} have a highly nonadditive character. Although they change the energy in opposite directions when considered separately, their simultaneous presence invariably lowers the energy. We thus need both components $U_1^{\mathrm{UHF}}(S,0)$, $S=0$ and 1, to transform the RHF wave function into the ground-state UHF solution.

Another interesting feature of these solutions is illustrated in Fig. 2. Although the UHF wave function properly describes the dissociation into the open-shell fragments (H atoms in ${}^2S$ states), the UHF energy curve has an incorrect shape in the intermediate region of R. In the vicinity of the triplet instability onset ($R=R_c=2.25$ a.u.), the UHF energy curve strongly deviates from the exact (FCI) curve describing the ${}^1\Sigma_g^+$ ground state, and for $R>R_c$, the UHF energy approximates the arithmetic average of the FCI energies associated with the lowest ${}^1\Sigma_g^+$ and ${}^3\Sigma_u^+$ states, $\frac{1}{2}[E^{\mathrm{FCI}}({}^1\Sigma_g^+)+E^{\mathrm{FCI}}({}^3\Sigma_u^+)]$, rather than the energy $E^{\mathrm{FCI}}({}^1\Sigma_g^+)$ itself, reflecting the presence of both ${}^1\Sigma_g^+$ and ${}^3\Sigma_u^+$ components in the UHF wave function. By projecting the desired ${}^1\Sigma_g^+$ component out of the UHF wave function [cf. Eqs. (72) and (80)] we obtain the energy curve that almost perfectly matches the exact FCI curve $E^{\mathrm{FCI}}({}^1\Sigma_g^+)$ (see Fig. 2). This indicates that the UHF wave function carries useful information about the lowest ${}^1\Sigma_g^+$ state, which can be retrieved by a suitable projection. In fact, in the triplet unstable region, the UHF wave function contains a fair amount of information about the lowest ${}^3\Sigma_u^+$ state (see the $P_{S=1}|\mathrm{UHF}\rangle$ curve in Fig. 2). This information can be retrieved by a suitable projection onto the triplet subspace [cf. Eq. (73)].

For larger many-electron systems, the spin contamination of the UHF wave function can be even more substantial, involving a number of higher multiplets. In general, it is laborious to project out the desired multiplets. Moreover, we cannot expect a simple UHF solution (or any broken-symmetry single-determinantal wave function) to contain complete information about the states involved due to an apparent lack of generality of the UHF wave function. On the other hand, we do not need all the information contained in the UHF solution in order to correct the closed-shell CCSD method in cases where it breaks. The CCSD method contains the most important pair components of the correlated wave function, so that we only have to estimate the missing connected cluster components, such as T_3 and T_4, to extend its applicability to quasidegenerate situations. This requires knowledge of the cluster structure of the single-determinantal, broken-symmetry solutions, such as UHF. We analyze this cluster structure next.

B. The general case

The above example of the DZ H_2 model illustrates that in general *ab initio* situations $U_1^X(0,0)$ does not vanish. In fact, we were able to confirm this observation in a number of other systems, such as various diatomics and triatomics, by using our program, which analyzes the structure of UHF solutions and computes the components $U_1^{\mathrm{UHF}}(0,0)$ and $U_1^{\mathrm{UHF}}(1,0)$ from the knowledge of UHF and RHF orbitals (for a brief description of this program, see Sec. V). It is interesting to observe that as long as $|\Phi_0\rangle$ represents the lowest symmetry-adapted (totally symmetric) RHF configuration, the corresponding $U_1^{\mathrm{UHF}}(0,0)$ component is totally symmetric as well, while $U_1^{\mathrm{UHF}}(1,0)$ does not contain the totally symmetric component. Realizing that in general *ab initio* situations both singlet and triplet components of U_1^X must be included in Eq. (52), we can write [cf. Eq. (56)]

$$P_{S=0}|\Phi_0^X\rangle \equiv P_{S=0}e^{U_1^X(0,0)}e^{U_1^X(1,0)}|\Phi_0\rangle = e^{U_1^X(0,0)}P_{S=0}e^{U_1^X(1,0)}|\Phi_0\rangle, \tag{82}$$

where we used the fact that $e^{U_1^X(0,0)}$ commutes with the projection operator $P_{S=0}$, as it contains only singlet components $(1/k!)[U_1^X(0,0)]^k$. Simultaneously, the projected $|\Phi_0^X\rangle$ wave function can be given the following form:

$$P_{S=0}|\Phi_0^X\rangle=(1+C^X)|\Phi_0\rangle\equiv e^K|\Phi_0\rangle, \tag{83}$$

where $C^X=\Sigma_{j=1}^N C_j^X$ is the corresponding CI excitation operator relative to $|\Phi_0\rangle$ [cf. Eq. (4)] and $K=\ln(1+C^X)=\Sigma_{j=1}^N K_j$ defines the cluster structure of the projected broken-symmetry solution, which is to be used to estimate T_3 and T_4. Comparison of Eqs. (82) and (83) suggests that the singlet component $U_1^X(0,0)$, albeit nonzero, cannot be engaged in forming the connected cluster components K_j with $j>1$. Let us analyze this fact and its possible implications for the CCSDQ′ formalism in detail.

If we apply the general relationship between the CI and CC excitation operators given by Eqs. (5)–(8) to many-body components of C^X and K, and compare the resulting relations with Eq. (82), we obtain

$$C_1^X=K_1=U_1^X(0,0), \tag{84}$$

$$C_2^X=K_2+\tfrac{1}{2}(K_1)^2=\tfrac{1}{2}[U_1^X(0,0)]^2+\tfrac{1}{2}P_{S=0}[U_1^X(1,0)]^2, \tag{85}$$

$$C_3^X=K_3+K_1K_2+\tfrac{1}{6}(K_1)^3=\tfrac{1}{6}[U_1^X(0,0)]^3 + \tfrac{1}{2}U_1^X(0,0)P_{S=0}[U_1^X(1,0)]^2, \tag{86}$$

$$C_4^X=K_4+\tfrac{1}{2}(K_2)^2+K_1K_3+\tfrac{1}{2}(K_1)^2K_2+\tfrac{1}{24}(K_1)^4 = \tfrac{1}{24}[U_1^X(0,0)]^4+\tfrac{1}{4}[U_1^X(0,0)]^2P_{S=0}[U_1^X(1,0)]^2 + \tfrac{1}{24}P_{S=0}[U_1^X(1,0)]^4. \tag{87}$$

The above system of equations can be easily solved for cluster components K_j, $j=1-4$. This allows us to write the following equations:

$$K_1=U_1^X(0,0), \tag{88}$$

$$K_2=\tfrac{1}{2}P_{S=0}[U_1^X(1,0)]^2, \tag{89}$$

$$K_3=0, \tag{90}$$

$$K_4=\tfrac{1}{24}P_{S=0}[U_1^X(1,0)]^4-\tfrac{1}{2}(K_2)^2. \tag{91}$$

We can see that the monoexcited cluster component K_1 is given by the singlet component $U_1^X(0,0)$, while higher excited components K_j $(j>1)$ are formed by powers of $U_1^X(1,0)$. Consequently, with the exception of monoexcited contribution K_1, all components K_j excited an odd number of times vanish. This becomes clear when we rewrite Eq. (82) as

$$P_{S=0}|\Phi_0^X\rangle=e^{K_1}P_{S=0}e^{U_1^X(1,0)}|\Phi_0\rangle, \tag{92}$$

and realize that odd (even) powers of $U_1^X(1,0)$ give the multiplets $|S,0\rangle$ with odd (even) values of S [cf., e.g., Eq. (78)], so that contributions to $e^{U_1^X(1,0)}$ excited an odd number of times are annihilated by the singlet projection $P_{S=0}$ and

$$P_{S=0}e^{U_1^X(1,0)}|\Phi_0\rangle=e^{K_2+K_4+\cdots}|\Phi_0\rangle. \tag{93}$$

In particular, no triexcited cluster component K_3 is present in the projected wave function $P_{S=0}|\Phi_0^X\rangle$.

Equations (88)–(91) are essential for the formulation of the CCSDQ′ approach. They show that no estimate of connected triexcited clusters can be obtained by analyzing the cluster structure of broken-symmetry, single-determinantal states, such as UHF. However, the projected UHF solution carries information about the connected quadruply excited clusters T_4, so that we can use the corresponding cluster components K_4, Eq. (91), as a substitute for true T_4 contributions in T_4-corrected CCSD equations, Eqs. (41) and (42). We discuss the resulting OSA CCSDQ′ approach in the next section.

IV. APPROXIMATE ACCOUNT OF T_4 CLUSTERS BY CCSDQ′ METHOD

We now describe basic equations of the PUHF-corrected CCSD formalism (referred to as the CCSDQ′ method), in which the T_4 components are estimated by cluster analyzing PUHF-type solutions. We employ the OSA formulation of CC theory (cf. Sec. II) and the results of cluster analysis of PUHF solutions (cf. Sec. III).

We have seen in the preceding section that K_4 is entirely described by the triplet component $U_1^X(1,0)$, making the presence or absence of the singlet component $U_1^X(0,0)$ in U_1^X irrelevant. Thus, the terms $\Theta_4[G_{rs}^{ab}(i)]$ that are required to correct the CCSD system of equations for T_4 contributions [cf. Eqs. (41)–(45)] are given by exactly the same formulas that were derived in Ref. [53], where $U_1^X(0,0)$ was neglected. We present below an independent derivation of these formulas, which is based on graphical methods of spin algebras.

It follows from Eq. (91) that the calculation of K_4 requires the knowledge of K_2. We thus need an explicit relationship between the amplitudes $\langle r||a\rangle_1$, defining the operator $U_1^X(1,0)$ [cf. Eq. (57)], and the OSA amplitudes $\langle rs|k_2|ab\rangle_i$ (or their unnormalized analogs $\langle rs|\kappa_2|ab\rangle_i$) defining pair clusters K_2,

$$K_2=\sum_{\substack{a\leqslant b\\ r\leqslant s}}\sum_{i=0}^{1}\langle rs|k_2|ab\rangle_i\, G_{ab}^{rs}(i) =\tfrac{1}{4}\sum_{a,b,r,s}\sum_{i=0}^{1}\langle rs|\kappa_2|ab\rangle_i\,\Gamma_{ab}^{rs}(i). \tag{94}$$

This relationship takes the form [cf. Eq. (89)]

$$\langle rs|k_2|ab\rangle_i=N_{ab}^{rs}\langle rs|\kappa_2|ab\rangle_i=\langle\Phi_0|G_{rs}^{ab}(i)K_2|\Phi_0\rangle =N_{rs}^{ab}(-1)^{i+1}[i]^{-1/2}\mathcal{S}^{ab}(i)\langle r||a\rangle_1\langle s||b\rangle_1, \tag{95}$$

where

$$\mathcal{S}_{kl}(i)\equiv\mathcal{S}^{kl}(i)=1+(-1)^i(kl) \tag{96}$$

designates the two-index symmetrizer $(i=0)$ or antisymmetrizer $(i=1)$, with (kl) representing the transposition of indices k and l. A simple diagrammatic proof of Eq. (95) is described in the Appendix, whereas the algebraic proof of Eq. (95) can be found in Ref. [53].

While the $\langle rs|k_2|ab\rangle_i$ amplitudes are important for the following developments, there is no need to calculate the

amplitudes defining K_4 clusters in order to evaluate $\Theta_4[G^{ab}_{rs}(i)]$ corrections. In fact, the K_4-corrected CCSD theory can be entirely formulated in terms of the k_2 components, Eq. (94). Let us concentrate on this aspect of the CCSDQ′ formalism.

Since $K_3=0$, the corresponding corrections $\Theta_3(G^{\dagger}_I)$ $[G_I=G^r_a,G^{rs}_{ab}(i)]$ and $\Theta_{1,3}[G^{ab}_{rs}(i)]$, Eqs. (43) and (45), vanish, so that the K_4-corrected CCSD system of equations becomes

$$\sum_{n=0}^{3}\Lambda_n(G^a_r)=0, \tag{97}$$

$$\sum_{n=0}^{4}\Lambda_n[G^{ab}_{rs}(i)]+\Theta^X_4[G^{ab}_{rs}(i)]=0 \quad (i=0,1), \tag{98}$$

where

$$\begin{aligned}\Theta^X_4[G^{ab}_{rs}(i)]&=\langle\Phi_0|G^{ab}_{rs}(i)(H_NK_4)_C|\Phi_0\rangle\\&=\langle\Phi_0|G^{ab}_{rs}(i)V_NK_4|\Phi_0\rangle=\Theta^X_{4;4}[G^{ab}_{rs}(i)]\\&\quad-\Theta^X_{4;2,2}[G^{ab}_{rs}(i)],\end{aligned} \tag{99}$$

with

$$\Theta^X_{4;4}[G^{ab}_{rs}(i)]=\langle\Phi_0|G^{ab}_{rs}(i)V_{N\frac{1}{24}}[U^X_1(1,0)]^4|\Phi_0\rangle, \tag{100}$$

$$\Theta^X_{4;2,2}[G^{ab}_{rs}(i)]=\langle\Phi_0|G^{ab}_{rs}(i)V_{N\frac{1}{2}}(K_2)^2|\Phi_0\rangle. \tag{101}$$

To obtain Eqs. (99)–(101), we used Eq. (91) and the fact that no vacuum disconnected diagrams (disconnected diagrams with no external lines; cf., e.g., Refs. [5] and [7]) can be formed from the operators $G^{ab}_{rs}(i)$, H_N or V_N, and K_4. We also dropped the projector $P_{S=0}$ from Eq. (100), since $G^{rs}_{ab}(i)$ generate singlet biexcitations. It can be further proved (cf. Ref. [53]) that the unlinked [5,7] components of $\Theta^X_{4;4}[G^{ab}_{rs}(i)]$ and $\Theta^X_{4;2,2}[G^{ab}_{rs}(i)]$ cancel out, so that $\Theta^X_4[G^{ab}_{rs}(i)]$, Eq. (99), reduces to

$$\Theta^X_4[G^{ab}_{rs}(i)]=\{\Theta^X_{4;4}[G^{ab}_{rs}(i)]\}_L-\{\Theta^X_{4;2,2}[G^{ab}_{rs}(i)]\}_L, \tag{102}$$

where the subscript L designates the linked part of a given expression. The easiest way to derive Eq. (102) is based on the observation that the unlinked part of $\Theta^X_{4;4}[G^{ab}_{rs}(i)]$ can be written as

$$\begin{aligned}\{\Theta^X_{4;4}[G^{ab}_{rs}(i)]\}_{UL}&\equiv\langle\Phi_0|\{G^{ab}_{rs}(i)V_{N\frac{1}{24}}[U^X_1(1,0)]^4\}_{UL}|\Phi_0\rangle\\&=\langle\Phi_0|G^{ab}_{rs}(i)\tfrac{1}{2}[U^X_1(1,0)]^2|\Phi_0\rangle\\&\quad\times\langle\Phi_0|V_{N\frac{1}{2}}[U^X_1(1,0)]^2|\Phi_0\rangle,\end{aligned} \tag{103}$$

where UL stands for the unlinked part of a given expression. Since $G^{rs}_{ab}(i)$ generate singlet biexcited configurations, we can reinsert the projector $P_{S=0}$ in front of $\frac{1}{2}[U^X_1(1,0)]^2$ to produce the cluster operator K_2 [cf. Eq. (89)]. In this way, we find that

$$\begin{aligned}\{\Theta^X_{4;4}[G^{ab}_{rs}(i)]\}_{UL}&=\langle\Phi_0|G^{ab}_{rs}(i)K_2|\Phi_0\rangle\langle\Phi_0|V_NK_2|\Phi_0\rangle\\&=\langle\Phi_0|\{G^{ab}_{rs}(i)V_{N\frac{1}{2}}(K_2)^2\}_{UL}|\Phi_0\rangle\\&\equiv\{\Theta^X_{4;2,2}[G^{ab}_{rs}(i)]\}_{UL}.\end{aligned} \tag{104}$$

Thus, the unlinked components of $\Theta^X_{4;4}[G^{ab}_{rs}(i)]$ and $\Theta^X_{4;2,2}[G^{ab}_{rs}(i)]$ cancel out.

In order to present the final K_4-corrected CCSD equations, we must derive explicit formulas for the linked terms $\{\Theta^X_{4;4}[G^{ab}_{rs}(i)]\}_L$ and $\{\Theta^X_{4;2,2}[G^{ab}_{rs}(i)]\}_L$. The latter term can be rewritten as follows:

$$\begin{aligned}\{\Theta^X_{4;2,2}[G^{ab}_{rs}(i)]\}_L&=\langle\Phi_0|\{G^{ab}_{rs}(i)V_{N\frac{1}{2}}(K_2)^2\}_L|\Phi_0\rangle\\&=\langle\Phi_0|\{G^{ab}_{rs}(i)[V_{N\frac{1}{2}}(K_2)^2]_C\}_L|\Phi_0\rangle\\&=\langle\Phi_0|G^{ab}_{rs}(i)[V_{N\frac{1}{2}}(K_2)^2]_C|\Phi_0\rangle\\&=\Lambda^{\mathrm{CCD}}_4[G^{ab}_{rs}(i)](T_2\rightarrow K_2),\end{aligned} \tag{105}$$

or, simply [cf. Eq. (40)],

$$\{\Theta^X_{4;2,2}[G^{ab}_{rs}(i)]\}_L=\sum_{k=1}^{5}\Lambda^{(k)}_4[G^{ab}_{rs}(i)](T_2\rightarrow K_2), \tag{106}$$

where we utilized the fact that no linked vacuum contributions can be formed from $G^{ab}_{rs}(i)$ and the disconnected part of $V_{N\frac{1}{2}}(K_2)^2$, and that no unlinked vacuum contributions can be obtained from $G^{ab}_{rs}(i)$ and $[V_{N\frac{1}{2}}(K_2)^2]_C$. We thus see that $\{\Theta^X_{4;2,2}[G^{ab}_{rs}(i)]\}_L$ reduces to the standard $\frac{1}{2}(T_2)^2$ term of the OSA CCD theory, Eq. (40), in which the T_2 clusters are replaced by their PUHF-type counterparts K_2 (which we indicated by the symbol $T_2\rightarrow K_2$). In other words, we obtain $\{\Theta^X_{4;2,2}[G^{ab}_{rs}(i)]\}_L$ by replacing the amplitudes $\langle rs|\tau_2|ab\rangle_i$ in the explicit expressions for $\Lambda^{\mathrm{CCD}}_4[G^{ab}_{rs}(i)]$ or $\Lambda^{(k)}_4[G^{ab}_{rs}(i)]$ $(k=1-5)$ of Ref. [44] by their $\langle rs|\kappa_2|ab\rangle_i$ analogs defined by Eq. (95).

It thus remains to derive the explicit equations for

$$\{\Theta^X_{4;4}[G^{ab}_{rs}(i)]\}_L\equiv\langle\Phi_0|\{G^{ab}_{rs}(i)V_{N\frac{1}{24}}[U^X_1(1,0)]^4\}_L|\Phi_0\rangle. \tag{107}$$

As shown in the Appendix (see, also, Ref. [53]), the linked part of $\Theta^X_{4;4}[G^{ab}_{rs}(i)]$ splits into three diagrammatic contributions,

$$\{\Theta^X_{4;4}[G^{ab}_{rs}(i)]\}_L=\Theta^X_{4;4}(\mathrm{a})+\Theta^X_{4;4}(\mathrm{b})+\Theta^X_{4;4}(\mathrm{c}), \tag{108}$$

where a, b, and c designate three Goldstone-Hugenholtz diagrams that can be obtained in this case. By using the diagrammatic method based on the graphical methods of spin algebras [69], we can prove that $\Theta^X_{4;4}(\mathrm{c})$ vanishes and that (cf. the Appendix)

$$\Theta^X_{4;4}(\mathrm{a}) = N^{ab}_{rs}[i]^{1/2} \sum_{a',b',r',s'} \langle a'b'||r's'\rangle \times \langle r'||a\rangle_1 \langle s'||b\rangle_1 \mathcal{S}_{rs}(i) \langle r||a'\rangle_1 \langle s||b'\rangle_1, \tag{109}$$

$$\Theta^X_{4;4}(\mathrm{b}) = N^{ab}_{rs}(-1)^{i+1}[i]^{-1/2} \sum_{a',b',r',s'} \langle a'b'||r's'\rangle \times \langle r'||b'\rangle_1 \mathcal{S}_{rs}(i) \mathcal{S}^{ab}(i) \langle r||a'\rangle_1 \langle s'||a\rangle_1 \langle s||b\rangle_1, \tag{110}$$

where $\langle r'||a\rangle_1$, etc. are the amplitudes occurring in Eqs. (57) and (58). Similar expressions for $\{\Theta^X_{4;4}[G^{ab}_{rs}(i)]\}_L$ were obtained in Ref. [53], where the algebraic rather than diagrammatic arguments were employed. We thus see that the linked part of $\Theta^X_{4;4}[G^{ab}_{rs}(i)]$ is given by rather simple algebraic expressions involving molecular integrals and the amplitudes $\langle r||a\rangle_1$ defining $U^X_1(1,0)$.

Interestingly enough, it can be further proved that

$$\Theta^X_{4;4}(\mathrm{a}) = [i]^2 \Lambda^{(5)}_4[G^{ab}_{rs}(i)](T_2 \to K_2), \tag{111}$$

$$\Theta^X_{4;4}(\mathrm{b}) = \Lambda^{(4)}_4[G^{ab}_{rs}(i)](T_2 \to K_2), \tag{112}$$

where on the right-hand side of Eqs. (111) and (112) are, respectively, the fifth and fourth diagrammatic contributions to the $\frac{1}{2}(T_2)^2$ term $\Lambda^{\mathrm{CCD}}_4[G^{ab}_{rs}(i)]$ of the CCD theory (cf. Fig. 1 of Ref. [57] or Fig. 4 of Ref. [22]), in which T_2 is replaced by K_2. To prove Eqs. (111) and (112), we must use Eqs. (109) and (110) and exploit the explicit relationship between the amplitudes $\langle r||a\rangle_1$ and the OSA amplitudes $\langle rs|k_2|ab\rangle_i$ or $\langle rs|\kappa_2|ab\rangle_i$ defining pair clusters K_2 [cf. Eq. (95)].

Inserting Eqs. (111) and (112) into Eq. (108) and combining the resulting expression with Eq. (106) allows us to write the following equation for the correction $\Theta^X_4[G^{ab}_{rs}(i)]$, Eq. (102),

$$\begin{aligned}\Theta^X_4[G^{ab}_{rs}(i)] &= \Lambda^{(4)}_4[G^{ab}_{rs}(i)](T_2 \to K_2) + [i]^2 \Lambda^{(5)}_4[G^{ab}_{rs}(i)](T_2 \to K_2) - \sum_{k=1}^{5} \Lambda^{(k)}_4[G^{ab}_{rs}(i)](T_2 \to K_2) \\ &= -\Lambda^{(1)}_4[G^{ab}_{rs}(i)](T_2 \to K_2) - \Lambda^{(2)}_4[G^{ab}_{rs}(i)](T_2 \to K_2) - \Lambda^{(3)}_4[G^{ab}_{rs}(i)](T_2 \to K_2) + 8\,\delta_{i1} \Lambda^{(5)}_4[G^{ab}_{rs}(i)](T_2 \to K_2).\end{aligned} \tag{113}$$

It is remarkable that the entire K_4 correction to CCSD equations can be expressed in terms of the $\frac{1}{2}(T_2)^2$ terms of the CCD theory, with T_2 replaced by K_2.

Equations (97) and (98), together with Eq. (113), are basic equations of the CCSDQ′ formalism. It is immediately obvious that they are no more complex than the standard OSA CCSD equations. The $\Theta^X_4[G^{ab}_{rs}(i)]$ term is evaluated only once, before we initiate the iterative procedure for solving the CC system of equations, by computing the CCD-like diagrammatic expressions using K_2 amplitudes, which are in turn evaluated using the $\langle r||a\rangle_1$ amplitudes and the relationship (95). The $\Theta^X_4[G^{ab}_{rs}(i)]$ term is then used to correct the absolute term [cf. Eq. (35) and, e.g., Ref. [44]]

$$\begin{aligned}\Lambda_0[G^{ab}_{rs}(i)] &= \langle \Phi_0|[G^{ab}_{rs}(i)]V_N|\Phi_0\rangle \\ &= N^{rs}_{ab}[i]^{1/2} \mathcal{S}_{rs}(i) \langle rs||ab\rangle.\end{aligned} \tag{114}$$

Clearly, the resulting formalism employs fewer amplitudes than the spin-orbital CCSD theory employing the UHF orbitals, and contrary to the latter method, the problem of spin contamination is entirely eliminated. We only have to know the amplitudes $\langle r||a\rangle_1$. A simple program, which allows us to calculate $\langle r||a\rangle_1$ from the knowledge of the UHF and RHF orbitals, is described in the next section. We should also notice that the CCSDQ′ equations (97), (98), and (113) reduce to the CCDQ′ equations of Ref. [53] when $T_1 = 0$.

We also recall that when the pair clusters $T_2 = K_2$ are exact (as, for example, in the strongly correlated $\beta = 0$ limit of the cyclic polyene model; cf. Ref. [56]), then the $\Theta^X_4[G^{ab}_{rs}(i)]$ correction cancels out the first three nonlinear diagrams of the CCD theory, $\Lambda^{(k)}_4[G^{ab}_{rs}(i)]$ $(k = 1-3)$, and slightly modifies the fifth contribution $\Lambda^{(5)}_4[G^{ab}_{rs}(i)]$. Indeed, in this special case the CCSDQ′ equations reduce to

$$\sum_{n=0}^{3} \Lambda_n(G^a_r) = 0, \tag{115}$$

$$\sum_{n=0}^{3} \Lambda_n[G^{ab}_{rs}(i)] + \Lambda^{\mathrm{ACCSD}'}_4[G^{ab}_{rs}(i)] = 0 \quad (i = 0,1), \tag{116}$$

where

$$\begin{aligned}\Lambda^{\mathrm{ACCSD}'}_4[G^{ab}_{rs}(i)] = \langle \Phi_0|G^{ab}_{rs}(i)\{H_N[\tfrac{1}{2}(T_1)^2 T_2 \\ + \tfrac{1}{24}(T_1)^4]\}_C|\Phi_0\rangle + \Lambda^{(4)}_4[G^{ab}_{rs}(i)] \\ + [i]^2 \Lambda^{(5)}_4[G^{ab}_{rs}(i)].\end{aligned} \tag{117}$$

Equations (115)–(117) are basic equations of the so-called ACCSD′ method, which reduces to the well-known ACPQ (or ACCD′) method of Ref. [53] when $T_1 = 0$. It should be emphasized that reduction of the CCSDQ′ equations to those of the ACCSD′ formalism is based on a rather strong assumption, namely, that both T_2 and T_4 components resulting from the cluster analysis of the PUHF solution are exact or nearly exact. This is indeed the case in the strongly corre-

lated regime of the PPP cyclic polyene model, but may not be the case in general *ab initio* situations. The CCSDQ′ formalism is based on a much weaker assumption requiring that only T_4 corrections are fairly well represented by the PUHF wave function, which is justified by a qualitatively good description of the bond-breaking phenomena by the PUHF solutions. We should also reiterate that the above simple relationship between the CCSDQ′ and ACCSD′ formalisms relies on the OSA formulation of the SRCC theory.

The general-purpose computer implementation of the CCSDQ′ and CCDQ′ methods is described in the next section. Together with CCSDQ′ and ACCSD′, we also consider the CCSDQ′[T] and ACCSD′[T] approaches, in which in addition to T_4 contributions estimated via Eq. (113) we also calculate T_3 energy corrections using Eq. (50). The relevant $\langle rs|t_2|ab\rangle_i$ amplitudes are then obtained from the CCSDQ′ and ACCSD′ calculations, respectively. Unfortunately, T_3 components cannot be obtained from cluster analysis of the PUHF solution, so that we must rely on some other approximation to estimate their contribution. We decided to use simple perturbative estimates T(CCSDQ′) or T(ACCSD′). Another possibility would be to consider the K_4 corrected CCSDT equations, which would result in a much more complex and computationally highly demanding CCSDT-like formalism. We do not pursue this approach, whose domain of applications would be rather limited.

V. COMPUTATIONAL DETAILS

All CC calculations reported in this paper were carried out with the general-purpose programs written in our laboratory. The CCSD, ACCSD′, CCSD[T], and ACCSD′[T] programs were described in Refs. [24] and [67]. The relevant OSA expressions for $\Lambda_n(G_I^\dagger)$ $[G_I=G_a^r,G_{ab}^{rs}(i)]$ and the CCSD energy were presented in Ref. [44], whereas the required OSA expressions for the triexcited corrections $\Delta E^{\mathrm{T}(X)}$ (X = CCSD, ACCSD′) were given in Ref. [22]. The CCSDQ′ and CCSDQ′[T] programs use the same type of expressions, so that they have the same structure as the CCSD and CCSD[T] codes, except for small differences in defining the absolute terms, which are computed only once before initiating the actual iterative procedure for solving the CC equations. Although the CCSDQ′ formalism can utilize any broken symmetry single-determinantal wave function to evaluate the $T_4=K_4$ corrections, the computer implementation described below uses the ground-state UHF wave function.

A. CCSDQ′ equations

Let us recall that the CCSD and ACCSD′, as well as CCSDQ′, programs are based on the iterative algorithm described in Ref. [30], which is in turn related to the reduced-linear equation (RLE) procedure of Purvis and Bartlett [86]. According to the procedure of Ref. [30], we express Eqs. (33) and (34) (for CCSD approach), (115) and (116) (for ACCSD′ approach), or (97) and (98) (for CCSDQ′ approach) in the form

$$\mathbf{A(T)}\cdot\mathbf{T}=\mathbf{B(T)}, \tag{118}$$

where $\mathbf{T}$ is a column vector consisting of cluster amplitudes, $\mathbf{B(T)}$ is a column vector containing negative of the absolute and of some or all nonlinear terms, and $\mathbf{A(T)}$ represents a square matrix with all linear and the remaining nonlinear terms that were moved from the right-hand side to the left-hand side of Eq. (118) and conveniently quasilinearized [30] (cf., also, Ref. [87]). In the case of CCSD and ACCSD′, the absolute terms occurring in $\mathbf{B(T)}$ are defined as $\Lambda_0(G_I^\dagger)$, Eq. (35), where $G_I=G_a^r,G_{ab}^{rs}(i)$. As explained in Sec. IV, the absolute terms of the CCSDQ′ formalism are defined by $\Lambda_0(G_r^a)$ for equations projected on singly excited configurations, and as

$$\Lambda_0^{\mathrm{CCSDQ}'}[G_{rs}^{ab}(i)]=\Lambda_0[G_{rs}^{ab}(i)]+\Theta_4^X[G_{rs}^{ab}(i)] \tag{119}$$

for equations projected on biexcited configurations [cf. Eqs. (113) and (114)].

We express the $(n+1)$st approximate of $\mathbf{T}$ as a linear combination of the initial guess $\mathbf{T}^{(1)}\equiv\mathbf{U}^{(1)}$ and n correction vectors $\mathbf{U}^{(k)}$, $k=2,\ldots,n+1$, calculated in subsequent iterations of the RLE procedure,

$$\mathbf{T}^{(n+1)}=\sum_{k=1}^{n+1}\alpha_k\mathbf{U}^{(k)}, \tag{120}$$

with scaling factors α_k chosen to minimize the Euclidean norm of the ''error'' vector

$$\mathbf{e}=\mathbf{A}(\mathbf{T}^{(n)})\cdot\mathbf{T}^{(n+1)}-\mathbf{B}(\mathbf{T}^{(n)}). \tag{121}$$

Typically, the corrections $\mathbf{U}^{(k)}$ are calculated by using the inverse of the diagonal part of $\mathbf{A(T)}$ [designated by $\mathbf{D(T)}$] to estimate $[\mathbf{A(T)}]^{-1}$,

$$\mathbf{U}^{(n+1)}=[\mathbf{D}(\mathbf{T}^{(n)})]^{-1}\cdot\mathbf{B}_D^{(n)}, \tag{122}$$

where

$$\mathbf{B}_D^{(n)}=\mathbf{B}(\mathbf{T}^{(n)})-\sum_{k=1}^{n}\mathbf{B}_k^{(n)},\quad \mathbf{B}_k^{(n)}=\mathbf{A}(\mathbf{T}^{(n)})\cdot\mathbf{U}^{(k)}. \tag{123}$$

In most cases, a simple first-order MBPT estimate of $\mathbf{T}^{(1)}$ gives a reasonable convergence. Other initial guesses, such as the second-order MBPT estimate for $\mathbf{T}^{(1)}$, or the previously converged amplitudes for the nearby geometry (in general, the converged amplitudes for the nearby values of the parameters used to describe the system), can also be used in our program.

An important feature of the above algorithm is the possibility to quasilinearize selected nonlinear terms. For example, in a number of quasidegenerate situations, it is useful to include the $\frac{1}{2}(T_2)^2$ clusters in $\mathbf{A(T)}\cdot\mathbf{T}$, so that the denominator matrix $\mathbf{D(T)}$ is modified by terms involving large pair-cluster amplitudes [30]. This is particularly important for the ACCSD′ and CCSDQ′ approaches, which are intended to be used in severe cases of quasidegeneracy, where the standard CCSD theory is no longer applicable or even breaks down. To improve the convergence of the CCSDQ′ algorithm in the region where the standard CCSD theory becomes singular, we introduced a new quasilinearization

scheme for $\frac{1}{2}(T_2)^2$ terms, in which we optionally quasilinearize and include in $\mathbf{A}(\mathbf{T})\cdot\mathbf{T}$ only the ACCD′-like nonlinear contributions $\Lambda_4^{(4)}[G_{rs}^{ab}(i)]$ and $[i]^2\Lambda_4^{(5)}[G_{rs}^{ab}(i)]$, while retaining the remaining $\frac{1}{2}(T_2)^2$ terms in $\mathbf{B}(\mathbf{T})$. This is justified by the fact that in severe cases of configurational quasidegeneracy the contributions of the first three nonlinear diagrams $\Lambda_4^{(k)}[G_{rs}^{ab}(i)]$ $(k=1-3)$, mutually cancel out [52], so that when we move the ACCD′-like terms $\Lambda_4^{(4)}[G_{rs}^{ab}(i)]$ and $[i]^2\Lambda_4^{(5)}[G_{rs}^{ab}(i)]$ to the left-hand-side of Eq. (118), the right-hand-side vector $\mathbf{B}(\mathbf{T})$ reduces to the negative of the vector containing the CCSDQ′ absolute terms $\{\Lambda_0(G_r^a),\Lambda_0^{\mathrm{CCSDQ}'}[G_{rs}^{ab}(i)]\}$. This quasilinearization improves the convergence of the CCSDQ′ scheme whenever the cluster analysis of the PUHF wave function yields very accurate cluster components (see the discussion below).

To further improve the convergence of our CC (in particular, CCSDQ′) algorithms, we decided to allow for better estimates of $[\mathbf{A}(\mathbf{T})]^{-1}$ for calculating $\mathbf{U}^{(n+1)}$, Eq. (122). Instead of relying on a simple approximation $\mathbf{A}(\mathbf{T})\approx\mathbf{D}(\mathbf{T})$, we write [88]

$$\mathbf{A}(\mathbf{T})=\mathbf{D}(\mathbf{T})+\mathbf{\Delta}(\mathbf{T}), \tag{124}$$

or (dropping for a moment the explicit dependence on $\mathbf{T}$)

$$\mathbf{A}^{-1}=\mathbf{D}^{-1}-\mathbf{D}^{-1}\cdot\mathbf{\Delta}\cdot(\mathbf{D}+\mathbf{\Delta})^{-1}, \tag{125}$$

where $\mathbf{\Delta}\equiv\mathbf{\Delta}(\mathbf{T})$ is the off-diagonal part of $\mathbf{A}(\mathbf{T})$. Expanding the right-hand side of Eq. (125), we obtain (retaining at most linear terms in $\mathbf{\Delta}$)

$$\begin{aligned}\mathbf{A}^{-1}&\approx\mathbf{D}^{-1}-\mathbf{D}^{-1}\cdot\mathbf{\Delta}\cdot\mathbf{D}^{-1}=\mathbf{D}^{-1}+\mathbf{D}^{-1}\cdot(\mathbf{D}-\mathbf{A})\cdot\mathbf{D}^{-1}\\&=2\mathbf{D}^{-1}-\mathbf{D}^{-1}\cdot\mathbf{A}\cdot\mathbf{D}^{-1},\end{aligned} \tag{126}$$

which allows us to express the improved correction vectors $\mathbf{U}^{(n+1)}$ as follows:

$$\begin{aligned}\mathbf{U}^{(n+1)}=&2[\mathbf{D}(\mathbf{T}^{(n)})]^{-1}\cdot\mathbf{B}_D^{(n)}\\&-[\mathbf{D}(\mathbf{T}^{(n)})]^{-1}\cdot\mathbf{A}(\mathbf{T}^{(n)})\cdot[\mathbf{D}(\mathbf{T}^{(n)})]^{-1}\cdot\mathbf{B}_D^{(n)}.\end{aligned} \tag{127}$$

Note that there is no need to store $\mathbf{A}(\mathbf{T})$ to calculate the improved vector $\mathbf{U}^{(n+1)}$, Eq. (127). The dimensions of arrays $\mathbf{D}(\mathbf{T}^{(n)})$ and $\mathbf{B}_D^{(n)}$ are the same as dimensions of $\mathbf{T}$ or $\mathbf{U}^{(k)}$, so that the matrix product $\mathbf{A}(\mathbf{T}^{(n)})\cdot[\mathbf{D}(\mathbf{T}^{(n)})]^{-1}\cdot\mathbf{B}_D^{(n)}$ can be calculated using the routines that are designed to calculate the products $\mathbf{B}_k^{(n)}$, Eq. (123). In fact, the same applies to higher-order analogs of the formula (127), which contain higher powers of $\mathbf{\Delta}$ [88], and which we included in our codes as well.

We found out that the improved estimate for $[\mathbf{A}(\mathbf{T})]^{-1}$ reduces the number of required iterations by as much as 30–40% (assuming the simple first-order MBPT estimate as the initial guess for T_2 and the convergence thresholds of 7–10 decimal places in the energy). Although every iteration requires more time when Eq. (127) is used, the overall benefit in cpu time is often substantial.

B. Cluster analysis

The most important new element of the current CC codes allowing for the CCSDQ′ calculations is the set of routines that perform the cluster analysis of the PUHF wave function and correct the CCSD equations by the relevant $\Theta_4^{\mathrm{UHF}}[G_{rs}^{ab}(i)]$ terms. According to the general theory of Sec. III, we must first extract the coefficients $\langle r||a\rangle_S$, defining the operators $U_1^{\mathrm{UHF}}(S,0)$, from the PUHF solution. These are in turn defined in terms of the spin-orbital coefficients $\langle r\sigma|u_1^{(\sigma)}|a\sigma\rangle$, where $\sigma=\alpha,\beta$ designates the spin-up and spin-down spin functions [see Eq. (58)]. The latter coefficients can be calculated using the transformation matrices $\mathbf{C}^{(\sigma)}\equiv||c_{kl}^{(\sigma)}||_{k,l=1}^{M}$ between the UHF and RHF orbitals,

$$\phi_{l,\sigma}^{\mathrm{UHF}}=\sum_{k=1}^{M}c_{kl}^{(\sigma)}\phi_k^{\mathrm{RHF}}. \tag{128}$$

Here, M is the number of RHF (UHF with α or β spins) orbitals or the dimension of the atomic orbital (AO) basis set used in the corresponding LCAO (linear combination of atomic orbitals) expansions defining both MO sets,

$$\phi_{k,\sigma}^{\mathrm{UHF}}=\sum_{\mu=1}^{M}a_{\mu k}^{(\sigma)}\chi_\mu, \tag{129}$$

$$\phi_k^{\mathrm{RHF}}=\sum_{\mu=1}^{M}b_{\mu k}\chi_\mu, \tag{130}$$

χ_μ $(\mu=1,\ldots,M)$ being the AO's. To find the desired relationship, we must expand the UHF wave function

$$|\Phi_0^{\mathrm{UHF}}\rangle=|\phi_{1,\alpha}^{\mathrm{UHF}}\alpha\phi_{1,\beta}^{\mathrm{UHF}}\beta\cdots\phi_{n,\alpha}^{\mathrm{UHF}}\alpha\phi_{n,\beta}^{\mathrm{UHF}}\beta| \tag{131}$$

in terms of the RHF configuration

$$|\Phi_0^{\mathrm{RHF}}\rangle=|\phi_1^{\mathrm{RHF}}\alpha\phi_1^{\mathrm{RHF}}\beta\cdots\phi_a^{\mathrm{RHF}}\alpha\phi_a^{\mathrm{RHF}}\beta\cdots\phi_n^{\mathrm{RHF}}\alpha\phi_n^{\mathrm{RHF}}\beta| \tag{132}$$

and various excited configurations relative to $|\Phi_0^{\mathrm{RHF}}\rangle$, using Eq. (128), and compute the coefficients at

$$\left|\begin{matrix}r\sigma\\a\sigma\end{matrix}\right\rangle\equiv\left|\begin{matrix}\phi_r^{\mathrm{RHF}}\sigma\\\phi_a^{\mathrm{RHF}}\sigma\end{matrix}\right\rangle=X_{r\sigma}^{\dagger}X_{a\sigma}|\Phi_0^{\mathrm{RHF}}\rangle, \tag{133}$$

where we rely on our labeling convention with $a=1,2,\ldots,n$ designating the occupied orbitals and $r=n+1,n+2,\ldots,M$ the unoccupied orbitals in $|\Phi_0^{\mathrm{RHF}}\rangle$.

Since we used the intermediate normalization in defining U_1^{UHF} [cf. Eq. (52)], the monoexcited coefficient $\langle r\sigma|u_1^{(\sigma)}|a\sigma\rangle$ is given by the ratio

$$\langle r\sigma|u_1^{(\sigma)}|a\sigma\rangle=\left\langle\begin{matrix}r\sigma\\a\sigma\end{matrix}\right|\Phi_0^{\mathrm{UHF}}\rangle\ \Big/\ \langle\Phi_0^{\mathrm{RHF}}|\Phi_0^{\mathrm{UHF}}\rangle. \tag{134}$$

The denominator is given by the product of two determinants: the determinant of a matrix with entries consisting of all possible overlaps between the occupied RHF MO's and the occupied UHF MO's associated with α spins, and a similar determinant for β spins,

$$\langle \Phi_0^{\mathrm{RHF}}|\Phi_0^{\mathrm{UHF}}\rangle = \det\|\langle \phi_k^{\mathrm{RHF}}|\phi_{l,\alpha}^{\mathrm{UHF}}\rangle\|_{k,l=1}^{n} \times \det\|\langle \phi_k^{\mathrm{RHF}}|\phi_{l,\beta}^{\mathrm{UHF}}\rangle\|_{k,l=1}^{n} = \det\|c_{kl}^{(\alpha)}\|_{k,l=1}^{n}\det\|c_{kl}^{(\beta)}\|_{k,l=1}^{n}. \quad (135)$$

An analogous formula can be obtained for the numerator, namely,

$$\left\langle \begin{matrix} r\sigma \\ a\sigma \end{matrix} \middle| \Phi_0^{\mathrm{UHF}} \right\rangle = \det\|\tilde{c}_{kl}^{(\sigma)}(a\rightarrow r)\|_{k,l=1}^{n}\det\|c_{kl}^{(\overline{\sigma})}\|_{k,l=1}^{n}, \quad (136)$$

where $\overline{\alpha}=\beta$, $\overline{\beta}=\alpha$, and $\|\tilde{c}_{kl}^{(\sigma)}(a\rightarrow r)\|_{k,l=1}^{n}$ is obtained from the matrix $\|c_{kl}^{(\sigma)}\|_{k,l=1}^{n}$ by replacing the ath ($a=1,2,\ldots,n$) row, containing the expansion coefficients $c_{al}^{(\sigma)}$, $l=1,2,\ldots,n$, for all occupied UHF MO's having σ spin, by the first n elements of the rth row of $\mathbf{C}^{(\sigma)}$ ($r=n+1,n+2,\ldots,M$) containing the coefficients $c_{rl}^{(\sigma)}$ that correspond to the given unoccupied orbital ϕ_r^{RHF}. The entries of the matrix $\|\tilde{c}_{kl}^{(\sigma)}(a\rightarrow r)\|_{k,l=1}^{n}$ are thus defined as follows:

$$\tilde{c}_{kl}^{(\sigma)}(a\rightarrow r)=\begin{cases} c_{rl}^{(\sigma)} & \text{if } k=a \\ c_{kl}^{(\sigma)} & \text{otherwise} \end{cases} \qquad (k,l=1,2,\ldots,n). \quad (137)$$

Substituting Eqs. (135) and (136) into Eq. (134), we arrive at the following result for $\langle r\sigma|u_1^{(\sigma)}|a\sigma\rangle$:

$$\langle r\sigma|u_1^{(\sigma)}|a\sigma\rangle = \det\|\tilde{c}_{kl}^{(\sigma)}(a\rightarrow r)\|_{k,l=1}^{n}/\det\|c_{kl}^{(\sigma)}\|_{k,l=1}^{n}. \quad (138)$$

Thus, the required monoexcited coefficients $\langle r\sigma|u_1^{(\sigma)}|a\sigma\rangle$ can be easily calculated using the $n\times n$ submatrices, $\|\tilde{c}_{l}^{(\alpha)}(a\rightarrow r)\|_{k,l=1}^{n}$ and $\|\tilde{c}_{kl}^{(\beta)}(a\rightarrow r)\|_{k,l=1}^{n}$, Eq. (137), of the relevant transformation matrices, $\mathbf{C}^{(\alpha)}$ and $\mathbf{C}^{(\beta)}$, respectively, between the RHF and UHF orbitals. The latter matrices can be conveniently expressed in terms of the LCAO coefficients defining both MO sets [cf. Eqs. (129) and (130)] and the overlap matrix $\mathbf{S}\equiv\|\langle\chi_\mu|\chi_\nu\rangle\|_{\mu,\nu=1}^{M}$ characterizing the AO set $\{\chi_\mu\}_{\mu=1}^{M}$. Indeed, it can be easily verified that

$$\mathbf{C}^{(\sigma)}=\mathbf{B}^{-1}\cdot\mathbf{A}^{(\sigma)}=\mathbf{B}^{\dagger}\cdot\mathbf{S}\cdot\mathbf{A}^{(\sigma)}, \quad (139)$$

where $\mathbf{A}^{(\sigma)}\equiv\|a_{\mu k}^{(\sigma)}\|_{\mu,k=1}^{M}$ and $\mathbf{B}\equiv\|b_{\mu k}\|_{\mu,k=1}^{M}$ are the transformation matrices between the UHF and RHF MO sets, $\{\phi_{k,\sigma}^{\mathrm{UHF}}\}_{k=1}^{M}$ and $\{\phi_k^{\mathrm{RHF}}\}_{k=1}^{M}$, respectively, and the AO set $\{\chi_\mu\}_{\mu=1}^{M}$. Equation (139) enables us to determine the transformation matrices $\mathbf{C}^{(\sigma)}$ ($\sigma=\alpha,\beta$), which are in turn exploited to calculate the coefficients $\langle r\sigma|u_1^{(\sigma)}|a\sigma\rangle$ via Eq. (138). The required OSA amplitudes $\langle r||a\rangle_S$, defining the singlet and triplet components of the monoexcitation operator U_1^{UHF}, are then given by Eq. (58). Finally, the triplet amplitudes $\langle r||a\rangle_1$ are used to calculate the cluster coefficients $\langle rs|k_2|ab\rangle_i$ defining the pair-cluster operator K_2 by employing the relationship (95).

The operations just outlined form an essential part of a small program that performs the cluster analysis of the PUHF wave function. The required LCAO coefficients, defining the UHF and RHF MO sets as well as the AO overlap matrix $\mathbf{S}$, are read into the program from the relevant files generated by GAMESS [73]. The resulting biexcited cluster amplitudes $\langle rs|k_2|ab\rangle_i$, as well as their monoexcited analogs defining K_1, which are clearly identical to the singlet coefficients $\langle r|u_1|a\rangle_0$ [see Eq. (88)],

$$\langle r|k_1|a\rangle=\langle r|u_1|a\rangle_0=2^{1/2}\langle r||a\rangle_0, \quad (140)$$

are then stored on a disk (the triplet coefficients $\langle r|u_1|a\rangle_1$ are not saved as they are only needed to construct $\langle rs|k_2|ab\rangle_i$ amplitudes). Both the amplitudes $\langle rs|k_2|ab\rangle_i$ defining K_2 and the singly excited singlet coefficients $\langle r|k_1|a\rangle$, Eq. (140), are read by the CCSDQ′ program. The $\langle rs|k_2|ab\rangle_i$ coefficients are primarily used to compute the $\Theta_4^{\mathrm{UHF}}[G_{rs}^{ab}(i)]$ corrections. We employed Eq. (113) for this purpose, since it allows us to utilize the routines that normally calculate the standard CCD diagrammatic contributions $\Lambda_4^{(k)}[G_{rs}^{ab}(i)]$. The resulting $\Theta_4^{\mathrm{UHF}}[G_{rs}^{ab}(i)]$ terms are then used to define the absolute term $\Lambda_0^{\mathrm{CCSDQ}'}[G_{rs}^{ab}(i)]$, Eq. (119). All these operations are carried out before initiating the actual iterative procedure for solving CC equations (see the discussion above). In addition, both $\langle rs|k_2|ab\rangle_i$ and $\langle r|k_1|a\rangle$ are used to evaluate the PUHF-based CCSD energy expression, in which the T_1 and T_2 clusters are replaced by their PUHF analogs K_1 and K_2, respectively,

$$\Delta E^{\mathrm{CCSD(PUHF)}}=\langle\Phi_0|[H_N(K_1+K_2+\tfrac{1}{2}K_1^2)]_C|\Phi_0\rangle. \quad (141)$$

The analogous CCD energy expression [$\Delta E^{\mathrm{CCD(PUHF)}}$, Eq. (141), with $K_1=0$] is evaluated as well. These energies are useful for assessing the quality of the monoexcited and biexcited cluster amplitudes, resulting from the analysis of the PUHF wave function (cf. the discussion below), and thus of the performance of the ACCSD′ approach, which assumes that the pair clusters T_2 are fairly well represented by the PUHF solution.

C. Code testing

Both the cluster analysis program and the final CCSDQ′ code were thoroughly tested. In particular, it was very useful to apply these programs to situations where the UHF or PUHF wave function provides exact values of the monoexcited and biexcited cluster amplitudes. These situations include the PPP and Hubbard cyclic polyene models in the strongly correlated ($\beta=0$) limit (we used $\beta=0$ benzene model for testing) and the so-called MBS S4 model [34], consisting of four hydrogen atoms arranged in a square (D_{4h}) configuration, in the dissociation ($H_4\rightarrow 4H$) limit. In the latter case, we were stretching the nearest-neighbor H−H separation to 10–50 a.u. In these cases, the cluster analysis program gave us the exact T_1 and T_2 components ($T_1=0$ for these models), which were independently obtained by the cluster analysis of the FCI wave function. Also, the CCSDQ′ energy was identical with $\Delta E^{\mathrm{CCSD(PUHF)}}$, Eq. (141), as well as with the UHF and FCI energies. The CCSDQ′ energy was also identical with the ACCSD′ energy, in agreement with the fact that diagram cancellation leading to ACCSD′ [cf. Eqs. (115)–(117)] is exact whenever (P)UHF gives exact T_2 and T_4 components.

In some cases, we were able to retrieve the T_4 components directly from the UHF wave function and compute $\Theta_4^{\rm UHF}[G_{rs}^{ab}(i)]$ using the standard spin orbital expression [14,27–29,62]

$$\Theta_4[E_{RS}^{AB}] \equiv \langle \Phi_0 | E_{RS}^{AB} (V_N T_4)_C | \Phi_0 \rangle$$
$$= \tfrac{1}{4} \sum_{R',S',A',B'} \langle A'B'|v|R'S' \rangle_{\mathcal{A}} \times \langle RSR'S'|t_4|ABA'B' \rangle_{\mathcal{A}}, \quad (142)$$

where $|K\rangle \equiv |k\sigma\rangle$ designate spin orbitals ($A,B,\ldots$ occupied; $R,S,\ldots$ unoccupied in $|\Phi_0\rangle$), $E_{RS}^{AB} \equiv (E_{AB}^{RS})^\dagger$ with

$$E_{AB}^{RS} = E_{RA} E_{SB}, \quad E_{RA} = X_R^\dagger X_A, \quad (143)$$

$\langle KL|v|K'L' \rangle_{\mathcal{A}}$ the antisymmetrized two-electron integrals,

$$\langle KL|v|K'L' \rangle_{\mathcal{A}} = \langle KL|v|K'L' \rangle - \langle KL|v|L'K' \rangle, \quad (144)$$

and $\langle RSR'S'|t_4|ABA'B' \rangle_{\mathcal{A}}$ the spin-orbital cluster amplitudes defining T_4 [the subscript $\mathcal{A}$ indicates their antisymmetric property with respect to interchanges of occupied (unoccupied) spin-orbital labels]. The OSA corrections $\Theta_4^{\rm UHF}[G_{rs}^{ab}(i)]$ could then be evaluated by forming the spin-free corrections

$$\Theta_4^{\rm UHF}(E_{rs}^{ab}) \equiv \sum_{\rho,\sigma=-1/2}^{1/2} \Theta_4^{\rm UHF}(E_{r\rho s\sigma}^{a\rho b\sigma}), \quad (145)$$

corresponding to spin-free biexcitation operators

$$E_{ab}^{rs} = E_{ra} E_{sb}, \quad (146)$$

and by subsequently converting the spin-free components (145) into the OSA form using the relationship

$$\Theta_4^{\rm UHF}[G_{rs}^{ab}(i)] = \tfrac{1}{2} N_{rs}^{ab}[i]^{-1/2} \mathcal{S}^{ab}(i) \Theta_4^{\rm UHF}(E_{rs}^{ab}), \quad (147)$$

which reflects an alternative formula for $G_{ab}^{rs}(i)$, namely [89],

$$G_{rs}^{ab}(i) = \tfrac{1}{2} N_{ab}^{rs}[i]^{-1/2} \mathcal{S}^{ab}(i) E_{ab}^{rs}. \quad (148)$$

We used this procedure to calculate $\Theta_4^{\rm UHF}[G_{rs}^{ab}(i)]$ for the MBS P4 model consisting of four hydrogen atoms (or, better, two interacting hydrogen molecules) arranged in a rectangular (D_{2h}) nuclear conformation [57] (cf. Sec. VI). In this case, there is only one tetraexcited amplitude defining T_4, which could easily be extracted from the CI-like expansion of the UHF wave function. The resulting corrections $\Theta_4^{\rm UHF}[G_{rs}^{ab}(i)]$ obtained in this way were invariably identical to those generated by our CCSDQ′ code, which uses for this purpose Eq. (113) and K_2 cluster amplitudes defined by Eq. (95). Finally, we used the monoexcited cluster amplitudes $\langle r||a\rangle_S$ or $\langle r|u_1|a\rangle_S$, generated by our cluster analysis program, to evaluate the CI-like expansion describing the UHF wave functions for small molecular systems, such as the MBS H4 model consisting of two interacting hydrogen molecules arranged in isosceles trapezoidal (C_{2v}) configuration [57] (cf. Sec. VI) and the DZ H_2 model described in Sec. III [cf. Eqs. (71)–(75)]. By computing the corresponding expectation values [cf. Eq. (79)], we were able to reproduce the UHF energy obtained independently in the standard GAMESS calculations, which use the UHF energy expression based on density matrices.

As in the case of our other CC programs [24,67,90], the current CCSDQ′ and CCSDQ′[T] codes allow for point-group symmetry adaptation and freezing of core and dropping of virtual orbitals. Exploitation of spin and spatial symmetries substantially increases the efficiency of these programs and enables us to study realistic cases on relatively small workstations. As pointed out in Sec. III, this is an important advantage of the PUHF corrected CCSD-RHF method, when compared with the CCSD-UHF approach. The CCSDQ′ approach uses the symmetry-adapted PUHF wave function to calculate $\Theta_4^{\rm UHF}[G_{rs}^{ab}(i)]$ and the lowest symmetry-adapted RHF solution as $|\Phi_0\rangle$, in contrast to the CCSD-UHF method, which uses the broken-symmetry UHF wave function as a reference. On the other hand, the CCSD-UHF method can be applied to several nonsinglet (doublet, triplet, etc.) problems of high-spin type, which cannot be treated at this point by the OSA CCSDQ′ approach discussed in this study. Examples of the CCSDQ′ and CCSDQ′[T] calculations are presented in the next section.

VI. EXAMPLES

To examine the performance of CCSDQ′ and related CCDQ′ and CCSDQ′[T] methods, as well as the ACCSD′ and ACCSD′[T] approaches, we performed a number of calculations for systems in which the configurational degeneracy can be continuously varied by changing a single parameter describing their geometries. These include the above mentioned H4 and P4 models, using both the MBS and DZP basis sets of Refs. [57] and [59], respectively, and the MBS H8 model [66], which is composed of four interacting hydrogen molecules arranged in a distorted octagonal configuration having D_{2h} spatial symmetry. The CCSDQ′ study of the DZP H4 system should explain the ''ill behavior'' of the ACCSD′ approach pointed out by Kucharski, Balková, and Bartlett in Ref. [40]. In all cases, the initial ground-state RHF and UHF orbitals were obtained with GAMESS, which was also used to perform the integral transformation from AO to MO basis sets and to calculate various limited and full CI results.

Geometries of all three models are defined by the two parameters a and α, but only α is varied. The parameter a is defined as the nearest-neighbor H-H internuclear separation and, as in previous studies of these models (cf. Refs. [24,31,33,34,36,40,50,57,59,66,67,91,92]), it is fixed at 2.0 a.u. [corresponding to slightly stretched hydrogen molecules in order to enhance quasidegeneracy effects (cf. Ref. [34])]. The second parameter α determines (i) the displacement of the two H_2 molecules from the square configuration for the H4 and P4 models, and (ii) the displacement of two opposite H_2 molecules from their position in the regular octagon for the H8 model. For the trapezoidal H4 model, α is the angular parameter that varies between 0 (square configuration) and 0.5 (linear configuration). For the rectangular P4 model, α varies between $a = 2.0$ a.u. (square configuration) and ∞, the latter limit corresponding to a dissociation of the H_4 system

TABLE I. A comparison of the FCI, RHF, UHF, and various CC energies (in hartree) for the ground electronic state of the MBS P4 model with $a=2.0$ a.u. and different values of α (in a.u.). In this case, CCD=CCSD, CCD(PUHF)=CCSD(PUHF), ACCD′=ACCSD′, and CCDQ′=CCSDQ′. The RHF solution is triplet stable for $\alpha>3.0$ a.u.

α	RHF	UHF	CCD(PUHF)	FCI	CCD	ACCD′	CCDQ′
2.0	−1.858241	−1.957155	−1.946785	−1.975862	−1.978696	−1.976017	−1.977885
2.01	−1.862506	−1.958413	−1.948910	−1.977266	−1.979877	−1.977887	−1.979064
2.02	−1.866709	−1.959682	−1.951045	−1.978778	−1.981176	−1.979791	−1.980364
2.05	−1.878956	−1.963553	−1.957480	−1.983905	−1.985742	−1.985718	−1.984944
2.1	−1.898211	−1.970183	−1.968162	−1.994026	−1.995178	−1.996274	−1.994436
2.15	−1.916113	−1.976985	−1.978601	−2.005366	−2.006086	−2.007475	−2.005424
2.2	−1.932761	−1.983905	−1.988659	−2.017204	−2.017658	−2.018988	−2.017082
2.3	−1.962643	−1.997916	−2.007346	−2.040617	−2.040802	−2.041775	−2.040387
2.4	−1.988497	−2.011891	−2.023944	−2.062315	−2.062386	−2.063047	−2.062100
2.5	−2.010868	−2.025579	−2.038457	−2.081741	−2.081760	−2.082207	−2.081574
3.0	−2.084760	−2.084766	−2.085322	−2.147821	−2.147794	−2.147857	−2.147794
4.0	−2.136758	−2.136758	−2.136758	−2.194027	−2.194017	−2.194002	−2.194017
5.0	−2.147975	−2.147975	−2.147975	−2.203366	−2.203363	−2.203354	−2.203363

into the two hydrogen molecules. In practice, it is sufficient to study the range 2.0–5.0 a.u. For the H8 model, α varies between 0 (regular octagonal configuration) and ∞; increasing α implies the process $H_8 \rightarrow H_4 + 2H_2$, where H_4 is the P4-like system formed by two ''spectator'' H_2 molecules that remain at all times in their initial position. In practice, it is sufficient to study the range 0–1.0 a.u. The values $\alpha=0$ for the H4 and H8 models and $\alpha=2.0$ a.u. for the P4 model describe the situation where the ground-state wave function has a two-configurational character: the ground-state RHF configuration has the same weight in the exact ground-state wave function as the doubly excited configuration involving the highest occupied (HOMO) and the lowest unoccupied (LUMO) MO's. As α increases, the degree of this configurational degeneracy decreases, so that the values $\alpha>0.1$ for the H4 and H8 models, and $\alpha>2.5$ a.u. for the P4 model, describe situations where the ground state is dominated by the RHF configuration with diminishing role of the HOMO–LUMO biexcitation (for more details see, e.g., Refs. [31,34,57,66]).

The results of our calculations are presented in Tables I–III (MBS P4 model), IV–VI (MBS H4 model), VII–IX (DZP H4 model), and X-XII (MBS H8 model). Consider first the MBS P4 model. In this case, the analysis of various cluster contributions to the electronic energy is drastically simplified by the absence of T_1 and T_3 components, which vanish due to the high symmetry of the model and the presence of only four MO's in the MBS basis set spanning four different irreducible representations of the D_{2h} group. Since $C_2=T_2$ and $C_4=T_4+\frac{1}{2}(T_2)^2$ in this case [cf. Eqs. (5)–(8)], we can easily assess the importance of the connected T_4 contribution by forming the energy difference FCI−CCD (FCI=CCDQ=CIDQ in this case, where CCDQ and CIDQ designate, respectively, CC and limited CI approaches with doubles and quadruples).

The results in Table I indicate that the CCDQ′ method represents a substantial improvement when compared with the ACCD′≡ACPQ approach for $\alpha\geqslant 2.05$ a.u. In this region, the errors in the CCDQ′ results relative to FCI do not exceed (in absolute value) 0.41 mhartree and are as small as −58 μhartree for $\alpha=2.15$ a.u. This should be compared to the −2.248-mhartree error obtained with the ACCD′ method at $\alpha=2.1$ a.u. or −1.8 to −2.1-mhartree errors obtained with this approach for $\alpha=2.15-2.2$ a.u. In fact, the region where the CCDQ′ approach gives by far the best results, i.e., the interval [2.1 a.u.,2.2 a.u.] (we exclude here negligible errors for all methods considered for $\alpha>3.0$ a.u., where RHF is triplet stable so that CCD=CCDQ′), coincides with the maximum errors in the ACCD′ results. This indicates that in this interval the T_2 cluster components are already relatively poorly described by the UHF approach, while the T_4 components extracted from the PUHF wave function remain quite close to their FCI counterparts. This becomes obvious when we compare individual FCI and PUHF cluster amplitudes. This can be easily done in this case, since in the MBS P4 model there are only six OSA biexcited amplitudes and one T_4 amplitude (see Table II). We find that the FCI T_4 amplitude almost perfectly matches K_4 for $\alpha=2.1-2.2$ a.u., in spite of the fact that the quality of K_2 amplitudes is relatively poor in this region. For example, we observe 17.7–26.1% errors for the dominant $\langle 33|t_2|22\rangle_0$ PUHF amplitude relative to FCI for $\alpha=2.1-2.2$ a.u., which should be compared to less than 4% error for the same amplitude for $\alpha\leqslant 2.02$ a.u. (here, 1 and 2 are occupied orbitals and 3 and 4 unoccupied ones in the RHF reference; 2 and 3 are HOMO and LUMO, respectively). The PUHF biexcited amplitudes $\langle 44|t_2|22\rangle_0$ and $\langle 33|t_2|11\rangle_0$, vanish, but are nonzero in the FCI case and begin to play an increasingly important role for $\alpha\geqslant 2.1$ a.u.

We believe that a good measure of the relative quality of the T_2 and T_4 amplitudes is the ratio

$$k_4^X=\langle t_4^X\rangle_C/\langle t_4^X\rangle_D, \tag{149}$$

where

TABLE II. Cluster amplitudes characterizing FCI and PUHF wave functions for the MBS P4 model with $a=2.0$ a.u. and different values of α (in a.u.). In this case, T_1 and T_3 components vanish. 1,2 (3,4) designate occupied (unoccupied) orbitals in the RHF reference; 2 and 3 are HOMO and LUMO, respectively. The quantity k_4 designates the ratio $\langle\Phi_0|G^{1122}_{3344}(0,0,0,0,0,0)T_4|\Phi_0\rangle/\langle\Phi_0|G^{1122}_{3344}(0,0,0,0,0,0)\frac{1}{2}(T_2)^2|\Phi_0\rangle$, where the operator $G^{1122}_{3344}(0,0,0,0,0,0)\equiv[G^{3344}_{1122}(0,0,0,0,0,0)]^{\dagger}=G^{11}_{33}(0)G^{22}_{44}(0)$ describes the projection onto the only available quadruply excited configuration $|3\alpha 3\beta 4\alpha 4\beta|$. For $\alpha>3.0$ a.u., the cluster components characterizing PUHF wave function vanish, since RHF is triplet stable in this region.

α	Method	$\langle 33\|t_2\|22\rangle_0$	$\langle 44\|t_2\|22\rangle_0$	$\langle 33\|t_2\|11\rangle_0$	$\langle 44\|t_2\|11\rangle_0$	$\langle 34\|t_2\|12\rangle_0$	$\langle 34\|t_2\|12\rangle_1$	$\langle 3344\|t_4\|1122\rangle_{0,0,0,0,0}$	k_4
2.0	FCI	−1.0	0.0	0.0	−0.065070	−0.265435	−0.153249	−0.046971	−0.419229
	PUHF	−1.0	0.0	0.0	−0.020182	−0.142064	−0.082021	−0.013455	−0.4
2.01	FCI	−0.949745	−0.005313	−0.006277	−0.064005	−0.261019	−0.147239	−0.042166	−0.398820
	PUHF	−0.968031	0.0	0.0	−0.020368	−0.140416	−0.081069	−0.013144	−0.4
2.02	FCI	−0.902579	−0.010342	−0.012199	−0.062998	−0.256857	−0.141542	−0.037854	−0.378566
	PUHF	−0.937381	0.0	0.0	−0.020544	−0.138771	−0.080120	−0.012838	−0.4
2.05	FCI	−0.778468	−0.023775	−0.027914	−0.060328	−0.245827	−0.126275	−0.027451	−0.319887
	PUHF	−0.852587	0.0	0.0	−0.021016	−0.133858	−0.077283	−0.011945	−0.4
2.1	FCI	−0.621275	−0.041230	−0.048013	−0.056966	−0.231696	−0.106285	−0.016354	−0.234101
	PUHF	−0.731412	0.0	0.0	−0.021618	−0.125743	−0.072598	−0.010541	−0.4
2.15	FCI	−0.510688	−0.053830	−0.062159	−0.054720	−0.221653	−0.091668	−0.010039	−0.167165
	PUHF	−0.630216	0.0	0.0	−0.021992	−0.117728	−0.067970	−0.009240	−0.4
2.2	FCI	−0.431746	−0.063002	−0.072133	−0.053286	−0.214435	−0.080848	−0.006337	−0.117772
	PUHF	−0.544583	0.0	0.0	−0.022146	−0.109819	−0.063404	−0.008040	−0.4
2.3	FCI	−0.330444	−0.075012	−0.084449	−0.051950	−0.205116	−0.066219	−0.002641	−0.056507
	PUHF	−0.408022	0.0	0.0	−0.021813	−0.094341	−0.054468	−0.005933	−0.4
2.4	FCI	−0.270238	−0.082279	−0.091141	−0.051773	−0.199539	−0.056828	−0.001053	−0.024471
	PUHF	−0.304581	0.0	0.0	−0.020675	−0.079355	−0.045815	−0.004198	−0.4
2.5	FCI	−0.231146	−0.087031	−0.094935	−0.052204	−0.195888	−0.050203	−0.000292	−0.007168
	PUHF	−0.224120	0.0	0.0	−0.018793	−0.064898	−0.037469	−0.002808	−0.4
3.0	FCI	−0.148270	−0.096691	−0.098999	−0.057506	−0.187813	−0.032584	0.000448	0.012342
	PUHF	−0.003625	0.0	0.0	−0.000667	−0.001555	−0.000898	−0.000002	−0.4
4.0	FCI	−0.108360	−0.098634	−0.094579	−0.069742	−0.183127	−0.017760	0.000195	0.005775
	PUHF	0.0	0.0	0.0	0.0	0.0	0.0	0.0	0.0
5.0	FCI	−0.097366	−0.096397	−0.091773	−0.078974	−0.181727	−0.010576	0.000053	0.001586
	PUHF	0.0	0.0	0.0	0.0	0.0	0.0	0.0	0.0

$$\langle t_4^X\rangle_C=\langle\Phi_0|G^{1122}_{3344}(0,0,0,0,0,0)T_4|\Phi_0\rangle \equiv\langle\Phi_0|G^{11}_{33}(0)G^{22}_{44}(0)T_4|\Phi_0\rangle\equiv\langle 3344|t_4|1122\rangle_{0,0,0,0,0} \tag{150}$$

and

$$\langle t_4^X\rangle_D=\langle\Phi_0|G^{1122}_{3344}(0,0,0,0,0,0)\tfrac{1}{2}(T_2)^2|\Phi_0\rangle \tag{151}$$

designate, respectively, the connected (T_4) and disconnected [$\frac{1}{2}(T_2)^2$] tetraexcited amplitudes obtained with method X (X=FCI, PUHF). In the PUHF case, it can be rigorously proved that this ratio is independent of α and equals -0.4, since

$$\langle t_4^{\mathrm{PUHF}}\rangle_C=-\frac{2}{3}\langle 3||2\rangle^2\langle 4||1\rangle^2, \tag{152}$$

and

$$\langle t_4^{\mathrm{PUHF}}\rangle_D=\frac{5}{3}\langle 3||2\rangle^2\langle 4||1\rangle^2. \tag{153}$$

As we can see from Table II, the FCI ratio k_4^{FCI} is far away from -0.4 for $\alpha\in$[2.1 a.u.,2.2 a.u.], and the primary reason for that is a poor quality of K_2 amplitudes in this region. As a result, the CCDQ′ approach works very well (K_4 is very good), whereas the ACCD′ approach, which is based on the assumption of good quality of both K_2 and K_4 clusters, gives maximum errors. The PUHF ratio $k_4^{\mathrm{PUHF}}=-0.4$ almost perfectly matches its FCI value k_4^{FCI} only for $\alpha<2.05$ a.u., where the degree of configurational quasidegeneracy reaches its maximum level. This explains why the ACCD′ approach gives extremely good results in the vicinity of the square configuration of the MBS P4 model [for $\alpha=2.0$ a.u., the error in ACCD′ results is only -0.155 mhartree, while CCD and CCDQ′ give more than 2-mhartree errors (in absolute value) relative to FCI; cf. Table I]. In fact, in the immediate vicinity of $\alpha=2.0$ a.u. limit, the ACCD′ approach provides us with a very good estimate of the T_4 contribution to the energy obtained by forming the energy difference ACCD′ −CCD (see Table III) and, as our experiments with the S4 model indicate, the superb quality of ACCD′ T_4 corrections is even better when we dissociate the H_4 cluster into four hydrogen atoms (this can be achieved using the parametrization of the P4 model by increasing $a=\alpha$ to ∞). In this case,

TABLE III. The effect of connected tetraexcited clusters on CCD=CCSD energies (in mhartree), as obtained by comparing CCDQ, CCDQ′, and ACCD′ methods, for the ground electronic state of the MBS P4 model with $a=2.0$ a.u. and different values of α (in a.u.). In this case, CCDQ=FCI and for $\alpha>3.0$ a.u. CCDQ′=CCD.

α	CCDQ −CCD	CCDQ′ −CCD	ACCD′ −CCD
2.0	2.834	0.811	2.679
2.01	2.611	0.813	1.990
2.02	2.398	0.812	1.385
2.05	1.837	0.798	0.024
2.1	1.152	0.742	−1.096
2.15	0.720	0.662	−1.389
2.2	0.454	0.576	−1.330
2.3	0.185	0.415	−0.973
2.4	0.071	0.286	−0.661
2.5	0.019	0.186	−0.447
3.0	−0.027	0.0	−0.063
4.0	−0.010	0.0	0.015
5.0	−0.003	0.0	0.009

$\langle t_4^{\mathrm{PUHF}}\rangle_C$ approaches the FCI value of $-\frac{2}{3}$ describing the dissociated S4 model, since $\langle 3||2\rangle=\langle 4||1\rangle=1$ in this limit. However, for $\alpha\geqslant 2.1$ a.u., the ACCD′ estimates of T_4 cluster contributions to energy become very poor (they have a wrong sign; see Table III), since pair clusters are no longer adequately represented by the PUHF approximation.

The CCDQ′ method exhibits totally different behavior. The CCDQ′ estimate of the T_4 contribution, as obtained by forming the energy difference CCDQ′−CCD, is invariably positive (we exclude in this analysis the $\alpha>3.0$ a.u. region where UHF=RHF), in agreement with its FCI analog obtained by forming the energy difference FCI−CCD =CCDQ−CCD. For $\alpha=2.1-2.2$ a.u., we obtain amazingly good agreement between CCDQ−CCD and CCDQ′−CCD energy increments (see Table III), in perfect agreement with the results of Table II.

Let us next consider the MBS H4 model. This model has lower (C_{2v}) symmetry and, as a result, the T_1 and T_3 contributions no longer vanish. We can thus explore the performance of the more complete CCSDQ′ and ACCSD′ approaches and of their perturbative CCSDQ′[T] and ACCSD′[T] analogs. The T_3 contributions are small enough to justify the use of perturbative estimates, such as CCSD[T], ACCSD′[T], and CCSDQ′[T], over a wide range of α values.

The results of Table IV indicate that for $\alpha>0.2$, the RHF solution is triplet stable (RHF=UHF), so that CCSDQ′=CCSD and CCSDQ′[T] = CCSD[T] in this region. It is immediately obvious from Table V that in the strongly degenerate region ($\alpha=0.01-0.1$), the CCSDQ′ and CCSDQ′[T] approaches are by far the best. In this region, the errors in CCSDQ′ and CCSDQ′[T] energies relative to FCI range between −0.85 mhartree for $\alpha=0.01$ and less than 0.1 mhartree (35 μhartree for CCSDQ′[T]) for $\alpha=0.1$. This should be compared to nearly −2-mhartree errors obtained for $\alpha=0.01$ with the CCSD, ACCSD′, CCSD[T], and ACCSD′[T] methods. For $\alpha>0.1$, the overall best results (errors less than 20 μhartree) are obtained with the standard CCSD approach indicating that T_3 and T_4 contributions cancel out. Inclusion of T_3 decreases and inclusion of T_4 (via FCI or CCSDQ′) increases the energy, and for $\alpha>0.1$ both effects are of a similar magnitude but of opposite sign.

The ACCSD′ and ACCSD′[T] approaches give the best result only in the immediate vicinity of the $\alpha=0$ limit (for $\alpha<0.01$) where, as in the P4 model, the PUHF T_2 and T_4 clusters are of good quality. For $\alpha>0.01$, the quality of the ACCSD′ results substantially deteriorates, whereas the errors in the CCSDQ′ energies monotonically decrease with increasing α. This indicates that for $\alpha>0.01$ we cannot rely on the PUHF estimates of both T_2 and T_4 components, since the former ones are rather poor. However, the K_4 clusters approximate FCI T_4 components rather well and, as a result, the CCSDQ′ method gives very good results for $\alpha>0.01$. This becomes obvious when we compare the energy differences CISDQ−CCSD and CIDQ−CCD [cf. Eqs. (5)–(8)]

TABLE IV. A comparison of the FCI, RHF, UHF, CCD(PUHF), and CCSD(PUHF) energies (in hartree) for the ground electronic state of the MBS H4 model with $a=2.0$ a.u. and different values of α. The RHF solution is triplet stable for $\alpha>0.2$.

α	RHF	UHF	CCD(PUHF)	CCSD(PUHF)	FCI
0.0	−1.858241	−1.957155	−1.946785	−1.946785	−1.975862
0.005	−1.871397	−1.961129	−1.953479	−1.953480	−1.980593
0.01	−1.883894	−1.965182	−1.960187	−1.960190	−1.986202
0.015	−1.895765	−1.969308	−1.966837	−1.966841	−1.992476
0.02	−1.907040	−1.973492	−1.973371	−1.973378	−1.999187
0.05	−1.963612	−1.998933	−2.008542	−2.008555	−2.040040
0.1	−2.025560	−2.036852	−2.049701	−2.049710	−2.090882
0.12	−2.042361	−2.049282	−2.061096	−2.061103	−2.105137
0.15	−2.061704	−2.064879	−2.074305	−2.074309	−2.121744
0.2	−2.083189	−2.083904	−2.089149	−2.089150	−2.140449
0.3	−2.104642	−2.104642	−2.104642	−2.104642	−2.159418
0.4	−2.113001	−2.113001	−2.113001	−2.113001	−2.166906
0.5	−2.115237	−2.115237	−2.115237	−2.115237	−2.168926

TABLE V. A comparison of the FCI and various CC energies (in hartree) for the ground electronic state of the MBS H4 model with $a=2.0$ a.u. and different values of α. For $\alpha>0.2$, CCDQ′=CCD and CCSDQ′=CCSD.

α	FCI	CCD	CCSD	ACCSD′	CCSD[T]	ACCSD′[T]	CCDQ′	CCSDQ′	CCSDQ′[T]
0.0	−1.975862	−1.978696	−1.978696	−1.976017	−1.978696	−1.976017	−1.977885	−1.977885	−1.977885
0.005	−1.980593	−1.982752	−1.982760	−1.981969	−1.982761	−1.981970	−1.981944	−1.981953	−1.981954
0.01	−1.986202	−1.987808	−1.987829	−1.988198	−1.987831	−1.988200	−1.987027	−1.987049	−1.987051
0.015	−1.992476	−1.993665	−1.993693	−1.994684	−1.993695	−1.994687	−1.992929	−1.992959	−1.992960
0.02	−1.999187	−2.000074	−2.000103	−2.001369	−2.000104	−2.001370	−1.999395	−1.999424	−1.999425
0.05	−2.040040	−2.040247	−2.040250	−2.041174	−2.040269	−2.041189	−2.039897	−2.039900	−2.039919
0.1	−2.090882	−2.090878	−2.090889	−2.091293	−2.090942	−2.091343	−2.090783	−2.090793	−2.090847
0.12	−2.105137	−2.105117	−2.105125	−2.105451	−2.105183	−2.105506	−2.105062	−2.105070	−2.105128
0.15	−2.121744	−2.121720	−2.121724	−2.121983	−2.121782	−2.122038	−2.121696	−2.121701	−2.121759
0.2	−2.140449	−2.140422	−2.140432	−2.140643	−2.140485	−2.140693	−2.140417	−2.140427	−2.140480
0.3	−2.159418	−2.159355	−2.159412	−2.159607	−2.159454	−2.159648	−2.159355	−2.159412	−2.159454
0.4	−2.166906	−2.166804	−2.166905	−2.167110	−2.166942	−2.167146	−2.166804	−2.166905	−2.166942
0.5	−2.168926	−2.168808	−2.168925	−2.169136	−2.168961	−2.169171	−2.168808	−2.168925	−2.168961

with analogous CC differences CC(S)DQ′−CC(S)D and ACC(S)D′−CC(S)D (cf. Table VI). It is apparent from Table VI that the ACCSD′ estimate of the T_4 energy contribution is reasonable only for $\alpha\approx 0$. In this region both ACCSD′ and ACCSD′[T] perform remarkably well. However, for $\alpha\geqslant 0.01$, the ACCSD′ T_4 energy contributions have a wrong sign, which is a consequence of the poor quality of K_2 clusters, even though K_4 mimics its ''exact'' CISDQ counterpart remarkably well, particularly for $0.01<\alpha<0.15$. The K_4 energy contribution is invariably positive, in agreement with the CISDQ results.

As in the case of the MBS P4 model, the CCSDQ′ results are best when the ACCSD′ ones are worst. This clearly indicates the need for an accurate treatment of T_1 and T_2 clusters prior to an approximate account of T_4. This is guaranteed by the CCSDQ′ approach but not by ACCSD′. A similar observation applies to T_3. Although it plays a minor role in the MBS H4 model, its perturbative account worsens the CCSD and ACCSD results for all α values, indicating the need for T_4 clusters to balance T_3 contributions. In the case of the CCSDQ′ approach, the perturbative T(CCSDQ′) correction improves the CCSDQ′ results for $\alpha=0.05-0.15$, which indicates that T_1, T_2, and T_4 are well represented by the CCSDQ′ method in this region. Actually, the CCSDQ′[T] has a clear advantage over ACCSD′[T] since the former method becomes CCSD[T] when RHF is triplet stable, which happens in the region in which T_4 plays a negligible role.

Most of the above remarks also apply to a more realistic (in a sense that larger basis set is employed) DZP H4 model, in which case RHF is triplet stable for $\alpha>0.3$ (see Table VII). There are, however, differences as well. Contrary to the MBS H4 model, where the CCSD energies were below the FCI energies for $\alpha\leqslant 0.1$ and above the FCI energies for $\alpha>0.1$ (cf. Table V), the CCSD energies are invariably above the FCI ones in the DZP case (see Table VIII). Thus,

TABLE VI. The effect of connected tetraexcited clusters on CCD and CCSD energies (in mhartree), as obtained by comparing CCDQ′, CCSDQ′, ACCD′, and ACCSD′ results with CIDQ and CISDQ data, for the ground electronic state of the MBS H4 model with $a=2.0$ a.u. and different values of α. For $\alpha>0.2$, CCDQ′=CCD and CCSDQ′=CCSD.

α	CIDQ −CCD	CISDQ −CCSD	CCDQ′ −CCD	CCSDQ′ −CCSD	ACCD′ −CCD	ACCSD′ −CCSD
0.0	2.834	2.834	0.811	0.811	2.679	2.679
0.005	2.167	2.168	0.808	0.807	0.786	0.791
0.01	1.626	1.629	0.781	0.780	−0.380	−0.369
0.015	1.214	1.217	0.736	0.734	−1.006	−0.991
0.02	0.911	0.916	0.679	0.679	−1.280	−1.266
0.05	0.234	0.232	0.350	0.350	−0.926	−0.924
0.1	0.091	0.085	0.095	0.096	−0.406	−0.404
0.12	0.080	0.075	0.055	0.055	−0.327	−0.326
0.15	0.074	0.070	0.024	0.023	−0.260	−0.259
0.2	0.069	0.071	0.005	0.005	−0.212	−0.211
0.3	0.066	0.071	0.0	0.0	−0.199	−0.195
0.4	0.062	0.070	0.0	0.0	−0.209	−0.205
0.5	0.060	0.070	0.0	0.0	−0.215	−0.211

TABLE VII. A comparison of the FCI, RHF, UHF, CCD(PUHF), and CCSD(PUHF) energies (in hartree) for the ground electronic state of the DZP H4 model with $a=2.0$ a.u. and different values of α. The RHF solution is triplet stable for $\alpha>0.3$.

α	RHF	UHF	CCD(PUHF)	CCSD(PUHF)	FCI
0.0	−1.931750	−2.023191	−2.010123	−2.010101	−2.063112
0.005	−1.941796	−2.025161	−2.014980	−2.014961	−2.065627
0.01	−1.951445	−2.027357	−2.019953	−2.019936	−2.069401
0.015	−1.960709	−2.029757	−2.024973	−2.024960	−2.074121
0.02	−1.969599	−2.032340	−2.029988	−2.029978	−2.079470
0.05	−2.015652	−2.050315	−2.058212	−2.058215	−2.114299
0.1	−2.069109	−2.081256	−2.093609	−2.093614	−2.160115
0.12	−2.084181	−2.092008	−2.103804	−2.103808	−2.173349
0.15	−2.101808	−2.105761	−2.115763	−2.115766	−2.188929
0.2	−2.121595	−2.122762	−2.129221	−2.129222	−2.206548
0.3	−2.141080	−2.141131	−2.142689	−2.142689	−2.224122
0.4	−2.148427	−2.148427	−2.148427	−2.148427	−2.230887
0.5	−2.150368	−2.150368	−2.150368	−2.150368	−2.232700

since T_4 contributions, as estimated by the difference between CCSDQ (CC singles, doubles, and quadruples approach, namely, the so-called CCSDQ-1a; see Ref. [40]) and CCSD energies, remain positive for all values of α (see Table IX), their inclusion in CCSD theory should increase the error relative to FCI. Only when simultaneously accounting for T_3 clusters, which compensate the error in CCSDQ results by lowering the CCSDQ energy, can accurate (exact) results be expected. It is remarkable how well the CCSDQ′ and CCSDQ′[T] methods follow this pattern. For example, for $\alpha=0.01$ (strongly degenerate region), the 3.602 mhartree error in CCSD energy increases to 4.363 mhartree when using CCSDQ′, and drops to only −0.192 mhartree for CCSDQ′[T]. The CCSD[T] method neglecting T_4 gives a −1.013-mhartree error. For comparison, the relatively small 1.747-mhartree error obtained with ACCSD′ (suggesting that ACCSD′ improves the CCSD energy although it should not) increases to a large (in absolute value) −3.737-mhartree error in the case of ACCSD′[T]. This shows that we cannot regard the ACCSD′ method as a reliable source of T_4 clusters per se, although it improves CCSD results for all α values (which is certainly a nice feature of this method from a practical point of view, considering its simplicity). Again, the reason for this behavior does not indicate the inadequacy of the underlying theoretical analysis leading to ACCSD′ theory, as one might wrongly conclude from the remarks made in Ref. [40], but from a simple fact that the PUHF K_2 components poorly approximate T_2 clusters that are needed to obtain T_4 (K_4) components by eliminating the disconnected $\frac{1}{2}(T_2)^2$ terms from the CI C_4 operator.

Analysis of the role of individual cluster components for the DZP H4 model is difficult because of the mutual cancellation of large T_3 and T_4 contributions and their highly nonadditive character in the strongly degenerate region. For $\alpha=0$, the errors in the CCSD, ACCSD′, CCSD[T], ACCSD′[T], CCSDQ′, and CCSDQ′[T] energies are rather large, namely, 5.508, 4.802, −3.968, −5.732, 6.334, and 3.070 mhartree, respectively. At the same time, our simple CCSDQ′[T] model is still the best among all the methods

TABLE VIII. A comparison of the FCI and various CC energies (in hartree) for the ground electronic state of the DZP H4 model with $a=2.0$ a.u. and different values of α. For $\alpha>0.3$, CCDQ′=CCD and CCSDQ′=CCSD.

α	FCI	CCD	CCSD	ACCSD′	CCSD[T]	ACCSD′[T]	CCDQ′	CCSDQ′	CCSDQ′[T]
0.0	−2.063112	−2.054869	−2.057604	−2.058310	−2.067080	−2.068844	−2.054050	−2.056778	−2.066182
0.005	−2.065627	−2.058604	−2.061154	−2.062709	−2.067626	−2.070232	−2.057806	−2.060349	−2.066751
0.01	−2.069401	−2.063415	−2.065799	−2.067654	−2.070414	−2.073138	−2.062662	−2.065038	−2.069593
0.015	−2.074121	−2.068955	−2.071192	−2.073044	−2.074646	−2.077162	−2.068260	−2.070489	−2.073893
0.02	−2.079470	−2.074930	−2.077039	−2.078752	−2.079746	−2.081951	−2.074296	−2.076397	−2.079065
0.05	−2.114299	−2.111409	−2.113037	−2.113863	−2.114259	−2.115177	−2.111080	−2.112704	−2.113915
0.1	−2.160115	−2.157889	−2.159204	−2.159608	−2.160039	−2.160461	−2.157788	−2.159103	−2.159935
0.12	−2.173349	−2.171228	−2.172490	−2.172844	−2.173273	−2.173640	−2.171167	−2.172428	−2.173209
0.15	−2.188929	−2.186897	−2.188118	−2.188435	−2.188856	−2.189184	−2.186868	−2.188088	−2.188826
0.2	−2.206548	−2.204561	−2.205778	−2.206078	−2.206481	−2.206791	−2.204553	−2.205770	−2.206473
0.3	−2.224122	−2.222083	−2.223374	−2.223685	−2.224064	−2.224386	−2.222082	−2.223374	−2.224064
0.4	−2.230887	−2.228775	−2.230137	−2.230467	−2.230831	−2.231173	−2.228775	−2.230137	−2.230831
0.5	−2.232700	−2.230560	−2.231948	−2.232285	−2.232645	−2.232994	−2.230560	−2.231948	−2.232645

TABLE IX. The effect of connected tetraexcited clusters on CCD and CCSD energies (in mhartree), as obtained by comparing CCDQ′, CCSDQ′, ACCD′, and ACCSD′ results with CCDQ-1a and CCSDQ-1a data, for the ground electronic state of the DZP H4 model with $a=2.0$ a.u. and different values of α. For $\alpha>0.3$, CCDQ′=CCD and CCSDQ′=CCSD.

α	CCDQ-1a [a] −CCD	CCSDQ-1a [a] −CCSD	CCDQ′ −CCD	CCSDQ′ −CCSD	ACCD′ −CCD	ACCSD′ −CCSD
0.0	1.094	1.155	0.819	0.826	−0.743	−0.706
0.005	0.706	0.754	0.798	0.805	−1.547	−1.555
0.01	0.451	0.489	0.753	0.761	−1.817	−1.855
0.015	0.290	0.317	0.695	0.703	−1.797	−1.852
0.02	0.188	0.207	0.634	0.642	−1.650	−1.713
0.05	0.015	0.019	0.329	0.333	−0.785	−0.826
0.1	0.000	0.002	0.101	0.101	−0.385	−0.404
0.12	0.003	0.005	0.061	0.062	−0.338	−0.354
0.15	0.006	0.009	0.029	0.030	−0.303	−0.317
0.2	0.010	0.013	0.008	0.008	−0.285	−0.300
0.3	0.011	0.015	0.001	0.000	−0.295	−0.311
0.4	0.011	0.014	0.0	0.0	−0.313	−0.330
0.5	0.010	0.013	0.0	0.0	−0.319	−0.337

[a]From Ref. [40].

considered. Actually, the CCSDQ′[T] results remain best for $\alpha<0.02$, while for $\alpha\geqslant 0.02$ CCSD[T] is better, giving errors smaller than 80 μhartree for $\alpha\geqslant 0.05$ (CCSDQ′[T] gives 55 −384 μhartree errors in the same region). It is not our goal, however, to prove the superiority of CCSDQ′-based approaches, but rather to see if they are capable of representing T_4 clusters better than ACCSD′ methods. For this reason, we compare in Table IX accurate estimates of T_4 cluster contributions as given by the energy differences CC(S)DQ-1a −CC(S)D with their CC(S)DQ′−CC(S)D and ACC(S)D′ −CC(S)D analogs. We find that ACCSD′ gives a wrong sign of T_4 energy contributions for all values of α, whereas CCSDQ′ approximates these contributions quite reasonably (K_4 contributions remain positive for all α values). Particularly impressive are the results for $\alpha<0.015$. Both the CCSDQ-1a and CCSDQ′ estimates of T_4 cluster contributions decrease to zero as α increases, even though for the CCSDQ-1a method this decrease is more rapid than in the CCSDQ′ case. Poor ACCSD′ estimates of T_4 cluster contributions result in rather large −0.294 to −4.605-mhartree errors for $\alpha=0.5-0.005$ obtained with the ACCSD′[T] approach, which should be compared to small 55-μhartree to −1.124-mhartree errors in the same region obtained with the CCSDQ′[T] method.

Let us look, finally, at the MBS H8 model. In this case, the manifold of quadruple excitations is larger than for the H4 and P4 models and up to eightfold excited configurations appear in the FCI wave function. The RHF solution is triplet stable only for $\alpha>0.5$ a.u. (see Table X). The MBS H8 model is very demanding for a variety of methods, including MRCC and MRCI investigated in Refs. [31,36,50,66,92]. It is also challenging for SRCC approaches, particularly in the degenerate $\alpha\leqslant 0.1$ a.u. region, where it is difficult to balance large T_3 and T_4 contributions [24,31,50]. For example, it is sufficient to add perturbative T(CCSD) correction to CCSD energies, which for $\alpha\leqslant 0.1$ a.u. give large errors relative to

TABLE X. A comparison of the FCI, RHF, UHF, CCD(PUHF), and CCSD(PUHF) energies (in hartree) for the ground electronic state of the MBS H8 model with $a=2.0$ a.u. and different values of α (in a.u.). The RHF solution is triplet stable for $\alpha>0.5$ a.u.

α	RHF	UHF	CCD(PUHF)	CCSD(PUHF)	FCI
0.0	−4.065533	−4.137980	−4.140227	−4.140278	−4.204793
0.0001	−4.065563	−4.137988	−4.140242	−4.140293	−4.204803
0.001	−4.065828	−4.138059	−4.140385	−4.140435	−4.204886
0.003	−4.066418	−4.138217	−4.140700	−4.140751	−4.205075
0.01	−4.068474	−4.138774	−4.141805	−4.141854	−4.205769
0.03	−4.074276	−4.140389	−4.144951	−4.144998	−4.208036
0.06	−4.082780	−4.142885	−4.149628	−4.149670	−4.212169
0.08	−4.088316	−4.144597	−4.152707	−4.152746	−4.215336
0.1	−4.093745	−4.146349	−4.155747	−4.155783	−4.218763
0.3	−4.142240	−4.165876	−4.183089	−4.183104	−4.257729
0.5	−4.180812	−4.188150	−4.203770	−4.203775	−4.293221
1.0	−4.242846	−4.242846	−4.242846	−4.242846	−4.352990

TABLE XI. A comparison of the FCI and various CC energies (in hartree) for the ground electronic state of the MBS H8 model with $a=2.0$ a.u. and different values of α (in a.u.). For $\alpha>0.5$, CCDQ′=CCD and CCSDQ′=CCSD.

α	FCI	CCD	CCSD	ACCSD′	CCSD[T]	ACCSD′[T]	CCSDT [a]	CCDQ′	CCSDQ′	CCSDQ′[T]	CCSDQ′ +T(CCSDT) [b]
0.0	−4.204793	−4.198759	−4.199754	−4.201009	−4.205774	−4.208932		−4.195415	−4.196320	−4.201529	
0.0001	−4.204803	−4.198773	−4.199767	−4.201025	−4.205780	−4.208941	−4.213165	−4.195430	−4.196334	−4.201537	−4.209732
0.001	−4.204886	−4.198900	−4.199884	−4.201176	−4.205828	−4.209016	−4.213168	−4.195567	−4.196461	−4.201603	−4.209745
0.003	−4.205075	−4.199185	−4.200147	−4.201511	−4.205942	−4.209188	−4.213182	−4.195873	−4.196746	−4.201757	−4.209781
0.01	−4.205769	−4.200211	−4.201099	−4.202693	−4.206408	−4.209824	−4.213279	−4.196978	−4.197780	−4.202363	−4.209960
0.03	−4.208036	−4.203376	−4.204082	−4.206143	−4.208256	−4.211921	−4.214008	−4.200368	−4.201001	−4.204598	−4.210927
0.06	−4.212169	−4.208643	−4.209147	−4.211518	−4.212151	−4.215762	−4.216327	−4.205970	−4.206418	−4.209018	−4.213598
0.08	−4.215336	−4.212410	−4.212816	−4.215225	−4.215284	−4.218708	−4.218595	−4.209950	−4.210308	−4.212459	−4.216087
0.1	−4.218763	−4.216321	−4.216649	−4.219016	−4.218714	−4.221902	−4.221328	−4.214061	−4.214350	−4.216165	−4.219029
0.3	−4.257729	−4.256887	−4.256929	−4.258253	−4.257699	−4.259119	−4.258105	−4.255973	−4.256010	−4.256753	−4.257186
0.5	−4.293221	−4.292531	−4.292534	−4.293356	−4.293092	−4.293936	−4.293304	−4.292249	−4.292252	−4.292806	−4.293022
1.0	−4.352990	−4.352372	−4.352444	−4.352785	−4.352799	−4.353145	−4.352965	−4.352372	−4.352444	−4.352799	−4.352965

[a]From Ref. [31].
[b]T(CCSDT) is defined as $E^{\mathrm{CCSDT}}-E^{\mathrm{CCSD}}$.

FCI (ranging between 2.442 and 6.034 mhartree), to obtain surprisingly small 49-μhartree to −0.981-mhartree errors (cf. the CCSD and CCSD[T] results in Table XI). This indicates that the perturbative T(CCSD), T(ACCSD′), and T(CCSDQ′) corrections grossly underestimate the magnitude of ''true'' T_3 energy contributions, which are in reality much larger when we estimate them by forming the energy difference CCSDT−CCSD (cf. Table XII and the results in Ref. [24]). For $\alpha\leqslant 0.1$ a.u., we obtain −4.7 to −13.4 mhartree for the ''true'' T_3 correction

$$\Delta E^{\mathrm{T(CCSDT)}}=E^{\mathrm{CCSDT}}-E^{\mathrm{CCSD}}, \tag{154}$$

whereas the perturbative $\Delta E^{\mathrm{T(CCSD)}}$, $\Delta E^{\mathrm{T(ACCSD')}}$, and $\Delta E^{\mathrm{T(CCSDQ')}}$ corrections range between −2 to −3 and −5 to −8 mhartree in the same region. Thus, CCSDQ′[T] overestimates the FCI energies by 2.6−3.3 mhartree for $\alpha\leqslant 0.1$ a.u. due to large positive T_4(PUHF) corrections that are not compensated by the T(CCSDQ′) term, instead of giving us small errors found for the H4 model.

The T_4 cluster components are reasonably well represented by the PUHF wave function, as the results in Table XII indicate. In this case, a comparison of the energy differences CC(S)DQ′−CC(S)D and ACC(S)D′−CC(S)D is made with the difference of CCSDTQ and CCSDT energies computed in Ref. [31]. Although the PUHF wave function seems to underestimate large T_4 contributions obtained by comparing more accurate CCSDTQ and CCSDT results, the agreement between CCSDTQ−CCSDT and CCSDQ′ −CCSD energy differences for $\alpha=0.06-0.1$ a.u. (particularly, for $\alpha=0.1$ a.u.) is rather good. We must not forget that T_3 and T_4 corrections are highly nonadditive in the MBS H8 model, and it is hard to objectively measure their magnitude. Again, ACCSD′ gives wrong (negative) signs for the energy

TABLE XII. The effect of connected tetraexcited and triexcited clusters on CCD and CCSD energies (in mhartree), as obtained by comparing CCDQ′, CCSDQ′, ACCD′, ACCSD′, CCSD[T], ACCSD′[T], and CCSDQ′[T] results with CCSDT and CCSDTQ data, for the ground electronic state of the MBS H8 model with $a=2.0$ a.u. and different values of α (in a.u.). For $\alpha>0.5$, CCDQ′=CCD and CCSDQ′=CCSD.

α	CCSDTQ [a] −CCSDT [a]	CCDQ′ −CCD	CCSDQ′ −CCSD	ACCD′ −CCD	ACCSD′ −CCSD	CCSDT [a] −CCSD	T(CCSD)	T(ACCSD′)	T(CCSDQ′)
0.0		3.344	3.434	−1.488	−1.255		−6.020	−7.923	−5.209
0.0001	8.327	3.343	3.433	−1.491	−1.258	−13.398	−6.013	−7.916	−5.203
0.001	8.248	3.333	3.423	−1.520	−1.292	−13.284	−5.944	−7.840	−5.142
0.003	8.073	3.312	3.401	−1.581	−1.364	−13.035	−5.795	−7.677	−5.011
0.01	7.478	3.233	3.319	−1.776	−1.594	−12.180	−5.309	−7.131	−4.583
0.03	5.944	3.008	3.081	−2.163	−2.061	−9.926	−4.174	−5.778	−3.597
0.06	4.137	2.673	2.729	−2.404	−2.371	−7.180	−3.004	−4.244	−2.600
0.08	3.242	2.460	2.508	−2.418	−2.409	−5.779	−2.468	−3.483	−2.151
0.1	2.551	2.260	2.299	−2.363	−2.367	−4.679	−2.065	−2.886	−1.815
0.3	0.374	0.914	0.919	−1.319	−1.324	−1.176	−0.770	−0.866	−0.743
0.5	0.083	0.282	0.282	−0.822	−0.822	−0.770	−0.558	−0.580	−0.554
1.0	−0.026	0.0	0.0	−0.343	−0.341	−0.521	−0.355	−0.360	−0.355

[a]From Ref. [31].

corrections due to T_4 which, as the CCSDTQ−CCSDT and CCSDQ′−CCSD energies indicate, should remain positive for all values of α. In consequence, small positive errors (for $\alpha=0.03-0.08$ a.u.) and small negative errors (for $\alpha\approx 0.1$ a.u.) in the ACCSD′ results change into large negative (−3.1 to −3.9-mhartree) errors when ACCSD′ is augmented by the perturbative T(ACCSD′) correction (cf., e.g., the ACCSD′[T] results in Table XI). In fact, these errors would be even larger were we to add the ''true'' T_3 correction, $\Delta E^{\mathrm{T(CCSDT)}}$, Eq. (154), to ACCSD′ energies (cf. the last four columns in Table XII). It is, in fact, instructive to consider the CCSDQ′+T(CCSDT) approach obtained by adding $\Delta E^{\mathrm{T(CCSDT)}}$, Eq. (154), to CCSDQ′ energies. In this case the errors reduce to as little as −751 to 27 μhartree for $\alpha>0.06$ a.u., as opposed to 2.877 to 0.191-mhartree errors obtained using the CCSDQ′[T] method in the same region. This indicates that the remaining T_1, T_2, and T_4 contributions are rather well represented by the CCSDQ′ approach and we only need better estimates of T_3 corrections. Unfortunately, the PUHF wave function does not provide us with any information about T_3 components.

Before summarizing our results, let us point out that there seems to be a straightforward correlation between the quality of CCSDQ′ and CCSDQ′[T] results and the magnitude of the energy difference

$$\delta^{\mathrm{PUHF}}\equiv E^{\mathrm{CCSD(PUHF)}}-E^{\mathrm{FCI}}=\Delta E^{\mathrm{CCSD(PUHF)}}-\Delta E^{\mathrm{FCI}}, \tag{155}$$

where $\Delta E^{\mathrm{CCSD(PUHF)}}$ is the PUHF-based CCSD energy expression defined by Eq. (141) and ΔE^{FCI} its exact (FCI) counterpart. When we analyze the results in Tables I, IV and V, VII and VIII, and X and XI, we immediately recognize that CCSDQ′ and CCSDQ′[T] methods perform best when δ^{PUHF}, Eq. (155), reaches its minimum value. Indeed, for all four models considered in this paper, δ^{PUHF} is a monotonically decreasing function of α in the strongly degenerate region and, after passing through its minimum value, it increases with α to reach the maximum value of $-\Delta E^{\mathrm{FCI}}$ in the region where the RHF solution is triplet stable, so that K_1, K_2, and $\Delta E^{\mathrm{CCSD(PUHF)}}$ vanish. The minimum values of δ^{PUHF} are reached: at $\alpha\sim 2.1$ a.u. for the MBS P4 model, at $\alpha\sim 0.015$ for the MBS and DZP H4 models, and at $\alpha\sim 0.06$ a.u. for the MBS H8 model. As we have seen before, these are the regions where CCSDQ′ and CCSDQ′[T] approaches perform best and provide the best description of T_4 clusters. Unfortunately, we cannot use δ^{PUHF}, Eq. (155), as a diagnostic tool, since it requires knowledge of the FCI energy. Nonetheless, the correlation between its magnitude and the performance of the CCSDQ′ and CCSDQ′[T] approaches is worth noting.

VII. SUMMARY

In this paper, we investigated the general cluster structure of broken-symmetry UHF solutions and the possibility of correcting the standard CCSD equations by T_4 contributions resulting from such an analysis. The aim of this study was to formulate, implement, and test the CCSDQ′ method, which approximately accounts for T_4 clusters by fixing their values to their PUHF estimates. It was shown that the PUHF wave function provides useful information about T_4 cluster components even when the PUHF estimates of T_2 components are rather poor.

The PUHF-based T_4 cluster components change the CCSD energy in exactly the same direction as the ''true'' T_4 components obtained in more accurate CCSDQ or CISDQ calculations. Thus, the CCSDQ′ approach carries a great deal of information about the true T_4 corrections. The same holds for the simpler ACCSD′ method, but only when the PUHF wave function provides a good estimate of both T_2 and T_4 clusters. Otherwise, the ACCSD′ method changes the CCSD energy in the wrong direction. This does not diminish the usefulness of the ACCSD′ approach, which is computationally simpler than CCSD and provides very good results, even in difficult *ab initio* situations involving complete bond breaking, such as those found for HF and N_2 [48,93].

We have shown that the monoexcited cluster operator U_1^{UHF}, defining the UHF wave function, generally possesses both singlet and triplet components. Although only the triplet component is responsible for the energy lowering, both components are needed to reach the variational energy minimum defining the broken-symmetry UHF solution in the region where RHF is triplet unstable. The singlet component of U_1^{UHF} defines the monoexcited clusters of the PUHF wave function, whereas all clusters excited an even number of times are solely determined by the triplet component. In spite of the presence of the monoexcited component in U_1^{UHF}, all clusters excited an odd number of times, except for T_1, are absent in the PUHF wave function. In particular, no T_3 clusters are present in the PUHF solution. We made an attempt to estimate the T_3 component perturbatively, while computing T_4 using the CCSDQ′ method, but the results are not conclusive. We think that better estimates of T_3 components are needed, and may be obtained with CASSCF rather than UHF wave function. Work in this direction is under way and the results will be presented elsewhere [77].

ACKNOWLEDGMENTS

The continued support by NSERC (J.P.) is gratefully appreciated. This work was also sponsored by Wrocław Technical University research Projects No. 341-473 and No. 331-359.

APPENDIX: DIAGRAMMATIC DERIVATION OF EQS. (95) AND (108)–(110)

In this Appendix, we use the diagrammatic approach [22,41–44] based on graphical methods of spin algebras [69] to derive fundamental Eqs. (95) and (108)–(110) for the OSA K_2 amplitudes and the OSA $\{\Theta^X_{4;4}[G^{ab}_{rs}(i)]\}_L$ corrections. These equations were obtained in Ref. [53] using algebraic arguments and the relationship between spin-free (i.e., nonorthogonally spin adapted) and OSA formalisms.

We first introduce basic orbital and spin diagrams needed to derive Eqs. (95) and (108)–(110), in particular a graphical representation of the operator $U_1^X(1,0)$. To facilitate our analysis, we consider a more general monoexcitation operator $U_1^X(S,0)$, Eq. (55), and set $S=1$ in final expressions. The orbital and spin diagrams defining $U_1^X(S,0)$ are shown in Fig.

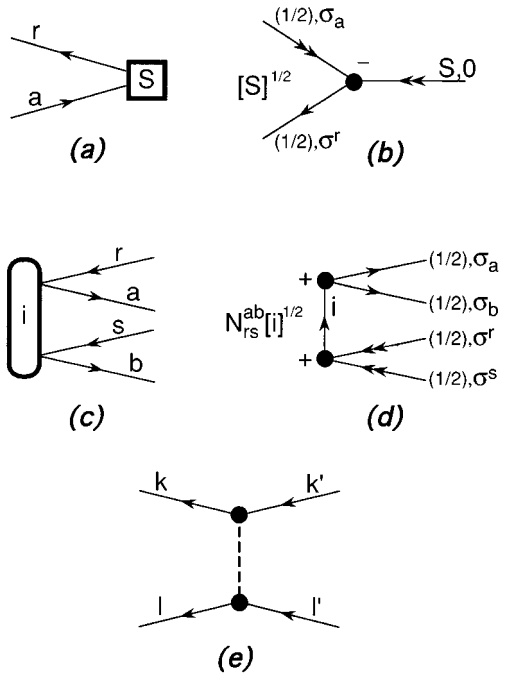

FIG. 3. Graphical representation of $U_1^X(S,0)$, Eq. (55) [(a) and (b)]; $G_{rs}^{ab}(i)\equiv[G_{ab}^{rs}(i)]^\dagger$, Eq. (28) [(c) and (d)]; and V_N, Eq. (13) [(e)]. (a), (c), and (e) are orbital and (b) and (d) spin diagrams.

3. We also need a graphical representation of the bra biexcitation operator $G_{rs}^{ab}(i)\equiv[G_{ab}^{rs}(i)]^\dagger$ and of the two-body part of the Hamiltonian V_N. They are given in Fig. 3 as well.

We begin with Eq. (95). Clearly,

$$\langle rs|k_2|ab\rangle_i=\langle\Phi_0|G_{rs}^{ab}(i)\tfrac{1}{2}[U_1^X(1,0)]^2|\Phi_0\rangle, \qquad \text{(A1)}$$

where we dropped the projector $P_{S=0}$, since $G_{ab}^{rs}(i)$ generates a singlet configuration. We thus consider a more general quantity

$$\Xi\equiv\langle\Phi_0|G_{rs}^{ab}(i)\tfrac{1}{2}[U_1^X(S,0)]^2|\Phi_0\rangle, \qquad \text{(A2)}$$

which reduces to Eq. (A1) when $S=1$. Following the general rules of the OSA diagrammatic formalism [22,41–44], we draw all possible Goldstone-Hugenholtz orbital diagrams (in Brandow representation) that arise in this case and the corresponding spin diagrams, and find the resulting orbital and spin factors. For the spin factors, we use graphical methods of spin algebras developed by Jucys and collaborators [69]. In case of Eq. (A2), only one Goldstone-Brandow orbital diagram can be drawn. It is shown together with its spin graph in Fig. 4. Notice the absence of the bra orbital diagram representing $G_{rs}^{ab}(i)$ in Fig. 4(a). As shown in Ref. [44] (cf., also, Refs. [22,42,43]), we do not have to draw the vertices representing projection operators, such as $G_{rs}^{ab}(i)$, in orbital diagrams, as they can always be accounted for by labeling the open paths of the remaining part of the diagram in all nonequivalent ways. In case of the operator $G_{rs}^{ab}(i)$, it is convenient to use for this purpose the symmetrizers $\mathcal{S}^{ab}\equiv\mathcal{S}^{ab}(0)$ and/or $\mathcal{S}_{rs}\equiv\mathcal{S}_{rs}(0)$. The symmetrizers $\mathcal{S}^{ab}$ and $\mathcal{S}_{rs}$ in orbital diagrams yield the (anti)symmetrizers $\mathcal{S}^{ab}(i)$ and $\mathcal{S}_{rs}(i)$ in the resulting algebraic expressions [44].

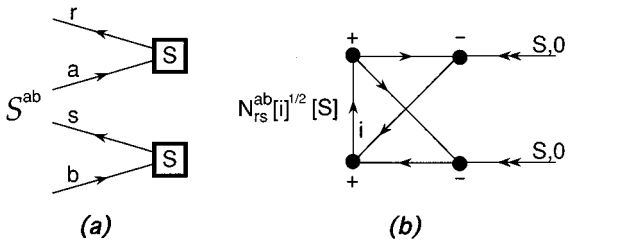

FIG. 4. Orbital (a) and spin (b) diagrams representing Ξ, Eq. (A2). The operator $\mathcal{S}^{ab}\equiv\mathcal{S}^{ab}(0)=1+(ab)$ represents two different ways of labeling the open paths in diagram (a). Lines carrying the spin $\frac{1}{2}$ in diagram (b) are left unlabeled.

The orbital factor corresponding to Fig. 4(a) is $\langle r|u_1|a\rangle_S\langle s|u_1|b\rangle_S$. The spin diagram of Fig. 4(b) has only two external lines, which can thus be joined to yield the $6-j$ symbol

$$U(i,S)=U(S,i)=\begin{Bmatrix}\frac{1}{2} & \frac{1}{2} & i\\ \frac{1}{2} & \frac{1}{2} & S\end{Bmatrix}, \qquad \text{(A3)}$$

introduced in Ref. [94]. As a result, we have

$$\Xi=N_{rs}^{ab}(-1)^{i+1}[i]^{1/2}U(i,S)\mathcal{S}^{ab}(i)\langle r|u_1|a\rangle_S\langle s|u_1|b\rangle_S. \qquad \text{(A4)}$$

In particular, for $S=1$ we obtain

$$\langle rs|k_2|ab\rangle_i=\tfrac{1}{2}N_{rs}^{ab}(-1)^{i+1}[i]^{-1/2}\times\mathcal{S}^{ab}(i)\langle r|u_1|a\rangle_1\langle s|u_1|b\rangle_1, \qquad \text{(A5)}$$

since [94]

$$U(i,1)=\tfrac{1}{2}[i]^{-1}. \qquad \text{(A6)}$$

Replacing $\langle r|u_1|a\rangle_1$ and $\langle s|u_1|b\rangle_1$ by $\langle r||a\rangle_1$ and $\langle s||b\rangle_1$, respectively, gives Eq. (95). Note that for $S=0$, we would obtain the formula for the $\frac{1}{2}(T_1)^2$ contribution to the OSA CCSD equations projected on double excitations [provided that we identify $U_1^X(0,0)$ with T_1; see Ref. [44]].

We next focus on Eqs. (108)–(110). Again, instead of $\{\Theta_{4;4}^X[G_{rs}^{ab}(i)]\}_L$, Eq. (107), we consider a more general quantity

$$\Upsilon\equiv\langle\Phi_0|\{G_{rs}^{ab}(i)V_N\tfrac{1}{24}[U_1^X(S,0)]^4\}_L|\Phi_0\rangle. \qquad \text{(A7)}$$

There are three distinct Goldstone-Hugenholtz diagrams that can be drawn in this case [cf. Eq. (108)]. Their Brandow representation is given in Figs. 5(a)–5(c), whereas the corresponding spin diagrams are shown in Figs. 6(a)–6(c). Thus, we write

$$\Upsilon=\Upsilon(a)+\Upsilon(b)+\Upsilon(c), \qquad \text{(A8)}$$

where the individual contributions $\Upsilon(x)$, $x=a,b,c$, correspond to diagrams 5(a), 5(b), and 5(c), respectively. Clearly, three contributions $\Upsilon(x)$, $x=a-c$, reduce to contributions $\Theta_{4;4}^X(x)$ of Eq. (108) when $S=1$.

The orbital factors associated with diagrams 5(a)–5(c) are

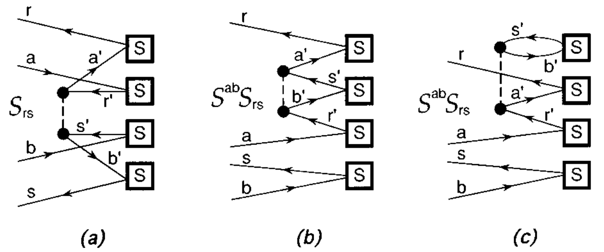

FIG. 5. Goldstone-Brandow orbital diagrams representing Υ, Eq. (A7). The operators $\mathcal{S}^{ab}\equiv\mathcal{S}^{ab}(0)=1+(ab)$ and $\mathcal{S}_{rs}\equiv\mathcal{S}_{rs}(0)=1+(rs)$ are used to represent different ways of labeling the open paths. The indices a',b' (r',s') are free summation labels of hole (particle) type.

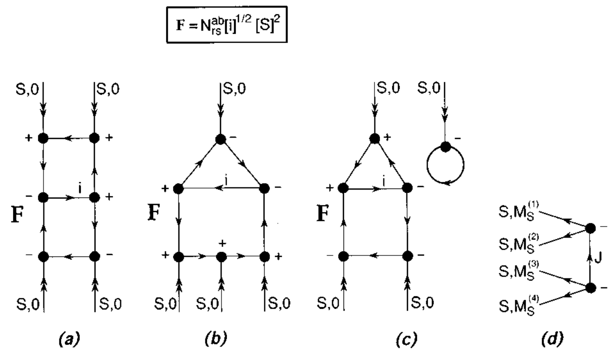

FIG. 6. Spin diagrams corresponding to the orbital diagrams of Fig. 5(a)– 5(c) [(a)–(c), respectively] and the 4-jm generalized Wigner coefficient (d) used to recouple the jm coefficients (a) and (b).

$$\Upsilon^{\rm orb}(a)=\langle a'b'||r's'\rangle\langle r|u_1|a'\rangle_S\langle r'|u_1|a\rangle_S \times\langle s|u_1|b'\rangle_S\langle s'|u_1|b\rangle_S, \tag{A9}$$

$$\Upsilon^{\rm orb}(b)=\langle a'b'||s'r'\rangle\langle r|u_1|a'\rangle_S\langle r'|u_1|a\rangle_S \times\langle s|u_1|b\rangle_S\langle s'|u_1|b'\rangle_S, \tag{A10}$$

$$\Upsilon^{\rm orb}(c)=-\langle a'b'||r's'\rangle\langle r|u_1|a'\rangle_S\langle r'|u_1|a\rangle_S \times\langle s|u_1|b\rangle_S\langle s'|u_1|b'\rangle_S. \tag{A11}$$

The corresponding spin factors $\Upsilon^{\rm spin}(x)$, $x=$a$-$c, can be easily evaluated by applying general rules described in Ref. [69] to diagrams 6(a)–6(c). Diagrams 6(a) and 6(b) have four external lines. We thus join these lines with the lines of the $4-jm$ generalized Wigner coefficient [69] depicted in Fig. 6(d). This results in the 4$-$jm coefficient

$$\begin{pmatrix} S & S & S & S \\ 0 & 0 & 0 & 0 \end{pmatrix}^{(1+2)+3}_J=(-1)^J\begin{pmatrix} S & S & J \\ 0 & 0 & 0 \end{pmatrix}\begin{pmatrix} J & S & S \\ 0 & 0 & 0 \end{pmatrix} =(-1)^J\begin{pmatrix} S & S & J \\ 0 & 0 & 0 \end{pmatrix}^2, \tag{A12}$$

where $\left(\begin{smallmatrix} j_1 & j_2 & j_3 \\ m_1 & m_2 & m_3 \end{smallmatrix}\right)$ is a standard 3–j (or 3–jm) symbol, in the final expressions for $\Upsilon^{\rm spin}(a)$ and $\Upsilon^{\rm spin}(b)$. Here, J is the intermediate spin coupling number that must be summed over from $J=0$ to $J=2$ (this summation must be accompanied by the factor $[J]$; cf. Ref. [69]). It is quite obvious from Figs. 6(a) and 6(b) that the resulting spin recoupling coefficients [obtained by joining the lines of 6(a) and 6(b) with 6(d)] are represented by diagrams that are separable over three internal lines. Thus, they factorize into products of much simpler $6-j$ symbols $U(X_1,X_2)$, Eq. (A3), and (cf. Ref. [94])

$$V(S,S,J)=\begin{Bmatrix} S & S & J \\ \frac{1}{2} & \frac{1}{2} & \frac{1}{2} \end{Bmatrix}. \tag{A13}$$

In this way, we arrive at the following expressions for the spin factors $\Upsilon^{\rm spin}(a)$ and $\Upsilon^{\rm spin}(b)$,

$$\Upsilon^{\rm spin}(a)=N^{ab}_{rs}(-1)^{i+1}[i]^{1/2}[S]^2\sum_{J=0}^{2}(-1)^J[J]U(i,J)V(S,S,J)^2\begin{pmatrix} S & S & J \\ 0 & 0 & 0 \end{pmatrix}^2, \tag{A14}$$

$$\Upsilon^{\rm spin}(b)=N^{ab}_{rs}(-1)^{i+1}[i]^{1/2}[S]^2\sum_{J=0}^{2}(-1)^J[J]U(i,S)V(S,S,J)^2\begin{pmatrix} S & S & J \\ 0 & 0 & 0 \end{pmatrix}^2. \tag{A15}$$

Two facts simplify these expressions further. The 6–j symbols $V(S,S,J)$ eliminate the $J=2$ term from Eqs. (A14) and (A15), since $V(S,S,2)=0$, whereas the 3–j symbol $\left(\begin{smallmatrix} S & S & J \\ 0 & 0 & 0 \end{smallmatrix}\right)$ eliminates the $J=1$ term, since $S+S+J$ must be even to give a nonzero value. As a result, J in Eqs. (A14) and (A15) must equal zero, so that

$$\Upsilon^{\rm spin}(a)=\tfrac{1}{4}N^{ab}_{rs}[i]^{1/2}, \tag{A16}$$

$$\Upsilon^{\rm spin}(b)=\tfrac{1}{2}N^{ab}_{rs}(-1)^{i+1}[i]^{1/2}U(i,S), \tag{A17}$$

since [94]

$$V(S,S,0)^2\begin{pmatrix} S & S & 0 \\ 0 & 0 & 0 \end{pmatrix}^2=\tfrac{1}{2}[S]^{-2}, \tag{A18}$$

and

$$U(0,i)=\tfrac{1}{2}(-1)^{i+1}. \tag{A19}$$

The spin factor $\Upsilon^{\rm spin}(c)$ is easier to evaluate since a loop diagram contributing to 6(c) introduces the Kronecker delta symbol $\delta_{S,0}$ [69]. As a result, the lines carrying S and the associated vertices representing 2–jm symbols (obtained by removing the $S=0$ line from each 3–jm vertex carrying S) can be eliminated, yielding after a simple manipulation,

$$\Upsilon^{\rm spin}(c)=\tfrac{1}{2}N_{rs}^{ab}\delta_{S,0}[i]^{1/2}. \tag{A20}$$

In consequence, the final formulas for $\Upsilon(x)$, $x=a-c$, obtained by combining the orbital and spin factors, $\Upsilon^{\rm orb}(x)$, Eqs. (A9)–(A11), and $\Upsilon^{\rm spin}(x)$, Eqs. (A16), (A17), and (A20), respectively, are

$$\Upsilon(a)=\tfrac{1}{4}N_{rs}^{ab}[i]^{1/2}\sum_{a',b',r',s'}\langle a'b'||r's'\rangle\langle r'|u_1|a\rangle_S\,\langle s'|u_1|b\rangle_S\,\mathcal{S}_{rs}(i)\langle r|u_1|a'\rangle_S\,\langle s|u_1|b'\rangle_S, \tag{A21}$$

$$\Upsilon(b)=\tfrac{1}{2}N_{rs}^{ab}(-1)^{i+1}[i]^{1/2}U(i,S)\sum_{a',b',r',s'}\langle a'b'||r's'\rangle\langle r'|u_1|b'\rangle_S\,\mathcal{S}_{rs}(i)\mathcal{S}^{ab}(i)\langle r|u_1|a'\rangle_S\,\langle s'|u_1|a\rangle_S\,\langle s|u_1|b\rangle_S, \tag{A22}$$

$$\Upsilon(c)=-\tfrac{1}{2}N_{rs}^{ab}[i]^{1/2}\delta_{S,0}\sum_{a',b',r',s'}\langle a'b'||r's'\rangle\mathcal{S}_{rs}(i)\mathcal{S}^{ab}(i)\langle r|u_1|a'\rangle_0\,\langle r'|u_1|a\rangle_0\,\langle s|u_1|b\rangle_0\,\langle s'|u_1|b'\rangle_0, \tag{A23}$$

where we interchanged the summation indices r' and s' in Eq. (A22). Clearly, for $S=1$, $\Upsilon(c)=\Theta_{4;4}^{X}(c)=0$. The remaining two contributions, $\Upsilon(a)$ and $\Upsilon(b)$, reduce to Eqs. (109) and (110) for $\Theta_{4;4}^{X}(a)$ and $\Theta_{4;4}^{X}(b)$, respectively, when we use Eq. (A6) to eliminate $U(i,1)$ from Eq. (A22) and replace $\langle r|u_1|a\rangle_1$ by $\langle r||a\rangle_1$.

It is interesting to notice that $\Upsilon(a)$, Eq. (A21), reduces to the $\frac{1}{24}(T_1)^4$ contribution to the OSA CCSD equations projected on biexcited configurations [44], once we set $S=0$ and identify $U_1^X(0,0)$ with T_1. The remaining two diagrams of Fig. 5 [i.e., $\Upsilon(b)$ and $\Upsilon(c)$] do not have such an interpretation, since they do not represent the connected diagrams of the CCSD theory.

As a last remark, let us notice that the general formula for the K_2 amplitudes $\langle rs|k_2|ab\rangle_i$, Eq. (95), that we derived in this Appendix, reduces to the expression for the exact pair-cluster amplitudes characterizing the $\beta=0$ limit of the cyclic polyene model with $N=4\nu+2=2n$ sites [56] (in this case, PUHF solution represents the exact wave function), once we realize that in this special case

$$\langle r\alpha|u_1^{(\alpha)}|a\alpha\rangle=\delta_{r,a+n}, \tag{A24}$$

$$\langle r\beta|u_1^{(\beta)}|a\beta\rangle=-\delta_{r,a+n}. \tag{A25}$$

To prove Eqs. (A24) and (A25), we must express the UHF orbitals for $\beta=0$ in terms of the corresponding RHF MO's and expand the UHF wave function for $\beta=0$ in terms of the RHF configuration and various excited configurations resulting from $|\Phi_0^{\rm RHF}\rangle$ in order to find the amplitudes defining the monoexcitations $|_{a\alpha}^{r\alpha}\rangle$ and $|_{a\beta}^{r\beta}\rangle$, Eq. (133) (see Appendix A in Ref. [56] for more detail). From Eqs. (58), (A24), and (A25) we immediately find

$$\langle r||a\rangle_0=0, \tag{A26}$$

$$\langle r||a\rangle_1=-\delta_{r,a+n}, \tag{A27}$$

so that $\langle rs|k_2|ab\rangle_i$ becomes

$$\begin{aligned}\langle rs|k_2|ab\rangle_i&=-N_{ab}^{rs}[i]^{-1/2}\mathcal{S}^{ab}(i)\,\delta_{r,b+n}\delta_{s,a+n}\\&=-N_{ab}^{rs}[i]^{-1/2}\delta_{r+s,a+b}\mathcal{S}^{ab}(i)\,\delta_{r,b+n},\end{aligned} \tag{A28}$$

where $\delta_{r+s,a+b}=1$ when $r+s=a+b(\mathrm{mod}N)$ and 0 otherwise, in perfect agreement with the results of Ref. [56]. Note that in this case, $U_1^X(0,0)=0$ [cf. Eq. (A26)], which was one of the main reasons for neglecting the singlet component of U_1^X in the initial study on CCDQ′ and ACCD′=ACPQ approaches [53].

[1] F. Coester, Nucl. Phys. **7**, 421 (1958); F. Coester and H. Kümmel, *ibid.* **17**, 477 (1960); J. Čížek, J. Chem. Phys. **45**, 4256 (1966); Adv. Chem. Phys. **14**, 35 (1969); J. Čížek and J. Paldus, Int. J. Quantum Chem. **5**, 359 (1971).

[2] J. Paldus, J. Čížek, and I. Shavitt, Phys. Rev. A **5**, 50 (1972).

[3] R.J. Bartlett, Annu. Rev. Phys. Chem. **32**, 359 (1981).

[4] R.J. Bartlett, J. Phys. Chem. **93**, 1697 (1989).

[5] J. Paldus, *Diagrammatic Methods for Many-Fermion Systems* (University of Nijmegen, Nijmegen, The Netherlands, 1981); in *New Horizons of Quantum Chemistry*, edited by P.-O. Löwdin and B. Pullman (Reidel, Dordrecht, 1983), pp. 31–60; R.J. Bartlett, C.E. Dykstra, and J. Paldus, in *Advanced Theories and Computational Approaches to the Electronic Structure of Molecules*, edited by C.E. Dykstra (Reidel, Dordrecht, 1984), pp. 127–159.

[6] M. Urban, I. Černušák, V. Kellö, and J. Noga, in *Methods in*

Computational Chemistry, Vol. 1: *Electron Correlation in Atoms and Molecules*, edited by S. Wilson (Plenum, New York, 1987), pp. 117–250.

[7] J. Paldus, in *Methods in Computational Molecular Physics*, Vol. 293 of *NATO Advanced Study Institute Series B: Physics*, edited by S. Wilson and G.H.F. Diercksen (Plenum, New York, 1992), pp. 99–194.

[8] J. Paldus, in *Relativistic and Electron Correlation Effects in Molecules and Solids*, Vol. 318 of *NATO Advanced Study Institute Series B: Physics*, edited by G.L. Malli (Plenum, New York, 1994), pp. 207–282.

[9] Theor. Chim. Acta **80** (2–6) (1991), topical issues on Coupled Cluster Theory of Electron Correlation in Many-Electron Systems, edited by R. J. Bartlett.

[10] B. Jeziorski and H.J. Monkhorst, Phys. Rev. A **24**, 1668 (1981); B. Jeziorski and J. Paldus, J. Chem. Phys. **88**, 5673 (1988).

[11] B. Jeziorski and J. Paldus, J. Chem. Phys. **90**, 2714 (1989).

[12] I. Lindgren and D. Mukherjee, Phys. Rep. **151**, 93 (1987).

[13] D. Mukherjee and S. Pal, Adv. Quantum Chem. **20**, 291 (1989).

[14] P. Piecuch, N. Oliphant, and L. Adamowicz, J. Chem. Phys. **99**, 1875 (1993).

[15] Y.S. Lee and R.J. Bartlett, J. Chem. Phys. **80**, 4371 (1984); Y.S. Lee, S.A. Kucharski, and R.J. Bartlett, *ibid.* **81**, 5906 (1984); **82**, 5761(E) (1985).

[16] J. Noga, R.J. Bartlett, and M. Urban, Chem. Phys. Lett. **134**, 126 (1987); G.W. Trucks, J. Noga, and R.J. Bartlett, *ibid.* **145**, 548 (1988).

[17] M. Urban, J. Noga, S.J. Cole, and R.J. Bartlett, J. Chem. Phys. **83**, 4041 (1985); S.J. Cole and R.J. Bartlett, *ibid.* **86**, 873 (1987).

[18] K. Raghavachari, J. Chem. Phys. **82**, 4607 (1985).

[19] K. Raghavachari, G.W. Trucks, J.A. Pople, and M. Head-Gordon, Chem. Phys. Lett. **157**, 479 (1989).

[20] J. Noga and R.J. Bartlett, J. Chem. Phys. **86**, 7041 (1987); **89**, 3401(E) (1988); J.D. Watts and R.J. Bartlett, *ibid.* **93**, 6104 (1990).

[21] G.E. Scuseria and H.F. Schaefer III, Chem. Phys. Lett. **152**, 382 (1988).

[22] P. Piecuch and J. Paldus, Theor. Chim. Acta **78**, 65 (1990).

[23] P. Piecuch, S. Zarrabian, J. Paldus, and J. Čížek, Phys. Rev. B **42**, 3351 (1990); J. Paldus and P. Piecuch, Int. J. Quantum Chem. **42**, 135 (1992).

[24] P. Piecuch, R. Toboła, and J. Paldus, Int. J. Quantum Chem. **55**, 133 (1995).

[25] S.A. Kucharski and R.J. Bartlett, Chem. Phys. Lett. **158**, 550 (1989).

[26] R.J. Bartlett, J.D. Watts, S.A. Kucharski, and J. Noga, Chem. Phys. Lett. **165**, 513 (1990).

[27] S.A. Kucharski and R.J. Bartlett, Theor. Chim. Acta **80**, 387 (1991).

[28] S.A. Kucharski and R.J. Bartlett, J. Chem. Phys. **97**, 4282 (1992).

[29] N. Oliphant and L. Adamowicz, J. Chem. Phys. **95**, 6645 (1991).

[30] P. Piecuch and L. Adamowicz, J. Chem. Phys. **100**, 5857 (1994).

[31] P. Piecuch and L. Adamowicz, J. Chem. Phys. **100**, 5792 (1994).

[32] G. Hose and U. Kaldor, J. Phys. B **12**, 3827 (1979); Phys. Scr. **21**, 357 (1980); Chem. Phys. **62**, 469 (1981); J. Phys. Chem. **86**, 2133 (1982); Phys. Rev. A **30**, 2932 (1984); U. Kaldor, J. Chem. Phys. **81**, 2406 (1984).

[33] K. Jankowski, J. Paldus, I. Grabowski, and K. Kowalski, J. Chem. Phys. **97**, 7600 (1992); **101**, 3085 (1994).

[34] J. Paldus, P. Piecuch, L. Pylypow, and B. Jeziorski, Phys. Rev. A **47**, 2738 (1993); P. Piecuch and J. Paldus, *ibid.* **49**, 3479 (1994); P. Piecuch, R. Toboła, and J. Paldus, Chem. Phys. Lett. **210**, 243 (1993).

[35] N. Oliphant and L. Adamowicz, J. Chem. Phys. **96**, 3739 (1992); Int. Rev. Phys. Chem. **12**, 339 (1993); P. Piecuch and L. Adamowicz, J. Chem. Phys. **102**, 898 (1995); V. Alexandrov, P. Piecuch, and L. Adamowicz, *ibid.* **102**, 3301 (1995).

[36] P. Piecuch and L. Adamowicz, Chem. Phys. Lett. **221**, 121 (1994).

[37] K.B. Ghose, P. Piecuch, and L. Adamowicz, J. Chem. Phys. **103**, 9331 (1995).

[38] J. Paldus and X. Li, in *Symmetries in Science VI: From the Rotation Group to Quantum Algebras*, edited by B. Gruber (Plenum, New York, 1993), pp. 573–592; X. Li and J. Paldus, J. Chem. Phys. **101**, 8812 (1994); **102**, 2013 (1995); **102**, 8059 (1995); **102**, 8897 (1995); **103**, 1024 (1995); **103**, 6536 (1995); Chem. Phys. Lett. **231**, 1 (1994).

[39] B. Jeziorski, J. Paldus, and P. Jankowski, Int. J. Quantum Chem. **56**, 129 (1995).

[40] S.A. Kucharski, A. Balková, and R.J. Bartlett, Theor. Chim. Acta **80**, 321 (1991).

[41] J. Paldus, B. Adams, and J. Čížek, Int. J. Quantum Chem. **11**, 813 (1977).

[42] J. Paldus, J. Chem. Phys. **67**, 303 (1977).

[43] B.G. Adams and J. Paldus, Phys. Rev. A **20**, 1 (1979).

[44] P. Piecuch and J. Paldus, Int. J. Quantum Chem. **36**, 429 (1989).

[45] B.G. Adams and J. Paldus, Phys. Rev. A **24**, 2302 (1981); **24**, 2316 (1981).

[46] J.F. Stanton, J. Gauss, J.D. Watts, and R.J. Bartlett, J. Chem. Phys. **94**, 4334 (1991).

[47] W.D. Laidig, P. Saxe, and R.J. Bartlett, J. Chem. Phys. **86**, 887 (1987).

[48] P. Piecuch, V. Špirko, A.E. Kondo, and J. Paldus, J. Chem. Phys. **104**, 4699 (1996).

[49] J. Paldus, M. Takahashi, and B.W.H. Cho, Int. J. Quantum Chem. Symp. **18**, 237 (1984).

[50] S.A. Kucharski, A. Balková, P.G. Szalay, and R.J. Bartlett, J. Chem. Phys. **97**, 4289 (1992).

[51] J. Paldus and M.J. Boyle, Int. J. Quantum Chem. **22**, 1281 (1982).

[52] J. Paldus, M. Takahashi, and R.W.H. Cho, Phys. Rev. B **30**, 4267 (1984); M. Takahashi and J. Paldus, Phys. Rev. B **31**, 5121 (1985).

[53] J. Paldus, J. Čížek, and M. Takahashi, Phys. Rev. A **30**, 2193 (1984).

[54] J. Planelles, J. Paldus, and X. Li, Theor. Chim. Acta **89**, 33 (1994).

[55] J. Paldus and P. Piecuch (unpublished).

[56] P. Piecuch and J. Paldus, Int. J. Quantum Chem. Symp. **25**, 9 (1991).

[57] K. Jankowski and J. Paldus, Int. J. Quantum Chem. **18**, 1243 (1980)

[58] B.G. Adams, K. Jankowski, and J. Paldus, Phys. Rev. A **24**, 2330 (1981).

[59] J. Paldus, P.E.S. Wormer, and M. Bénard, Coll. Czech. Chem. Commun. **53**, 1919 (1988).
[60] R.A. Chiles and C.E. Dykstra, Chem. Phys. Lett. **80**, 69 (1981); S.M. Bachrach, R.A. Chiles, and C.E. Dykstra, J. Chem. Phys. **75**, 2270 (1981); S.-Y. Liu, M.F. Daskalakis, and C.E. Dykstra, *ibid.* **85**, 5877 (1986); D.E. Bernholdt, S.-Y. Liu, and C.E. Dykstra, *ibid.* **85**, 5120 (1986); C.E. Dykstra, S.-Y. Liu, M.F. Daskalakis, J.P. Lucia, and M. Takahashi, Chem. Phys. Lett. **137**, 266 (1987); C.E. Dykstra, *Ab Initio Calculation of the Structure and Properties of Molecules* (Elsevier, Amsterdam, 1988).
[61] J. Planelles, J. Paldus, and X. Li, Theor. Chim. Acta **89**, 59 (1994).
[62] J. Paldus and J. Planelles, Theor. Chim. Acta **89**, 13 (1994).
[63] D.J. Thouless, *The Quantum Mechanics of Many-Body Systems*, 2nd ed. (Academic, New York, 1974).
[64] J. Paldus, in *Self-Consistent Field: Theory and Applications*, edited by R. Carbó and M. Kłobukowski (Elsevier, Amsterdam, 1990), pp. 1–45.
[65] B.W. Char, K.O. Geddes, G.H. Gonnet, M.B. Monagan, and S.M. Watt, *Maple Reference Manual*, 5th ed. (Watcom Publications, Waterloo, Ontario, 1988); B.W. Char, K.O. Geddes, G.H. Gonnet, M.B. Monagan, and S.M. Watt, *MAPLE, First Leaves, A Tutorial Introduction to Maple*, 3rd ed. (Watcom Publications, Waterloo, Ontario, 1990); B.W. Char, K.O. Geddes, G.H. Gonnet, B.L. Leong, M.B. Monagan, and S.M. Watt, *Maple V, Maple Language Reference Manual*, pre-publication manuscript (Waterloo Maple Publishing, Waterloo, Ontario, 1991).
[66] K. Jankowski, L. Meissner, and J. Wasilewski, Int. J. Quantum Chem. **28**, 931 (1985).
[67] P. Piecuch and J. Paldus, J. Chem. Phys. **101**, 5875 (1994).
[68] G. E. Scuseria, Chem. Phys. Lett. **176**, 27 (1991).
[69] A. Jucys, J. Levinsonas, and V. Vanagas, *Mathematical Apparatus of the Theory of Angular Momentum* (Institute of Physics and Mathematics of the Academy of Sciences of the Lithuanian S.S.R., Vilnius, 1960) (in Russian); English translations: (Israel Program for Scientific Translations, Jerusalem, 1962), (Gordon and Breach, New York, 1964); A. Jucys and A. Bandzaitis, *The Theory of Angular Momentum in Quantum Mechanics*, 2nd ed. (Mokslas, Vilnius, 1977) (in Russian); D.M. Brink and G.R. Satchler, *Angular Momentum*, 2nd ed. (Clarendon, Oxford, 1968); E. El Baz and B. Castel, *Graphical Methods of Spin Algebras in Atomic, Nuclear and Particle Physics* (Marcel Dekker, New York, 1972); for a brief review of these methods, see, e.g., Appendices of Ref. [41] and P. Piecuch, in *Molecules in Physics, Chemistry and Biology, Vol. 2*: *Physical Aspects of Molecular Systems*, edited by J. Maruani (Kluwer, Dordrecht, 1988), pp. 417–505.
[70] J. Paldus and J. Čížek, Adv. Quantum Chem. **9**, 105 (1975).
[71] J. Paldus, J. Chem. Phys. **61**, 5321 (1974); in *Theoretical Chemistry, Advances and Perspectives*, edited by H. Eyring and D.J. Henderson (Academic, New York, 1976), Vol. 2, pp. 131–290; in *Mathematical Frontiers in Computational Chemical Physics*, edited by D.G. Truhlar (Springer, Berlin, 1988), pp. 262–299; in *Contemporary Mathematics* (American Mathematical Society, Providence, RI, 1994), Vol. 160, pp. 209-236.
[72] L. Stolarczyk, Chem. Phys. Lett. **217**, 1 (1994).
[73] M. Dupuis, D. Spangler, and J.J. Wendoloski, The GAMESS system of programs, National Resource for Computations in Chemistry, Software Catalog, University of California, Berkeley, CA 1980, Program QG01; M.W. Schmidt, K.K. Baldridge, J.A. Boatz, S.T. Elbert, M.S. Gordon, J.H. Jensen, S. Koseki, N. Matsunaga, K.A. Nguyen, S.J. Su, T.L. Windus, M. Dupuis, and J.A. Montgomery, J. Comput. Chem. **14**, 1347 (1993).
[74] M. Dupuis, F. Johnston, and A. Marquez, *HONDO 8.5 from CHEM-Station* (IBM Corporation, Kingston, NY, 1994).
[75] M.J. Frisch, G.W. Trucks, M. Head-Gordon, P.M.W. Gill, M.W. Wong, J.B. Foresman, B.G. Johnson, H.B. Schlegel, M.A. Robb, E.S. Replogle, R. Gomperts, J.L. Andres, K. Raghavachari, J.S. Binkley, C. Gonzalez, R.L. Martin, D.J. Fox, D.J. Defrees, J. Baker, J.J.P. Stewart, and J.A. Pople, GAUSSIAN 92, Revision E.2, Gaussian, Inc., Pittsburgh PA, 1992.
[76] K. Andersson, M.R.A. Blomberg, M.P. Fülscher, V. Kellö, R. Lindh, P.-Å. Malmqvist, J. Noga, J. Olsen, B.O. Roos, A.J. Sadlej, P.E.M. Siegbahn, M. Urban, and P.-O. Widmark, MOLCAS 3, University of Lund, Lund, Sweden, 1994.
[77] R. Toboła, P. Piecuch, J. Paldus, and H. Chojnacki (unpublished); G. Peris, J. Planelles, and J. Paldus (unpublished).
[78] J. Paldus, E. Chin, and M.G. Grey, Int. J. Quantum Chem. **24**, 395 (1983).
[79] J. Čížek and J. Paldus, J. Chem. Phys. **47**, 3976 (1967).
[80] J. Paldus and J. Čížek, Phys. Rev. A **2**, 2268 (1970).
[81] R.J. Bartlett and G.D. Purvis III, Phys. Scr. **21**, 255 (1980).
[82] A. Igawa and H. Fukutome, Prog. Theor. Phys. **64**, 491 (1980); H. Fukutome, Int. J. Quantum Chem. **20**, 955 (1981).
[83] P.-O. Löwdin, Phys. Rev. **97**, 1509 (1955); J. Appl. Phys. (Suppl.) **33**, 251 (1962); Rev. Mod. Phys. **34**, 520 (1962); in *Quantum Theory of Atoms, Molecules and the Solid State, A Tribute to John C. Slater*, edited by P.-O. Löwdin (Academic, New York, 1966), p. 601; Adv. Chem. Phys. **14**, 283 (1969).
[84] P.-O. Löwdin, *Symposium on Molecular Physics* (Maruzen, Tokyo, 1953), p. 13; R. Pauncz, *Alternant Molecular Orbital Method* (Saunders, Philadelphia, 1967).
[85] H. Fukutome, Prog. Theor. Phys. **40**, 998 (1968); **40**, 1227 (1968); **45**, 1382 (1971); **52**, 115 (1974); **52**, 1766 (1974); **53**, 1320 (1975).
[86] G.D. Purvis III and R.J. Bartlett, J. Chem. Phys. **75**, 1284 (1981).
[87] N. Oliphant and L. Adamowicz, Chem. Phys. Lett. **190**, 13 (1992).
[88] P. Piecuch and J. Paldus (unpublished).
[89] J. Paldus and B. Jeziorski, Theor. Chim. Acta **73**, 81 (1988).
[90] A.E. Kondo, P. Piecuch, and J. Paldus, J. Chem. Phys. **102**, 6511 (1995); *ibid.* (in press).
[91] S. Wilson, K. Jankowski, and J. Paldus, Int. J. Quantum Chem. **23**, 1781 (1983); **28**, 525 (1985); U. Kaldor, *ibid.* **28**, 103 (1985); N. Iijima and A. Saika, *ibid.* **27**, 481 (1985); S. Zarrabian and J. Paldus, *ibid.* **38**, 761 (1990).
[92] L. Meissner, K. Jankowski, and J. Wasilewski, Int. J. Quantum Chem. **34**, 535 (1988); K. Jankowski, J. Paldus, and J. Wasilewski, J. Chem. Phys. **95**, 3549 (1991).
[93] V. Špirko, P. Piecuch, A.E. Kondo, and J. Paldus, J. Chem. Phys. **104**, 4716 (1996).
[94] P. Piecuch and J. Paldus, Theor. Chim. Acta **83**, 69 (1992).